Partial Discharge Location Technique for Covered-Conductor Overhead Distribution Lines

Muzamir Isa

Partial Discharge Location Technique for Covered-Conductor Overhead Distribution Lines

Muzamir Isa

Doctoral dissertation for the degree of Doctor of Science in Technology to be presented with due permission of the Aalto University School of Electrical Engineering for public examination and debate held in Auditorium S1 at the Aalto University School of Electrical Engineering (Espoo, Finland) on the 11th of January 2013, at 12 noon.

Supervising professor
Professor Dr. Matti Lehtonen

Preliminary examiners
Dr. Joseph M. Wetzer, Principal Consultant Asset Management,
KEMA Nederland B.V., The Netherlands

Associate Professor Dr. Charles J. Kim, Howard University,
Washington, USA

Opponent
Professor Dr. Akihiro Ametani, Doshisha University, Kyoto, Japan

NORDIC ECOLABEL

441   697
Printed matter

Author
Muzamir Isa

Abstract

In Finland, covered-conductor (CC) overhead lines are commonly used in medium voltage (MV) networks because the loads are widely distributed in the forested terrain. Such parts of the network are exposed to leaning trees which produce partial discharges (PDs) in CC lines.

This thesis presents a technique to locate the PD source on CC overhead distribution line networks. The algorithm is developed and tested using a simulated study and experimental measurements. The Electromagnetic Transient Program-Alternative Transient Program (EMTP-ATP) is used to simulate and analyze a three-phase PD monitoring system, while MATLAB is used for post-processing of the high frequency signals which were measured. A Rogowski coil is used as the measuring sensor. A multi-end correlation-based technique for PD location is implemented using the theory of maximum correlation factor in order to find the time difference of arrival (TDOA) between signal arrivals at three synchronized measuring points. The three stages of signal analysis used are: 1) denoising by applying discrete wavelet transform (DWT); 2) extracting the PD features using the absolute or windowed standard deviation (STD) and; 3) locating the PD point. The advantage of this technique is the ability to locate the PD source without the need to know the first arrival time and the propagation velocity of the signals. In addition, the faulty section of the CC line between three measuring points can also be identified based on the degrees of correlation.

An experimental analysis is performed to evaluate the PD measurement system performance for PD location on CC overhead lines. The measuring set-up is arranged in a high voltage (HV) laboratory. A multi-end measuring method is chosen as a technique to locate the PD source point on the line. A power transformer 110/20 kV was used to energize the AC voltage up to 11.5 kV/phase (20 kV system). The tests were designed to cover different conditions such as offline and online measurements.

The thesis evaluates the possibility of using a Rogowski coil for locating faults in MV distribution lines and a test bench of a 20 kV distribution network is developed. Different fault scenarios are simulated including earth and phase faults, arcing faults and faults caused by leaning trees. Results favourably show the possibility of using a Rogowski coil for locating faults in distribution networks.

Acknowledgments

Author's declaration

I hereby declare that I am the sole author of this thesis, having the main responsibility for all contents of the thesis, for doing all analyses and simulations and also for developing and writing the corresponding published papers. This work has been carried out at Aalto University, School of Electrical Engineering, Espoo, Finland, under the supervision of Professor Matti Lehtonen.

Table of contents

List of symbols

Symbol	Description	Units
Γ	Reflection coefficient	-
ε	Error	-
λ_j	Threshold value	-
σ_n	Estimated noise standard deviation	-
τ	Damping time constant of the partial discharge pulse	s
$\psi(.)$	Mother wavelet	-
A	Amplitude of the partial discharge pulse	A
C_l	Lumped capacitance of Rogowski coil	F
CR	Correlation	-
CR_{BA}	Correlation between vector B and vector A	-
d_1	Internal diameter of Rogowski coil	m
d_2	External diameter of Rogowski coil	m
d_{rc}	Net diameter of Rogowski coil	m
f	Frequency of signal	Hz
g	Time-varying arc conductance	p.u.
G	Stationary arc conductance	p.u.
H	Sensitivity of Rogowski coil	-
$i(t)$	Current flowing in the conductor-core	A
L	Length of CC line	m
L_{AB}	Length between A and B	m
L_{BC}	Length between B and C	m
L_l	Lumped inductance of Rogowski coil	H
LR	Ratio of difference distance	-
M	Mutual inductance of the Rogowski coil	H
MCR_{AA}	Maximum correlation factor of signal A	-
MCR_{BB}	Maximum correlation factor of signal B	-
n	Number of samples	-
N_{rc}	Number of turns of Rogowski coil	-
r	Series resistance per-unit length	Ω/m
R_l	Lumped resistance of Rogowski coil	Ω
S_n	Gaussian white noise	-
t	Time	s

t_o	Time of partial discharge occurrence	s
TD_{BA}	Time difference between B and A	s
TD_{BC}	Time difference between B and C	s
v	Propagation velocity	m/s
$v_{rc}(t)$	Voltage induced in Rogowski coil	V
$v_{out}(t)$	Output voltage of Rogowski coil	V
$WF_A(.)$	Sampling window for vector A after extraction	-
$WF_B(.)$	Sampling window for vector B after extraction	-
$WF_C(.)$	Sampling window for vector C after extraction	-
$WS_A(.)$	Sampling window for vector A before extraction	-
$WS_B(.)$	Sampling window for vector B before extraction	-
$WS_C(.)$	Sampling window for vector C before extraction	-
z	Series impedance per-unit length	Ω/m
Z_{out}	Terminating impedance of Rogowski coil	Ω

List of acronyms

AC	Alternating current
CC	Covered-conductor
CCC	Cyclic cross-correlation
CT	Current transformer
DC	Direct current
DGA	Dissolved gas analysis
DSI	Discrete spectral interference
DSO	Digitizing oscilloscope
DWT	Discrete wavelet transform
EMD	Electromagnetic disturbances
EMI	Electromagnetic interference
EMTP-ATP	Electromagnetic transient program-Alternative transient program
FFT	Fast Fourier transform
FM	Frequency modulation
GCC	Generalized cross-correlation
GPS	Global positioning system
GWN	Gaussian white noise
HDPE	High density polyethylene
HPLC	High performance liquid chromatography
HV	High voltage
IEC	International electrotechnical commission
km	kilometer
kV	kilovolt
LV	Low voltage
MATLAB	Matrix laboratory
MHz	Mega hertz
MV	Medium voltage
nC	nano coulomb
PD	Partial discharge
RF	Radio frequency
RLC	Resistance inductance capacitance
SNR	Signal to noise ratio
STD	Standard deviation
TACS	Transient analysis control system

TDOA	Time difference of arrival
TNA	Transient network analyzer
VHF	Very high frequency
XLPE	Cross-linked polyethylene

1- Introduction

1.1   Background and problem statement

Electrical insulating materials are used in various forms to provide insulation for any kind of apparatus dealing with high voltage (HV) equipments. The insulating materials may be solid, liquid, gas, or even a combination of these. These materials should possess good insulating properties over a wide range of operating parameters, such as a wide temperature range and a wide frequency range, from direct current (DC) to several Mega Hertz (MHz) in the radio and high frequency ranges. These insulating materials are, for instance, the cross-linked polyethylene (XLPE) or high density polyethylene (HDPE) used in 20 kV covered-conductor (CC) lines which usually has a thickness of 2.3 mm. It is used to cover the conductor material, which is normally an aluminum alloy. CCs are insulated overhead conductors without metal sheaths. They are used to improve the reliability of the distribution of electricity, and help to make the line corridors narrow, which is particularly an advantage in built-up or forest areas. Several years usage has demonstrated the CC system to be both extremely functional and reliable. Interruptions and faults caused by snow, ice or storms have been diminished remarkably [1], [2]. The CC and its cross-sectional view are shown in Fig. 1.1 [3].

Aluminum alloy conductor   **HDPE covering**
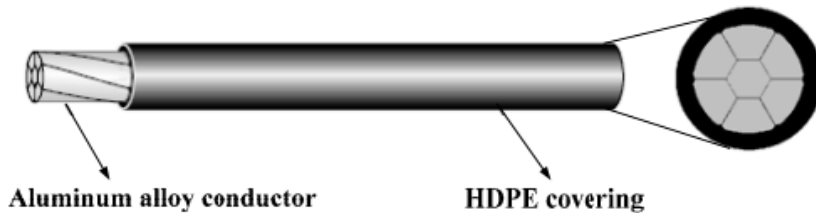
Fig. 1.1 Cross-sectional view of covered-conductor used in distribution networks [3].

CCs for overhead distribution networks or medium voltage (MV) lines have been used in Finland for more than 40 years [1], [2]. In the middle of the 1990's the use of CC was expanded to the HV level which is 110 kV. Fig.1.2 shows two CC overhead lines (MV and HV) in Tuusula, Finland. The basic idea for using CCs in Finland is to make the line more tolerant to conductor clashing and trees leaning on the conductor. These contribute a lot to space saving between the trees and conductor, and the spacing between the conductors itself [1]. Fig. 1.3 shows the condition of CC overhead lines covered with snow during the winter season.

From the statistical data on CC overhead lines installed in Finland, there are around 0.9 fault cases per year per 100 km as reported in [2]. This low value of fault cases supports the

application of CC overhead lines in the forest area as in Finland. Although CC overhead line faults occur infrequently, power failures are impossible to completely avoid.
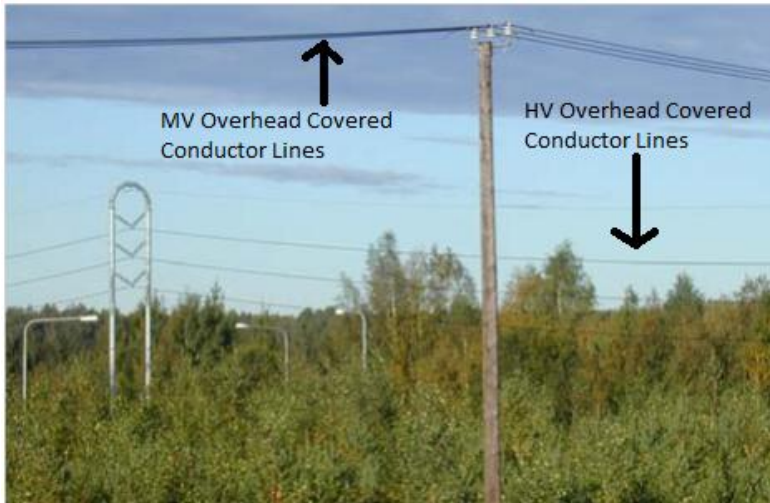
Fig. 1.2 MV and HV covered-conductor lines in Tuusula, Finland [1].

Fig. 1.3 MV covered-conductor lines covered with snow during winter in Finland [1].

CC lines being manufactured using modern extruded synthetic insulation materials will unavoidably be subjected to mechanical failures and subsequent electric breakdown [3]. In contrast to failures on bare overhead lines, CC line faults are often permanent and the faulty section of the line has to be removed. Thus, although CC line faults are rare, these failures may be severe and cause excessive power interruption to customers and large costs for the distributor. Furthermore, the mean time of failure for installed CC overhead lines based on

modern extruded synthetic insulation materials is unknown. There is, therefore, understandable anxiety over the future reliability of these power networks and a need to develop accurate monitoring systems to predict failures.

One of the major problems associated with the CC line that remains a concern is the initiation of partial discharges (PDs). This happens when an insulator is not functioning as it should be, due to structural damage or pollution on the insulator surface. The other main reason is especially after leaning of a tree on the line as shown in Fig. 1.4. A tree in contact with a CC will distort the electric field around the conductor and causes PDs after a certain period of time through chemical, thermal, and electrical mechanisms [4], [5]. The PD pulse is then propagates along the CC lines in both directions from its source. PDs can be observed and it is usually an early indicator of imminent failure of the insulator. If the PD on the CC is undetected for a certain period of time, it will lead to an outage of the distribution network connected to the CC.

Fig. 1.4 Leaning trees on covered conductor lines in Forest–Sax Line [1].

PDs are small discharges caused by strong and inhomogeneous electrical fields. The reason for such fields could be voids, bubbles, or defects in an insulating material. The detection of a PD is performed in order to ascertain the condition of the insulating material in HV elements, such as cables and CCs. Since a PD usually occurs before complete breakdown, PD monitoring provides a warning to remove the power system component from service before catastrophic failure occurs. Therefore, the area of PD measurement and diagnosis is accepted as one of the most valuable non-destructive means of assessing the quality and technical integrity of HV power apparatus and cables.

An important aspect of PD detection and localization is the possibility to reliably detect and accurately estimate the activity and location of a PD source on CC overhead lines [5]. The

detection and the ability to locate the PD on the CC line at the earliest stage possible are of great importance for maintenance purposes. Further corrective action can be prepared more precisely to prevent unpredicted outages in operation of the CC overhead distribution networks. Early detection and replacement of a damaged CC line will save a lot of unnecessary repair costs and annoying electricity cuts to paying customers [6]. These benefits have led the PD detection and location techniques to become a valuable tool for condition assessment of MV networks consisting of CC overhead lines.

Currently, there are two types of measurement techniques carried out to test if there are any faults along the CC line. They are offline and online measurements. For the offline kind, PD measurements have been carried out with special equipment, which entail interruptions in the normal operation. Due to this limitation, online PD measurements have been introduced and practiced recently [3], [5]. With the online measurement, the power line continues working as normal and no disruption of service is required. The methods currently available use very high frequency (VHF) antennas, infrared sensors, capacitive coupling and a Rogowski coil [3], [5], [9]. Sensors used for PD detection can be divided into capacitive and inductive sensors, measuring the voltage and current on the CC overhead lines, respectively. Their physical properties and limitations often decide which sensor type can be employed [10]-[12]. The choice of sensors also depends on the properties of the power system and the installation requirements. The ongoing research into online PD diagnostics has produced several devices that have been commercialized [7], [8].

In this work, a Rogowski coil is chosen as a PD sensor because of its property of having a wide bandwidth frequency which is needed for the detection of the PD due to the leaning of a tree on the CC line. It is also a non-intrusive method to detect the PD. The Rogowski coil features have a very good linearity due to a structure which has no iron core nor magnetic materials. Furthermore, its circuitry is simple and the cost is low [3], [13]-[15], [62]. In [15], the comparison of different kinds of current measuring sensors has been summarized, with the Rogowski coil shown to have more advantages in comparison to the others.

In [62], different sensor types were tested to determine the optimal sensor for on-line PD detection in HV power cables. Three different sensors characteristics which are the capacitive sensor, axial magnetic sensor and Rogowski coil sensor have been compared and summarized as shown in Table 1.1 [62]. From the Table, Rogowski coil sensor is favored in terms of sensitivity, installation feasibility and frequency response. Although in this particular work [62], the performances of the Rogowski coil for PD detection was assessed in HV power cables, it is also found suitable for use in detection of PD signal in CC overhead lines as presented in [3].

4

Table 1.1 PD sensors characteristic comparison [62]

	Capacitive sensor	Axial magnetic field sensor	Rogowski coil
Sensitivity	Low	Low	High
Universal applicability	Wide	Limited to helical structure of shield cable	Wide
Frequency response	High (up to 200-300 MHz)	Low (up to few MHz)	High (up to 40 MHz)
Time resolution	A few ns	Tens of ns	A few ns
Installation difficulty	Easy	Easy	Easy

The PD in CC overhead lines will induce high frequency current pulses in the conductor, propagated at both sides along the CC lines. A Rogowski coils located at certain distance will pick up the high frequency current pulses associated with the PD.

As the Rogowski coil is capable of extracting the PD signals, their location can be found using traveling wave fault locator principles [3], [21]. The single-end traveling wave locator function is not that suitable to locate the distance of the PD source. However, the multi-end traveling wave locator with two-end synchronized measuring method gives better accuracy for PD location, but it needs information about the wave propagation velocity over the feeder, which is a function of the feeder parameters and tower configuration.

In [20], single-end and double-end online PD detection and location of underground power cables have been introduced, while single-end PD detection and location on MV CC overhead lines has been explained in [5]. Both of these works have shown good results in PD detection, but produce an error and inconsistency in determining the PD source location. This is due to their dependency on the characteristic of propagation velocity for both CC overhead and underground cables. The propagation velocity is relatively affected by physical parameters such as temperature and the level of height of the CC line with respect to the ground surface [22], [23]. In addition, propagation velocity is frequency-dependent and it increases by increasing the frequency of the propagated signals.

PD measurement with alternating current (AC) source supplied on the line is always affected by electromagnetic disturbances (EMD) and noise. A different PD measurement location will be affected by different types of noise. The noise can be classified as follows; discrete spectral interference (DSI) caused by radio broadcast signal, periodical pulse shaped disturbances from power electronic equipments, stochastic pulse shaped disturbance due to lightning or switching operations, and white noise which is broadband interference caused by the measuring instrument itself [5]. Using a PD sensor with a suitable frequency bandwidth,

then followed by post processing for denoising, is the best way to eliminate the noise problem in PD measuring signals.

Many different noise reduction techniques have been proposed including filtering, spectral analysis and wavelet analyses [16]-[18]. The closed-loop technique refers to a situation where a reference signal is used to measure the noise, for example, using an external antenna [19]. The use of advanced signal processing has been extensively applied, especially since the cost and time of processing power has decreased.

An estimation of PD source location based on first arrival time has been discussed in [24]-[26]. Noise and interferences are the main problems to accurately stamp first arrival times using this method. Meanwhile, an energy-based correlation method for locating the PD in transformer winding has been discussed in [27], [28]. This technique is based on the correlation of radio frequency (RF) signals measured by a few antennas that act as PD sensors concentrated on the transformer device to detect and locate PD sources. It is, however, hard to apply to widely distributed underground cables or CC overhead lines.

1.2 Research objective

This investigation is driven by the motivation to develop a function for locating the PD source in order to localize such faults. The main objective of this research is to develop reliable and efficient techniques for online monitoring of PDs due to leaning trees on CC overhead distribution lines. Detection and localization of PD activity in the overhead power network is an application which can benefit from the features of the traveling wave along the CC line. This study will provide protection improvements against the breakdown in the distribution network due to leaning trees, particularly in Finnish electricity networks.

The expected result of this project is an increased understanding of the difficulties and remedies in the measurement, detection and localization of the PD source in power networks. This will reduce the gap between the theoretical models, the signal processing algorithms, the laboratory scale prototypes and the low cost and highly reliable monitoring systems that are required by the industry. Eventually, it is hoped that this will lead to improved detection and localization reliability. With the increasing range of using CC overhead lines in the distribution power network, especially in Finland, the potential impact of this application is great. It is believed that the signal analysis approach and PD locator algorithm developed in this work will lead to enhanced methods for the detection and localization of insulation degradation in medium and HV power networks.

1.3 Thesis contribution

Based on single-end measurement, a three-phase PD monitoring system on CC overhead lines in distribution systems network has been modeled in EMTP-ATP. A Clark CC line is used as the CC overhead lines model. The comparative study of an online three-phase PD monitoring system using Clark and JMarti CC line models has been performed.

Using the frequency-dependent CC line model (JMarti), a new model of online three-phase PD monitoring system is developed for double-end measurement. The propagation of the PD pulse from the source location towards its both-end feeders is measured. The localization process is done using a locator function which is based on the stamping time of arrival (TOA) and the propagation velocity for the measured signals.

An experimental analysis has been performed to evaluate the PD measurement system performance for PD location on CC overhead lines. A multi-end measuring method with three measuring points is introduced as a technique to locate the PD source point on the line. The tests have been carried out under different measurement conditions, such as offline and online PD measuring systems. For the offline measurements, the pulse calibrator is used to inject the PD source to the CC overhead lines. Meanwhile for the online measurements, two methods were used to generate live PD signals with an energized CC overhead line via a power transformer. The methods are firstly, by twisting a coil around the CC and secondly, by leaning a tree againts the CC line. The chirp detector is used as a signal processing tool to extract the high frequency signals in order to determine the TOA of the signals at each of the measuring sensors. The locator function algorithm for multi-end measurement is developed. The localization of PD source on CC overhead lines is done without the need to consider the propagation velocity of the signals.

Next, a multi-end correlation technique for the PD source locator is employed in order to eliminate the problem encountered in previous online PD detection and location. This new proposed technique is a combination of three different stages of signal analysis, which are, firstly, denoising by applying discrete wavelet transform (DWT), secondly, extracting the PD features using the absolute or windowed-standard deviation (STD) and thirdly, by locating the PD point by correlating the measured signals of three Rogowski coils. Besides the ability to locate the PD source without the need to know the propagation velocity of the signals, the faulty section of the line also can be identified based on the degrees of correlation. The algorithm outline and its derivative are discussed in chapters 5 and 6. The algorithm is evaluated using Electromagnetic transient program-Alternative transient program (EMTP-ATP) simulated PD cases and verified using experimental measurements results. The multi-end measured signals are considered as synchronized signals.

For unsynchronized measured signals, the locator function algorithm is developed based on the two-end correlation of the signals. The ratio of correlation is then plotted against its ratio of distance. The hyperbolic sine equation is found as the best function correlated with this plotted curve. Referring to the plotted graph, the PD source on the CC overhead lines can be localized. This method helps to solve the problem of the unsynchronized measured signals between two measuring points.

There are possibilities that faults on CC overhead lines occur for reasons other than PD, for instance, the arcing fault which has the characteristics of intermittent faults. As a precautionary step, the capability of the Rogowski coil to work on capturing different fault transients traveled from source location is evaluated. This evaluation is useful in order to make it possible to implement a fault locator technique using the same technique used to locate the PD. Different values of fault resistances and inception angles due to earth and phase faults are tested on the MV distribution networks in order to investigate the performance of the Rogowski coil.

1.4   Organization of thesis

The thesis is organized into the following chapters:

Chapter 2 presents the basic concept of the PD phenomenon in HV equipment. An overview of the Rogowski coil as a PD sensor used in this work is also presented. The physical configuration and equivalent circuits of the Rogowski coils are shown.

Chapter 3 presents the models of an online three phase PD monitoring system on CC overhead lines distribution networks concerning PD due to a leaning tree on the CC line. The models are based on single-end measurement. The comparison performance of the online PD monitoring system which has been developed using two different types of CC line, i.e., Clark and JMarti models, is presented.

Chapter 4 presents an investigation for the possibilities of implementing an online three-phase PD monitoring system using a Rogowski coil sensor to detect PD caused by a leaning tree on CC overhead distribution lines at both-ends.

Chapter 5 presents an evaluation of the measurement systems performance for locating PD in energized CC overhead lines. The measurement is done using a multi-end measuring method.

Chapter 6 presents a multi-end correlation technique for locating PD sources on CC overhead lines. This technique overcomes the difficulty of identifying the faulty section of the line for multi-end measurement from the previous technique as discussed in Chapter 5.

Chapter 7 presents a correlation of the unsynchronized two-end windows technique for locating the PD source on CC overhead lines.

Chapter 8 presents an evaluation of Rogowski coil performance with different fault scenarios such as different fault types, different fault resistances and different inception angles. Furthermore, the fault due to leaning trees and the arcing fault which has the characteristics of intermittent faults are considered in the study.

2- Basic concepts of partial discharge and Rogowski coil

2.1   Classification of partial discharge

According to the International Electro-technical Commission (IEC) standard 60270, partial discharge (PD) is a localized electrical discharge that incompletely bridges the insulation between conductors [29]. Generally, local electrical stress concentrations in insulation or on the surface of insulation results in PD. The PD is in the form of various voltage impulses and current impulses, with duration of less than 1 second [29]. The activities of PD which usually have been observed in high voltage (HV) equipment, for example in on HV insulation system, causes a movement of charge. The charge movement tends to reduce the potential between the electrodes until more charge arrives from the supply.

The forms of insulators are mostly impure and due to this impurity, bubbles (void) are created within the insulating material. As a result, the insulation region is weakened and it causes PD to appear. The phenomena can be explained simply: the dielectric constant of the void is less compared to its surroundings which consequently causes insulation failure in HV equipment. PDs usually occur at the void, subsequently creating bad conductor profiles in the devices. As time passes by, the discharge causes a significant degradation to the insulator although such discharges have less magnitude. Failure will then occur in the insulation system due to the occurrence of discharge.

PD detection and measurement is therefore important and necessary to foresee the insulation life in HV power equipment. Three types of PD phenomena are as shown in Fig. 2.1(a-d) [29]:

(a)   *Corona discharge*: Non-uniformity of electric field on sharp edges of the conductor results in corona discharge. For the aforementioned type of discharge, the insulation supplied is either gas, air or liquid [29]. The discharge appears for a long duration around the bare conductor. The insulation systems are not directly affected by them, contrary to system-like internal and surface discharge. Only by the indirect action of ozone formed by corona deteriorates insulating materials used.

(b)   *Surface discharge*: Surface discharge usually takes place outside the power equipment or on interfaces of dielectric material. This may occur in bushing, underground cable, overhead lines terminals or any point on insulator surface between electrodes. Various factors affect the occurrence of such discharge, such as permittivity of the dielectric material used, voltage

distribution between the conductors and the properties of the insulating medium where PD occurs. PD produced due to leaning trees on CC lines is known as surface discharges.

(c)   *Internal discharge*: Internal discharge occurs inside a system. The discharge which happens in the void belongs to such a PD type. The properties of the insulating material which is used in HV power equipment are given by the PD measurement system. The PD measurements are executed using different methods. The generation and dissipation of energy related with electrical discharge is the principle behind the measurement of PD, i.e. generation of electromagnetic waves, dissipation of heat energy, light and formation of noise, etc. A number of types of discharge, such as cavity discharge and treeing channel are included among the internal discharge PD phenomena [29], [30].

> (i)   *Treeing channel*: high intensity fields produced at the sharp edges in an insulating material which consequently deteriorate the insulating material. As a result, continuous PD, called a treeing channel is produced.

> (ii)   *Cavity discharge*: Usually happens in solid or liquid insulating materials since the cavities are generally formed in those materials. The cavity is generally filled with gas or air. The discharges take place when the gas in the cavity is over stressed.
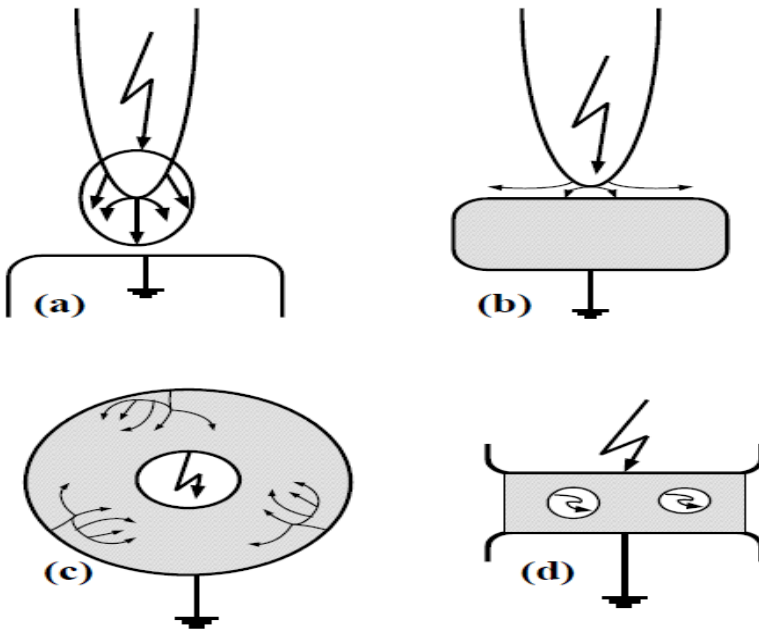
Fig. 2.1 Various types of PD in the HV insulating material. (a) Corona or gas discharges, (b) surface discharges, (c) treeing channel and (d) cavity discharge [9].

2.2   PD effect on insulating system

The main reason for the degradation and electrical breakdown of insulating material is the appearance of PD. The repetition of discharge is the reason for degradation of the insulating material, both mechanically and chemically. The effect of discharge on the insulation system of HV equipment is severe. Chemical changes in the dielectric result in the rising conductivity of the insulating material. Dielectrics are classified into several types, i.e. inorganic dielectrics and organic dielectrics. Generally the inorganic dielectrics such as porcelain, glass and mica have higher immunity. Polymer dielectrics belong to the class of organic dielectrics.

In general, PD generates energy in the heat form. The main reason for degradation of the insulation is the heat energy. This effect is known as the thermal effect on insulating materials used. For HV power equipment, the PD activities make it possible to know the deterioration of the insulation. Time to time monitoring of PD activity by the power engineer or power manager at the time of manufacturing as well as during operation should be performed. Careful design and manufacturing, and selection of proper insulating material can help to prevent the PD. In other words, PDs prevention and detection are essential for a secure, long-period of operation of HV equipment.

2.3   PD detection methods

There are various methods for PD measurement based on both electrical and non-electrical phenomena. The most well-known methods for measurement of PDs are [38]-[44]:

(a)   *Optical detection method*: In this method, light is dissipated in the form of ionization excitation process during the appearance of the discharge. The emission of the light is dependent on the insulating medium used and other parameters like temperature and pressure. An insulating material which is transparent type is usable for this detection method. Difficulties arise in cases of HV transformer implementation due to the opaque nature of mineral oil.

(b)   *Acoustic detection method*: Acoustic sensors are placed outside the HV equipment for detection of PDs for this kind of method [31], [32]. The method is efficient to perceive and encode the acoustic signal generated during a PD event. Acoustic methods have many advantages over the other methods, for example it is unaffected by electromagnetic disturbances (EMD), which can reduce the sensitivity of electrical methods [32]. However, due to the nature of acoustic wave propagation, it is complicated to be applied in a non-homogeneous device such as a HV transformer.

(c)   *Chemical detection method*: In the chemical method, PDs are detected by observing the chemical changes in the composition of insulating material used in HV power equipment. In this method, PD diagnosis extensively uses dissolve gas analysis (DGA) and high performance liquid chromatography (HPLC). DGA gives the PD information in terms of the volume of gas produced and the products, such as glucose and degraded forms of glucose produced due to degradation of the insulation, are measured by HPLC [31], [32]. The chemical detection method does not give the information about PD characteristics and the location of PDs, which are the drawbacks in this detection technique. This happens because of the insolubility properties of glucose in mineral oil and the degraded form of it, is unstable in nature. Furthermore, complicated instrumentation and its analysis process are required during online monitoring PD activity.

(d)   *Electrical detection method*: The electrical detection method is one of the most popular methods in HV power equipment for PD measurement. It focuses on the appearance of the current and voltage pulse generated by the current streamer in the void as well as impurities [31]. The pulses are of less than one second duration and the variation of frequency components are in the range of kHz to MHz. The shape of the pulse and occurrence of phase location within the alternating current (AC) cycle gives the information about PD type and information about insulation failure. A time domain recording device is used to observe PD impulses in this detection method. Various signal processing methods are applicable for identification and location of the PD signal. This method is also applicable for online electrical PD detection. Both broadband and narrowband electrical noises are found during the operation of HV power equipment. It is not easy to separate these noises and PDs. The impulses which are received in this detection method depend on the location of the PD source. This method has some drawbacks but has wide application in power systems which helps the power engineer and technician by giving necessary and important information regarding the characteristics, appearance of different PD types as well as about the occurrence of insulation failure in HV power equipment (for instance, transformer, cable, overhead CC, etc). In this work, the electrical detection method has been used in a simulated study and experimental set-up to measure and localize PD in CC overhead lines in a distribution system.

2.4   Factors influencing the dielectric strength of insulating material

There are some essentials requirements for the insulating materials used for HV equipment [29]. The first thing that should be taken into account is that the insulation resistance and the dielectric strength of the material should be high. The insulating material should also

have good mechanical properties. In addition, the materials should be unaffected by any other chemicals. In term of high dielectric strength, there are some factors, or conditions, which affect the dielectric strength of the materials. These main factors are temperature, spacing between the electrodes and the presence of impurity.

The function of the insulation depends on the operating temperature. When the temperature gets higher, so does the degree of degradation and this will lower the life of the insulating material. Thus, temperature has an undesirable effect on the dielectric strength of the insulating material and depends upon the types of materials used in the HV power equipment. The temperature at which the power equipment operates is responsible for degradation of insulating material used. The characteristics of the strength of the material used and the temperature at which equipment operates is, therefore, inversely proportional.

The breakdown strength of the insulation depends upon its width, electrode shape and the material used for insulation. The size and shape of the electrodes are responsible for determining the volume of medium subjected to high electrical stress. The impurity content particles increase with increases in volumes. A large content of impurity particles will lower the breakdown voltage of the space between electrodes and the presence of impurity has a direct effect on the insulating material which is used on the power equipment. The strength of the dielectric liquid used in HV equipment decreases to 70% as a consequence of impurity content such as metal particles. Impurity includes solid particles: carbon, wax, cellulose fiber and acids. Moreover impurity content creates imperfections on the insulation region.

The dielectric strength of insulating material which is used in power equipment is also affected by other factors, i.e. the thickness of the specimen and the level of humidity. The thickness of the specimen is directly proportional to the dielectric strength of the insulating material, where as a surface condition like humidity is inversely proportional to the dielectric strength of the material.

When a solid or a liquid electrical insulation system is under HV stress, a small portion of the system might go through a process of dielectric breakdown. Such a process is called PD. The PDs within an insulation system may or may not reveal any visible discharges as the discharge events tend to have a more sporadic character. The effects of PD within CC, cables and other HV equipment can lead to complete malfunction and thus should not be treated lightly. PD can potentially cause serious problems amongst HV equipment. The PD phenomenon usually commences within the voids, cracks, in bubbles within liquid dielectrics or inclusion within the solid insulating medium. In addition, PDs also occur at the boundaries between the different insulating materials, contamination, poor conductor profiles and floating metal-work in the HV equipment [33]-[36]. The electrical PD detection methods are based on the appearance of the PD current or voltage pulse across the test object or large HV power apparatus. In this work, the CC line is the object for the PD test and the measuring sensor

employed is the Rogowski coil.

2.5   Rogowski coil as a PD sensor

Since 1912, the Rogowski coil has been used to measure the magnetic fields and has been extensively used for measuring fast, high-frequency transient currents in the range of mega-amperes rather than for measurements in power systems [6], [64], [65]. The Rogowski coils have become more suitable for those applications since the microprocessor-based protection relays and measurement devices have been improved and have generally been used [9]. Due to their advantages of low insertion loss and reduced size as compared to an equivalent current transformer (CT), Rogowski coils have become an increasingly popular method of measuring current within power electronics equipment [14]. They are the favored method of high frequency current measurements having more suitable features than CTs and other iron-cored devices. The inherent linearity and wide dynamic range features of the Rogowski coils make them useful for transient measurements. The geometry and construction of the Rogowski coil, and its corresponding simulated circuit are shown in Fig. 2.2 and Fig. 2.3. In Fig. 2.2, d_1, d_2, and d_{rc} are the inner, outer, and transducer diameters of the Rogowski coil, respectively.
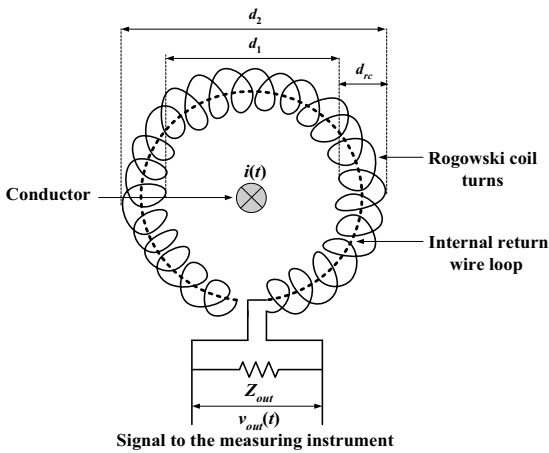
Fig. 2.2 Geometry and construction of the Rogowski coil [3].
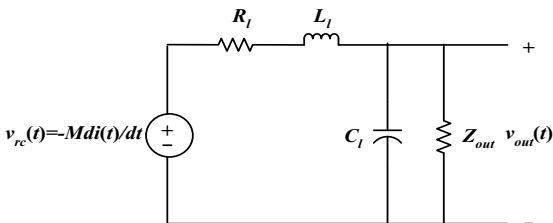
Fig. 2.3 The Rogowski coil corresponding circuit (lumped parameters model) [3].

The working principle of the Rogowski coil has been explained in [3], where the Rogowski coil operates on the basic principle of Faraday's law. The air-cored coil is placed around the conductor and the current pulses produced by PDs are to be measured. These pulses produce a magnetic field and the rate of change in current induces a voltage in the coil given as [3]:

$$v_{rc}(t) = -M \frac{di(t)}{dt} \tag{2.1}$$

$v_{rc}(t)$ is the voltage induced in the coil, $i(t)$ is the current flowing in the conductor, and M is the the mutual inductance between the main current and the coil. Meanwhile, Z_{out} is the terminating impedance of the Rogowski coil, where R_l, L_l, and C_l are the lumped resistance, inductance, and capacitance of the coil, respectively [3], [37].

By assuming that the Rogowski coil has negligible impedance, the approximate measured voltage at the output terminal becomes [3]:

$$v_{out}(t) \approx v_{rc}(t) \approx -M \frac{di(t)}{dt} \tag{2.2}$$

So the current following through the conductor is [3]:

$$i(t) = -\frac{1}{M} \int v_{out}(t) dt \tag{2.3}$$

The Rogowski coil sensor has a very wide frequency response and there is no conductive coupling between the coil sensors and the test object. Furthermore, the coil installation does not require disconnection of the grounding leads of the test objects and therefore becomes a non-intrusive sensor which is a very important aspect for on-site, online monitoring. It can posses a high signal to noise ratio (SNR) with a broad frequency bandwidth. Since there is no saturation due to the air-cored coil, it is not damaged by over current. Due to the absence of magnetic materials, it also has very good linearity. The Rogowski coil based PD measurement system is a low cost solution and can easily be implemented on-site due to its light weight [3]. These advantages are important for online PD measurements. It is for all these reasons that Rogowski coils are preferred over conventional PD sensors to take measurements for detecting leaning trees on CC overhead distribution lines.

3- Single-end measurement-based online three-phase PD monitoring system for CC overhead lines

An Electromagnetic transient program-Alternative transient program (EMTP-ATP) simulation environment is used to evaluate the performance of an online three-phase partial discharge (PD) monitoring system for covered-conductor (CC) overhead distribution lines. The model is developed using an EMTP-ATP environment, brief details of the set-up are given below.

3.1 Electromagnetic transient program-Alternative transient program (EMTP-ATP)

The EMTP is a computer program for simulating electromagnetic, electromechanical, and control system transients on multiphase electric power systems. It was first developed as a digital computer counterpart to the analogue transient network analyzer (TNA). Many other capabilities have been added to the EMTP over the years and it has become a standard program. One of the EMTP's major advantages is its flexibility for accurate modeling and experienced users can apply the program to a wide variety of studies. The cost and space considerations of analogue simulation give preference to the EMTP program. For example, it is not possible with scaled down analogue models to simulate the distributed nature of transmission line parameters [45]-[47].

The ATP was started as a new program updated from the EMTP, but with different commercialization. Therefore, the ATP manual is just a complete set of rules for EMTP inputs and outputs. However, there are slight differences such as circuit-breaker models which are embedded in the EMTP but they are not set in the ATP. To overcome this drawback, the ATP includes transient analysis control system (TACS) controlled resistance that can provide breaker arc interaction. For more flexible of a programming language, MODELS has been recently introduced to interact with the source code of the ATP.

ATPDraw is a graphical and mouse-driven preprocessor to the ATP version of the EMTP program on the Microsoft-Windows platform where the user can construct an electrical circuit using the mouse and by selecting components from menus [50], [51]. Then, an ATP input file is generated according to its codes. Most of the standard components of the ATP, as well as TACS and MODELS are supported in ATPDraw. Line or cable modeling is also included where the user specifies the geometry and material data and has an option to view the cross-section graphically and to verify the model in the frequency domain.

The EMTP-ATP contains various models to represent CC overhead distribution lines. These models can account for tower geometry, bundling and earth resistivity. The user can select any of these models for overhead CC lines such as lumped or distributed parameters, frequency independent or frequency-dependent models. The choice of the CC overhead line model is dependent on a number of factors, such as the length of the lines, the nature of the simulation (fault, surges, dynamic stability, etc), and the fidelity of the results. The following are the various options for CC overhead line models in the EMTP-ATP [51], [52]:

1. *Bergeron/Clark model*: Distributed parameter model including the traveling wave phenomena. However, it represents the line resistances at both ends as a lumped element.

2. *PI-model*: Nominal PI-equivalent model with lumped parameters, which is suitable for the simulation of short lines.

3. *Noda-model*: Frequency-dependent model. This algorithm models the frequency-dependent transmission lines and cables directly in the phase domain.

4. *Semlyen-model*: Frequency-dependent simple fitted model. The Semlyen model was one of the first frequency-dependent line models. It may, however give inaccurate or unstable solutions at high frequencies.

5. *JMarti-model*: Frequency-dependent model with constant transformation matrix that is suitable for simulating the traveling wave phenomena in long transmission lines.

3.2   Overview of experimental set-up for online single-phase PD monitoring system

For single-end measurement, an online single-phase PD monitoring system designed to measure a PD due to a leaning tree on CC overhead lines has already been simulated and experimentally verified by a previous researcher as presented in [3]. The corresponding model of the PD monitoring system (including CC line and Rogowski coil) is shown in Fig. 3.1, where three main parts of the model are a pulse calibrator as a PD source, a Rogowski coil as a PD sensor, and the CC as the medium for distribution lines. The parameters model is listed in Table 3.1. The online single-phase PD monitoring system was modeled in an EMTP-ATP simulation environment.

In [3], two sets of PD measurements have already been performed on the CC line. Here, the summary of the work is explained. First measurement was done to calibrate the PD monitoring system where a pulse of known magnitude is injected into the conductor by a pulse calibrator, and the Rogowski coil measurements are taken at points P_1 and P_2, as shown in Fig. 3.2 (a). In the second measurement, the conductor is energized with 20 kV distribution voltages and knife traces are made on the conductor insulation. A pine tree is leaned against the

conductor at point P_T on the conductor where the knife traces are made and the Rogowski coil measurements are taken at point P_2 as shown in Figs. 3.2 (b), 3.3 and 3.4, respectively.
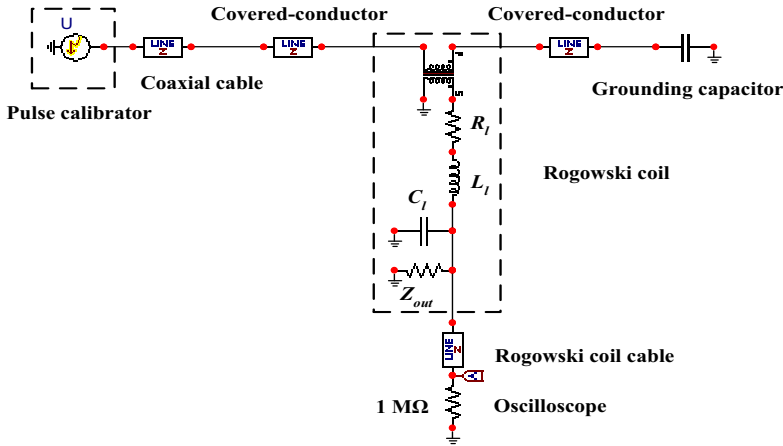
Fig. 3.1 ATPDraw circuit for online single-phase PD monitoring system [3].

Table 3.1 Parameters model for online single-phase PD monitoring system [3]

Model parameters	Measured or used values
Resistance, R_l	0.11 Ω
Inductance, L_l	0.6 μH
Capacitance, C_l	50.3 pF
Terminating impedance, Z_{out}	2 kΩ
Impedance of Rogowski coil cable	50 Ω
Impedance of CC line	350 Ω
Grounding capacitor	500 pF
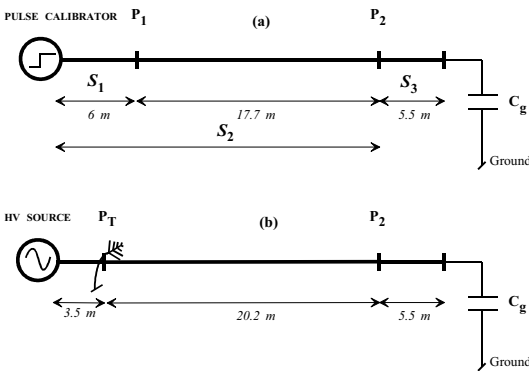
Fig. 3.2 Single-line diagram for online PD measuring system with: (a) pulse calibrator, (b) leaning tree with the line is energized with a 20 kV supply [3].

19

Fig. 3.3 A pine tree leaning on the CC line [3].

Fig. 3.4 Knife traces are made and a pine tree is leaned on the conductor insulation [3].

From the simulated study and experimental measurements in [3] and [5] as shown in Fig. 3.2, it was summarized that the PD produced due to the leaning of a single tree is about equivalent to 3 nC. However an average value of a 5 nC pulse calibrator is used for the simulated cases as a PD source in order to make the real analysis of a single pine tree leaning on the CC line. The amplitude of the PD signal captured by the Rogowski coil due to the leaning of a pine tree on a CC line at a distance of 3.5 km is less than 1 mV. There are further two important points which have been found from the measurements and simulations above. First, the PD signals are highly attenuated while propagating along the CC line. The second

point is that the PD signals measured at different locations will have different frequency bands which are in the range of MHz [3].

3.3 Comparative study of online three-phase PD monitoring systems for CC overhead lines

In this work, which is a continuation or extended model to the online single phase PD monitoring system in [3], a three-phase PD monitoring system for CC overhead distribution lines is developed based on single-end measurement. It would be interesting to analyze the PD measurements for practical three-phase CC lines that are normally mounted at a height of more than 8 m. For this purpose, the CC line characteristics for a real situation at a height of 8 m above ground level can be calculated from the theoretical model, and are used in simulation with the parameters of: resistance, 0.54 Ω/m, propagation velocity 288 x10^6 m/s, and characteristic impedance, 475 Ω [53], [99]. The simulated models for the online three-phase PD monitoring system are shown in Figs. 3.5 and 3.10. These models have been developed using two different types of CC overhead lines, which are, the Clark and JMarti models. The model includes the Rogowski coil as PD sensor, the three-phase CC overhead lines and the capacitance as terminating impedance at the end of CC lines. The pulse calibrator is used to produce a simulated PD signal similar to the PD pulse which results from a leaning tree on CC overhead lines. In [3], the PD pulse produced due to a leaning pine tree on a CC line has already been calculated, and is simulated in EMTP-ATP (see Fig. 3.6). The PD signal will travel towards the end of CC lines. The Rogowski coils located at a certain distance will measure the traveled PD signals. The Rogowski coil parameters for simulations are the same as what have been used in the modeling of the single-phase PD monitoring system [3]. However, the sensors are located on each phase which are labeled as RC_A, RC_B, and RC_C.

The present model is investigated under various PD source conditions. The performance comparisons of the online PD monitoring system modeling are evaluated. Then the localization of the PD source is done by using a time of arrival (TOA) method for a single-end measurement. The best model for CC overhead lines is evaluated, and then used for the next following work.

3.3.1 PD monitoring system using Clark model as CC line

In the simulations, four scenarios which produce PD are investigated. The scenarios are:

  i. A tree is leaning on phase A (the pulse calibrator is injected on phase A)

  ii. A tree is leaning on phases A and B (the pulse calibrator is injected on phase A and B)

  iii. A tree is leaning on each phase A, B, and C (the pulse calibrator is injected on phases A, B, and C)

  iv. Two trees are leaning on phase A (the pulse calibrator with magnitude twice as much as the first three scenarios is injected on phase A).

The PD measurements are taken at a distance of 3.5 km from the leaning trees on the CC lines. This distance is used to avoid the interference of any signal reflections coming from the termination of the CC line into the actual PD measurements [55].
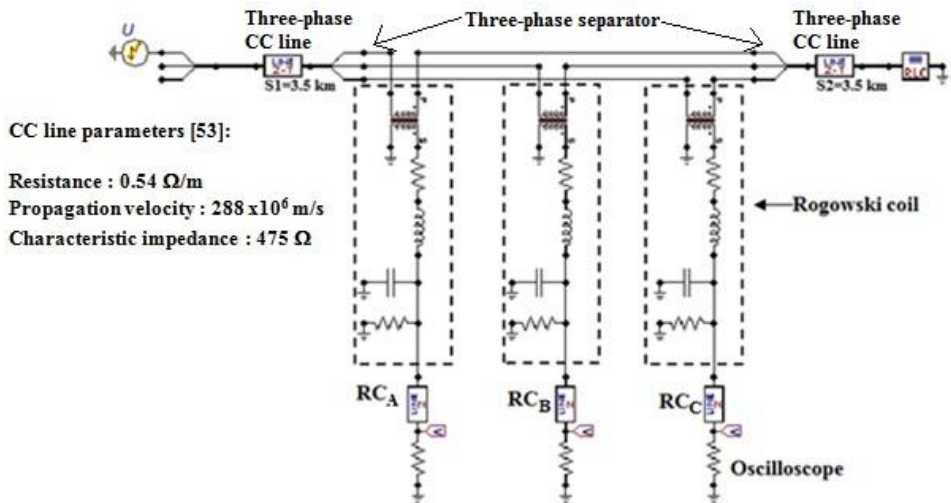
Fig. 3.5 ATPDraw circuit for online three-phase PD monitoring system for CC lines using Clark model [56].

  The PD monitoring system for CC line using Clark model is done for the three various scenarios (cases i, ii, and iii). The simulation results are shown in Figs. 3.7, 3.8, and 3.9, respectively. For case (i), the PD pulse captured by the Rogowski coil at phase A initiates at $t = 12.16$ μs as shown in Fig. 3.7 (a). The value of propagation velocity v used in simulations is 288×10^6 m/s. Therefore, the distance traveled by the signal until it reaches the point of insertion of the Rogowski coil is $s = vt = 3.502$ km, which is in good agreement with the value used in simulation (3.5 km). This reveals that the simulated PD monitoring system can be used

to detect the PDs resulting from a leaning tree as well as localizing the leaning tree on the CC lines.

The signal at the PD sensor at phase A is stronger due to the leaning of a tree on the same phase. However, the signals captured at phases B and C are very weak as shown in Fig. 3.7(b), because no trees are leaning on these phases. There is a small amount of PD signals due to the coupling capacitances of these phases.

Similar results are also obtained for case (ii) where the PD sensor mounted at phase C could not detect the leaning tree on phases A and B as shown in Fig. 3.8. In case (iii), all PD sensors have almost similar measurement signals which result from the leaning of a tree on each phase as shown in Fig. 3.9. It is worth mentioning that the quantity of PD magnitude detected by PD sensors reduces when a tree falls on more than one phase, i.e. PD magnitude is less when a tree is leaning on phases A and B, and even lesser when a tree is leaning on all phases. The quantity of PD magnitude increases linearly if the number of leaning trees on the same phase increases as given in case (iv).
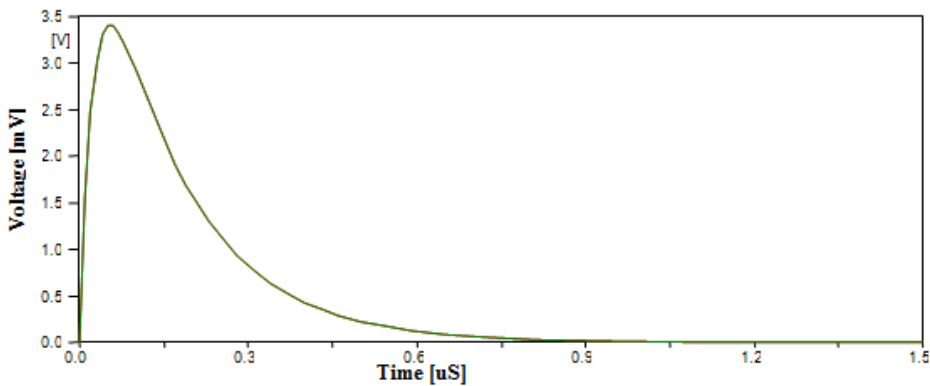
Fig. 3.6 Simulated 5 nC calibrator pulses as PD input voltage.

(a)

(b)

Fig. 3.7 Current flowing in CC line and Rogowski coil PD measurements (voltage signals) resulting from the leaning of a tree on phase A, (a) measurements at phase A, (b) measurements at phases B and C.

(a)

(b)

Fig. 3.8 Current flowing in CC line and Rogowski coil PD measurements (voltage signals) resulting from the leaning of a tree on phase A, and B, (a) measurements at phase A and B, (b) measurements at phase C.
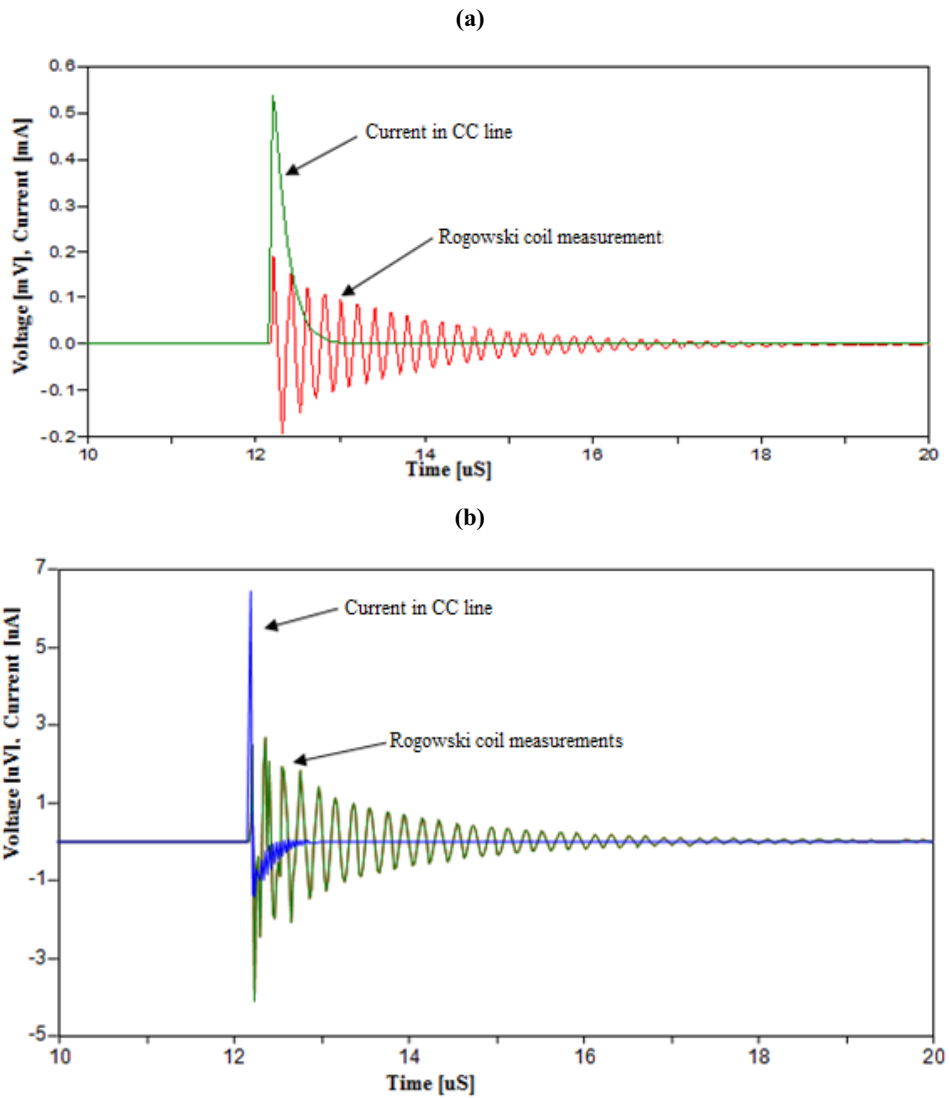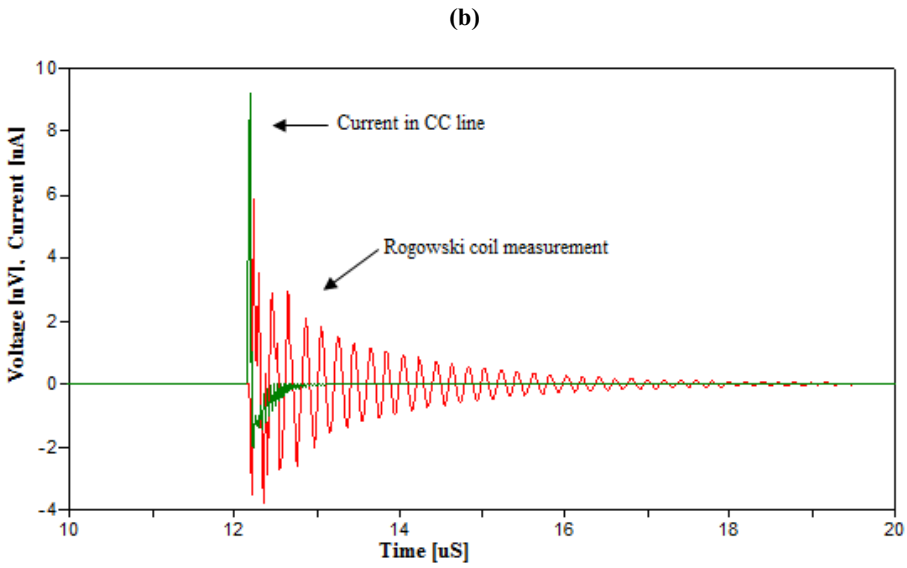
Fig. 3.9 Current flowing in CC line and Rogowski coil PD measurements (voltage signals) resulting from the leaning of a tree on phase A, B, and C.

3.3.2 PD monitoring system using JMarti model as CC line

It is interesting to model and analyze the online three-phase PD monitoring system for CC overhead distribution lines using the frequency-dependent JMarti line model. This model is more practical compared to the Clark line model. The main limitation of the Clark model is the assumption of considering the parameters constant with respect to the frequency variation. Variations of line parameters such as R, L and C as a function of frequency are simply ignored when using the Clark model of line. In order to address this deficiency, a frequency-dependent line model was developed by J. Marti [57]. In addition, the JMarti (frequency-dependent) line model shows a good correlation with actual line responses, being efficient and accurate for most simulation cases [58].

The PD monitoring system which uses the JMarti model for CC line is shown in Fig. 3.10(a), and the CC lines which consider the medium voltage (MV) feeder configuration are given in the Fig. 3.10(b). In order to overcome the numerical instability during ATP execution, a separation between the power network and the Rogowski coil is carried out. This separation is performed by exporting the measured switch current into the TACS field using sensors type 91. Then, a transfer function of unity is used in order to overcome the looping issue. The output of the transfer function is considered to be able to control the value of the TACS controlled current source. This current source is used as an input to saturable the current transformer (CT) when the secondary side is connected by the Rogowski coil cable to the oscilloscope. Simulation results for the aforementioned various scenarios explained in 3.3.1 are shown in Figs. 3.11, 3.12, and 3.13, respectively.
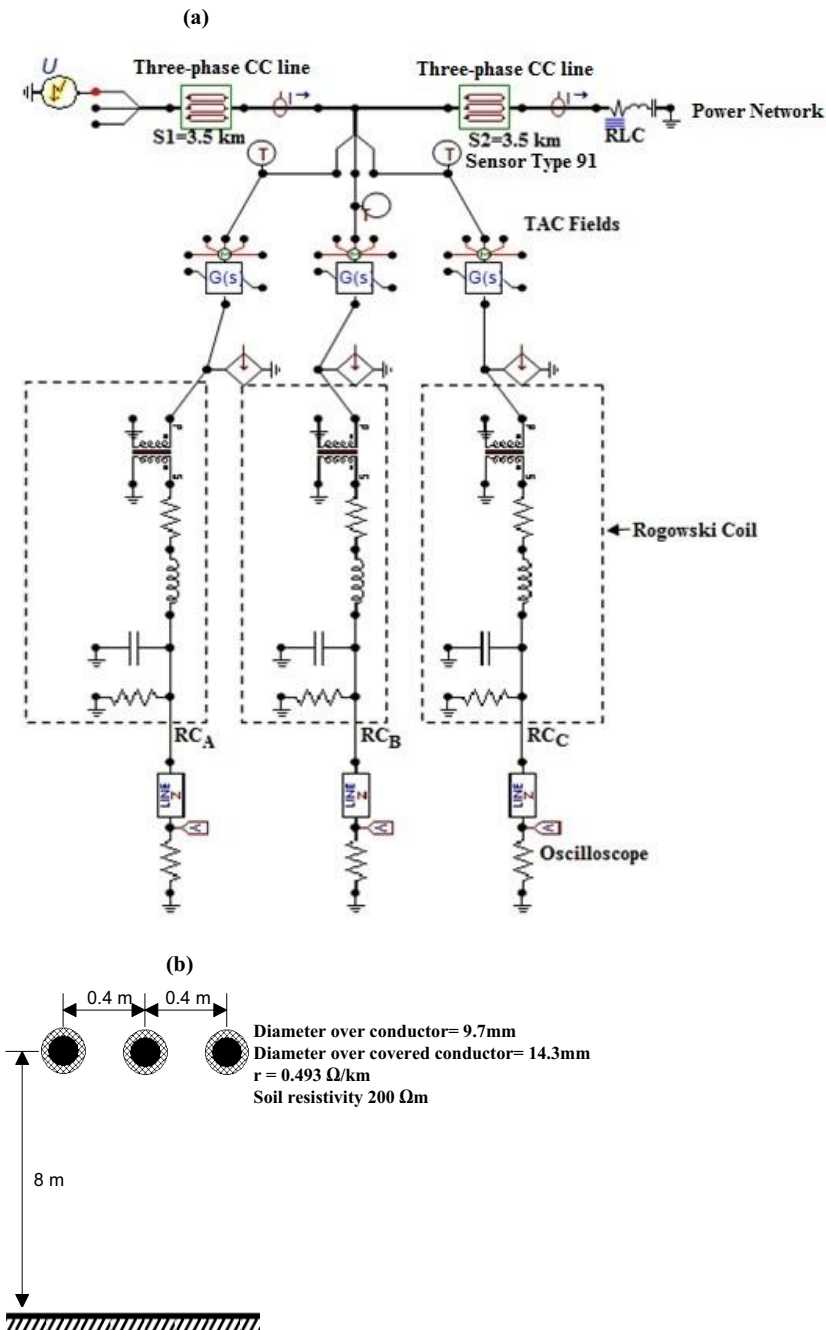
Fig. 3.10   (a) ATPDraw circuit for online three-phase PD monitoring system for CC lines using the JMarti model [60], (b) the MV feeder configuration [63].

The PD pulses for both types of CC lines models are almost similar in time response, but have different magnitudes measured by the Rogowski coil. Two pulses which can be seen in the JMarti simulations are due to the reflection effect from the CC line. A different impedance value, z for both types of CC lines, may cause these results. The impedance z of the CC line for the Clark model is manually determined [59]. Whereas for the JMarti CC line model, the impedance z is automatically determined by the system. For all cases, the PD pulses captured by the Rogowski coil at each faulty phase where the tree is leaning initiate at $t = 12.18$ μs (Clark line model) and 12.15 μs (JMarti line model). The value of propagation velocity v used in simulations is 286.69 x 10^6 m/s for the JMarti line model. Therefore, the distance traveled by the PD signal until it reaches the point of insertion of the Rogowski coil is, $s = vt = 3.483$ km, which is almost accurate with the distance used in simulations (3.5 km). The result shows that the simulated PD monitoring system can be used to detect the PDs which result from a leaning tree as well as localizing the tree on the CC lines.

One of the major advantages of using the JMarti model is that the faulty phase where the tree is leaning can be recognized on the basis of the polarities of the PD pulses obtained from the Rogowski coil. The positive polarities of the PD pulses give the value of the PD signals detected and negative polarities give information of the phase where there is no PD. However, there will be a small signal at the negative polarity due to coupling capacitances produced between different phases. The impact of coupling capacitances between the phases is higher for the JMarti CC line model compared to the Clark model. It can be seen from the simulation results where the signal caused by the coupling capacitance captured by the Rogowski coil is higher for the JMarti CC line model.
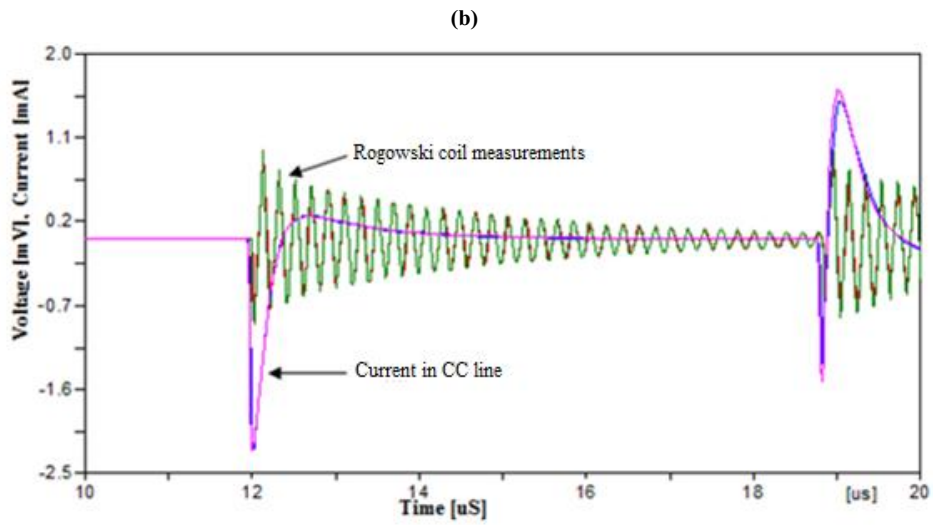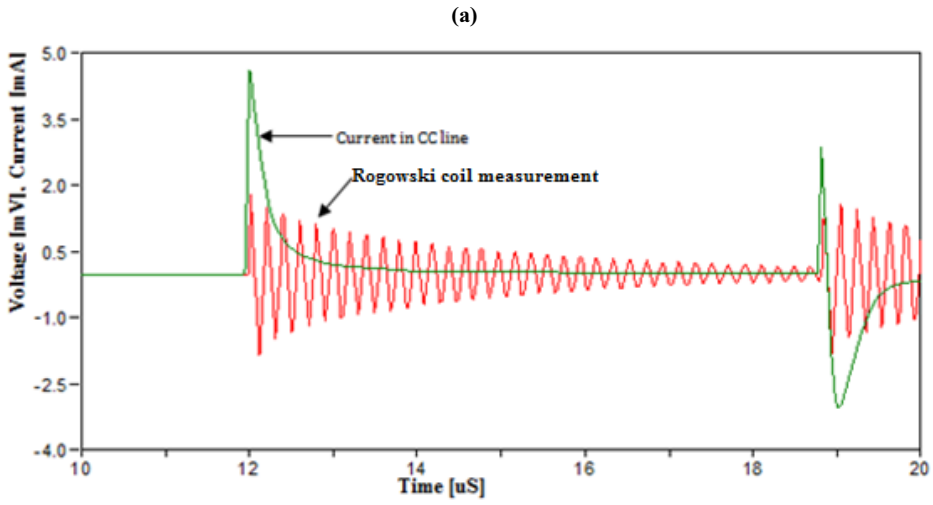
Fig. 3.11 Current flowing in CC line and Rogowski coil PD measurements (voltage signals) resulting from the leaning of a tree on phase A, (a) measurements at phase A, (b) measurements at phases B and C.
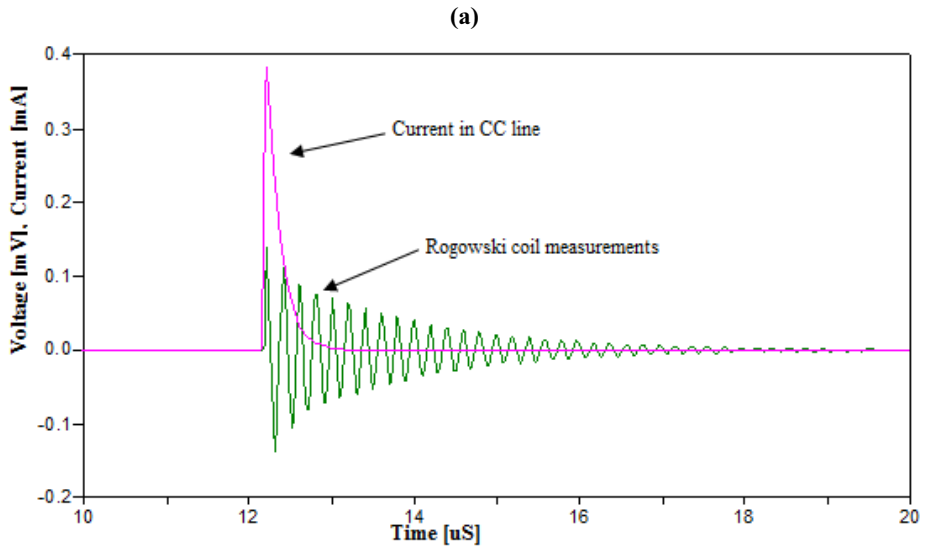
(a)

(b)
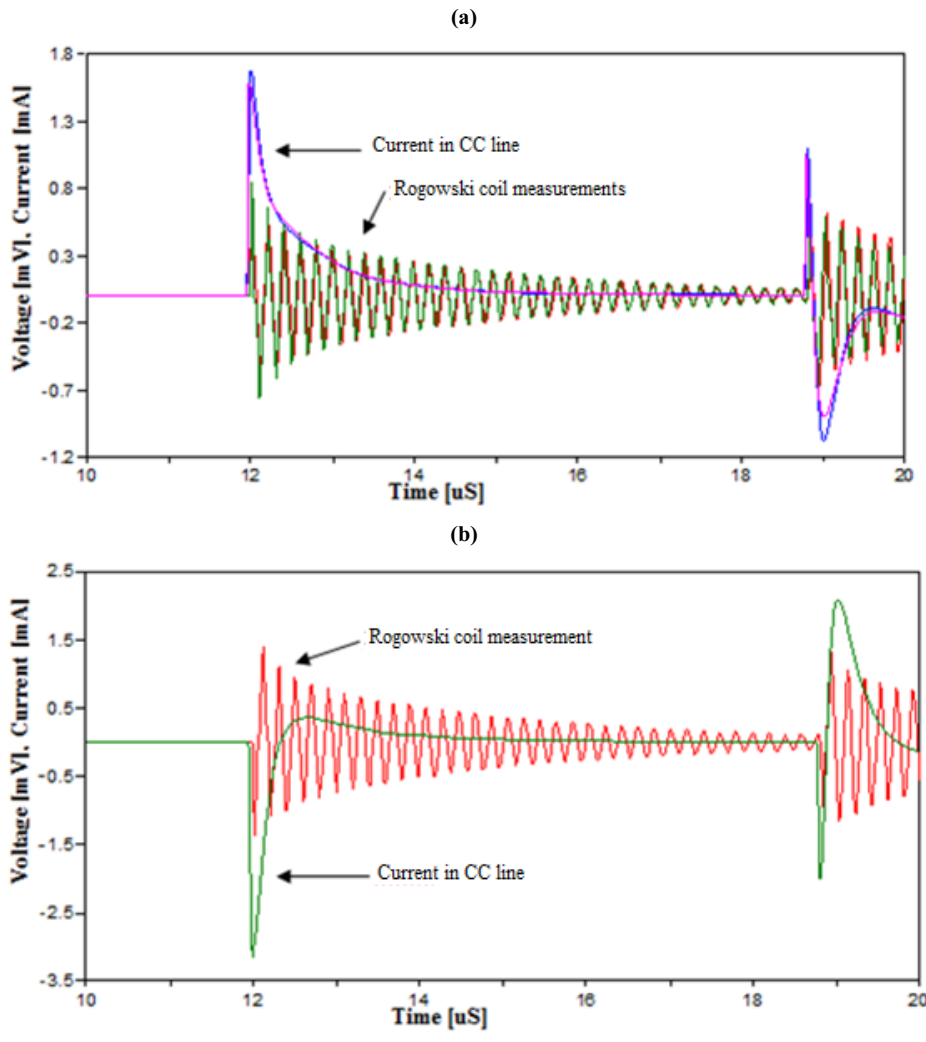
Fig. 3.12 Current flowing in CC line and Rogowski coil PD measurements (voltage signals) resulting from the leaning of a tree on phase A and B, (a) measurements at phase A and B, (b) measurements at phase C.
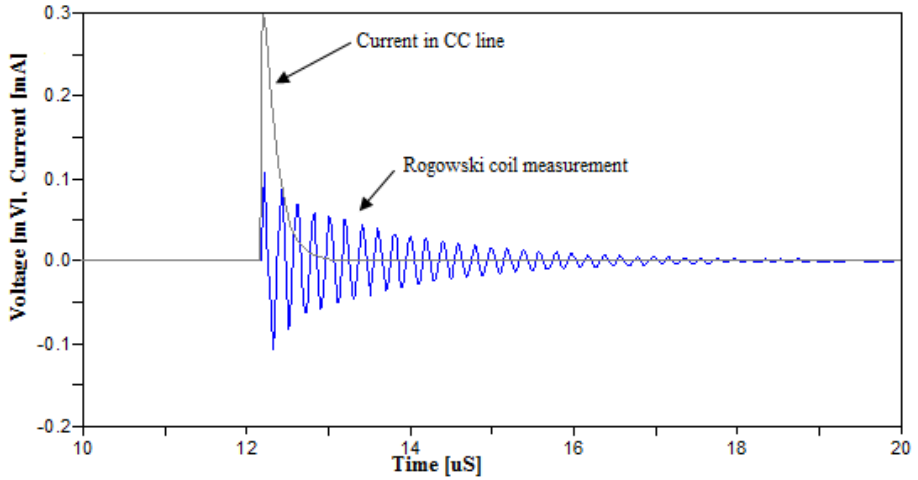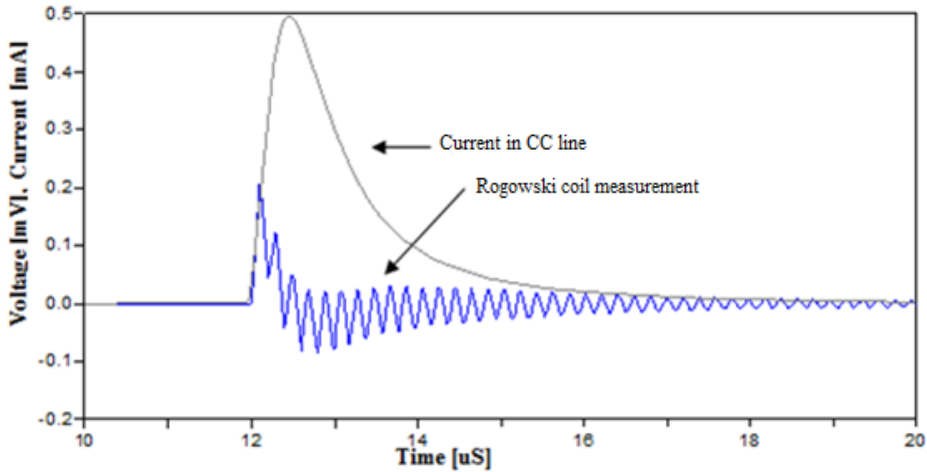
Fig. 3.13 Current flowing in CC line and Rogowski coil PD measurements (voltage signals) resulting from the leaning of a tree on phase A, B, and C.

3.4   Discussion

The online three-phase PD monitoring system based on single-end measurement is simulated in an EMTP-ATP simulation environment. The amplitude of the PD signal captured as the result of a tree leaning on a CC line at a distance of 3.5 km is around 0.2 mV in the case of a three-phase PD monitoring system. This means we need more PD sensors in three-phase cases in a fully working system. It is possible to detect PD signals beyond a distance of 4 km, provided there are a few trees leaning on the line or the scratches are impressed on the CC insulation by the leaned of trees.

A comparison of performance between two online three-phase PD monitoring systems for CC overhead distribution lines has been performed. Both models can be used to design an online PD modeling system for a CC overhead line. However, more practical results can be obtained using the JMarti CC line model, especially for a long CC line. The Clark model is acceptable for designing a short CC line. Within the context of this thesis, the JMarti frequency-dependent model is used for simulating and modeling of CC overhead distribution lines. In the following chapters, proposed model is extended to measure the PD source at the double-end of CC overhead lines in a distribution system, and the locator algorithm is developed.

4- Double-end measurement-based online three-phase PD monitoring system for CC overhead lines

This chapter extends the previous investigation to the possibilities of implementing an online three-phase partial discharge (PD) monitoring system using a Rogowski coil sensor at both-ends to detect the PD resulting from a leaning tree on covered-conductor (CC) overhead distribution lines. Various PD producing scenarios for a leaning tree on a CC line are also investigated. The PD source is detected and localized by comparing the arrival times of the pulses captured at different locations and the attenuation of the pulses while propagating over the line.

4.1   Three-phase PD monitoring system-based on double-end measurement

The investigation is carried-out to detect and localize the PD caused by a tree leaning on CC lines at different phases (various scenarios). Fig. 4.1 shows the schematic concept of the online three-phase PD monitoring system when the tree falls onto the CC line. After a certain period of time, the PD will be produced [56]. The PD pulse is split into two identical pulses traveling in opposite directions provided the impedance seen by the PD source is equal in both directions. The location of discharge is found out using the traveling wave technique.

The Rogowski coils which act as PD measuring sensors were placed in every phases at 1 km and 3 km from the PD source at its left and right side, respectively. Rogowski coils RC_1, RC_2, and RC_3 (shown in Fig. 4.1) are used to detect the PD pulse traveling to the left side of the PD source. The coils RC_{11}, RC_{22}, RC_{33} are used to detect the PD pulse traveling to the right hand side. The PD source location and the affected CC lines (where the tree is leaning) can be recognized by comparing the arrival times and signal polarities measured by each Rogowski coil. Knowing the total cables length L between the two Rogowski coils and the propagation velocity v, the location x from the left hand side of the PD source can be determined as follows [61]:

$$x = \frac{1}{2}\left[v(t_1 - t_2) + L\right]$$

(4.1)

where t_1 and t_2 are the arrival time stamped at the Rogowski coils on the left and right hand sides, respectively.

The simulated system is illustrated in Fig. 4.2. The CC lines model is simulated using the Electromagnetic transient program-Alternative transient program (EMTP-ATP), in which the processing is created using ATPDraw. The CC lines are represented using a frequency-

dependent JMarti model type which considers the feeder configuration given in Fig. 4.3. The CC line model and the feeder configuration are the same as in Chapter 3 which has been explained thoroughly in Section 3.3.2. An RLC branch is added at both terminals of the feeder for connecting the conductor-end to the ground. The first three scenarios as listed in Chapter 3 are again considered for modeling. The simulation results are discussed in the next section.
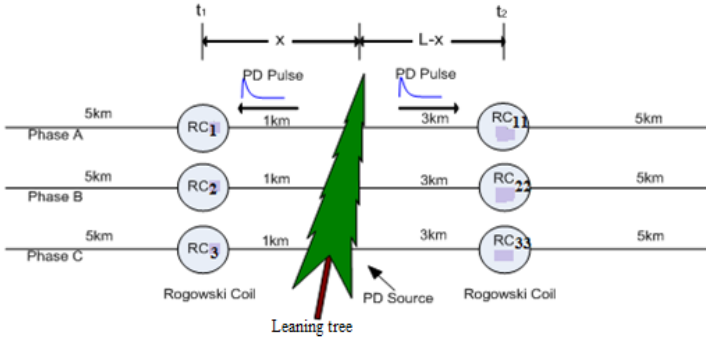
Fig. 4.1 Schematic of online three-phase PD monitoring system for CC overhead distribution lines [63].

Fig. 4.2 ATPDraw circuit for online three-phase PD monitoring systems for CC overhead distribution lines based on double-end measurement [63].
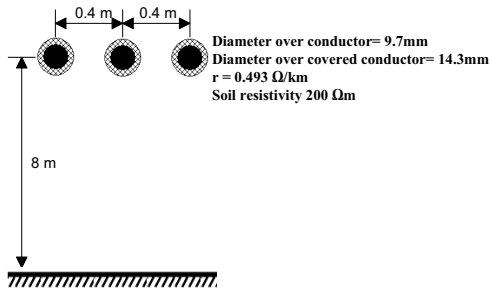
Fig. 4.3 The MV feeder configuration [63].

4.2 Simulation results

Figs. 4.4, 4.5, and 4.6 show the PD measurements for scenarios (i), (ii), and (iii), respectively. These measurements are done on each phase at both sides in both time and in frequency domains.

The attenuation of the PD pulses on each phase and each case are almost identical. The comparison is carried out using the time domain performance and Fast Fourier Transform (FFT) analysis. For case (i), the PD pulses measured by Rogowski coils RC_1 and RC_{11} at phase A initiate at $t_1 = 3.45$ µs and $t_2 = 10.28$ µs, as shown in Figs. 4.4 (a) and (b), respectively. The propagation velocity v obtained from the simulation in EMTP-ATP is 286.69 x 10^6 m/s for the JMarti CC line model [59]. Using Equation (4.1), the distance of the PD source on phase A is calculated to be 1.021 km and 2.979 km from the Rogowski coils located at the left side and right side, respectively. From the FFT analysis in Figs. 4.4 (c) and (d), it is clear that the PD pulse amplitude is higher at the faulty phase (phase A) compared to the other two phases. The resonance frequency of the Rogowski coil occurs at ≈ 5.1 MHz.

(a)
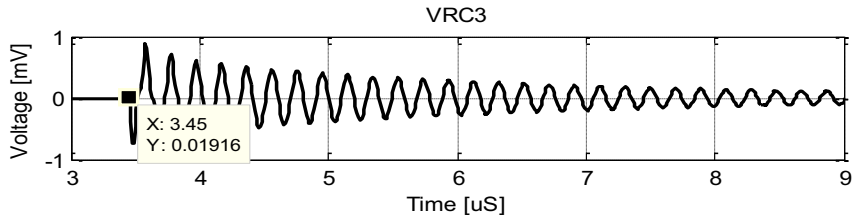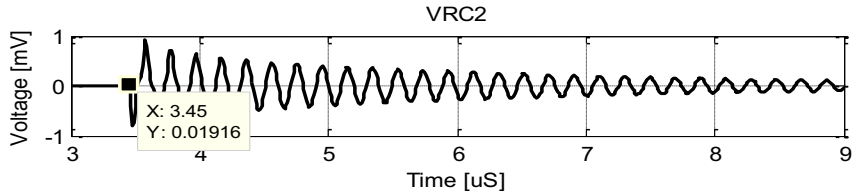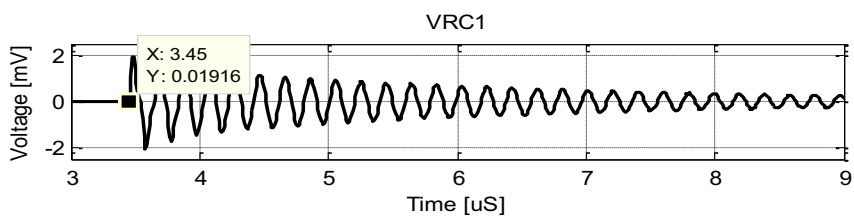
(b)
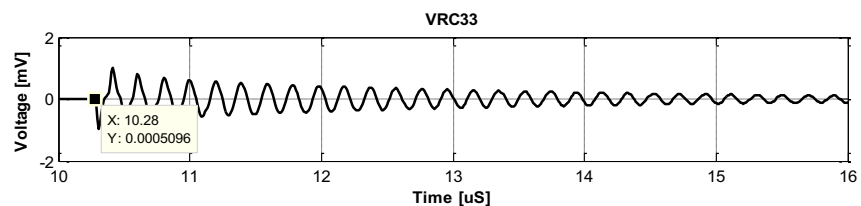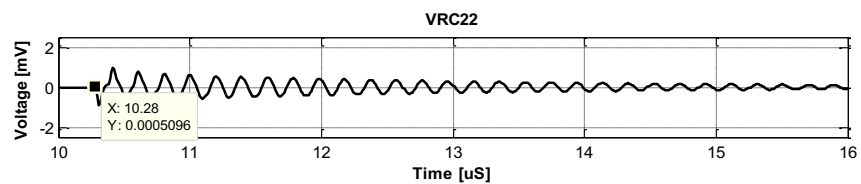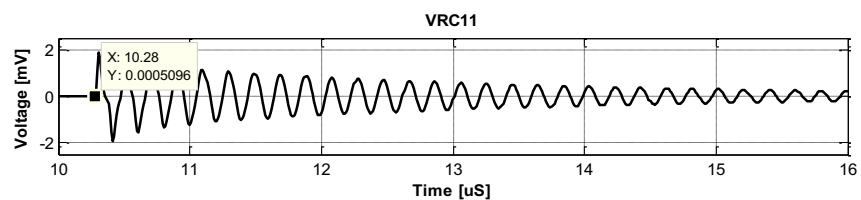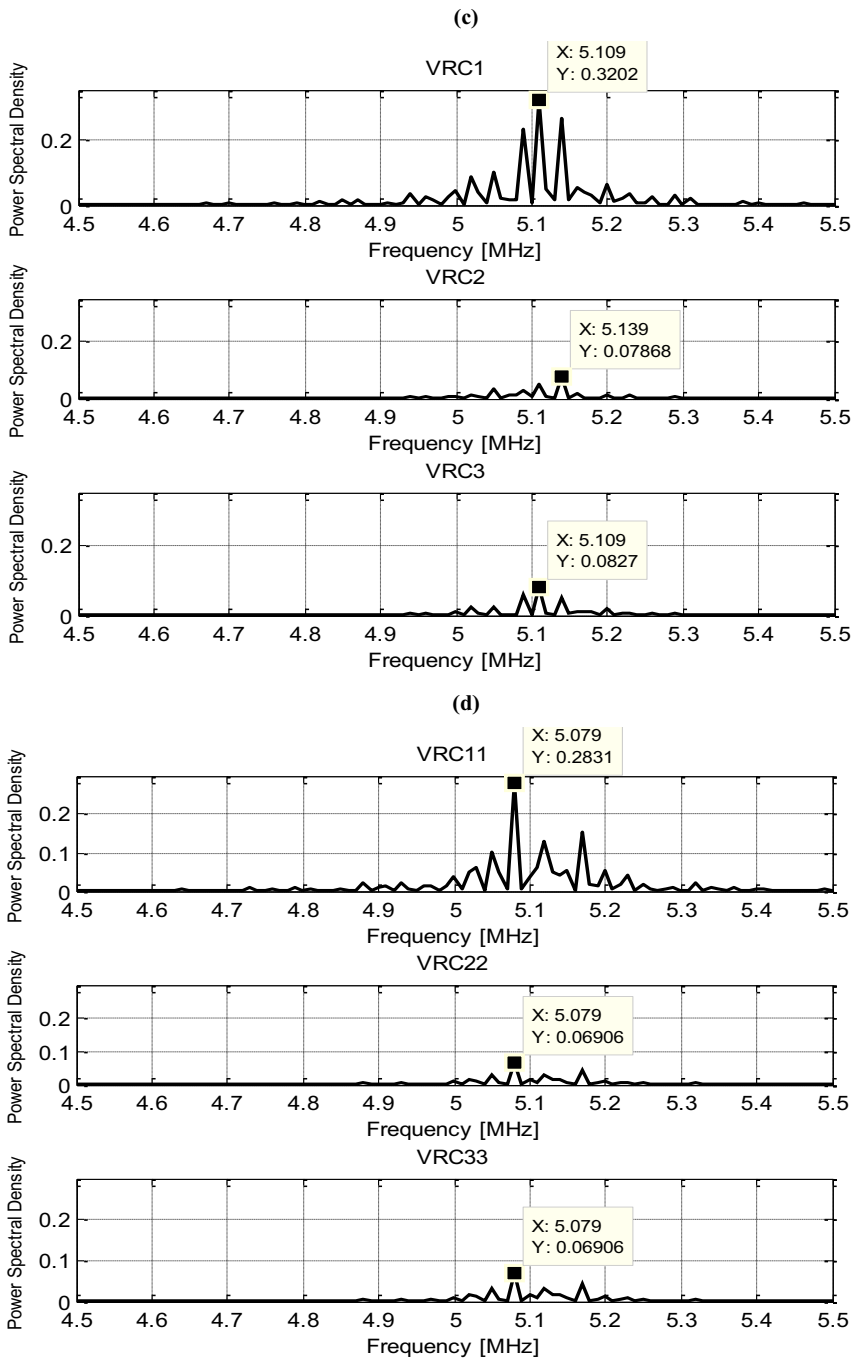
Fig. 4.4 Rogowski coils response for each phase resulting from a leaning tree at phase A in the time domain [(a), (b)], the frequency domain [(c), (d)].

For case (ii), referring to Figs. 4.5 (a), and (b), same concept can be applied to detect the PD location and the faulty phase caused by a leaning tree. The PD signals measured by Rogowski coils RC_1, RC_2, RC_{11}, and RC_{22} are in positive polarity. Although the amplitude measured by Rogowski coils RC_3 and RC_{33} at phase C is slightly higher, it is in negative polarity. This means that the tree has fallen on phase A and B but not on phase C. The distance of the PD source is 1.020 km and 2.980 km from Rogowski coils located at the left and right sides, with the arrival time of t_1 = 3.44 µs and t_2 = 10.28 µs respectively. The FFT analysis in Figs. 4.6 (c) and (d) show that the dominant frequency containing the PD pulse lies in the frequency range of 5.0 - 5.2 MHz. The amplitude of measured voltage signal at phase C is higher due to the summation of coupling capacitances effect from phase A and B.

(a)

37

(b)

VRC11

VRC22

VRC33

(c)

VRC1

VRC2

VRC3

38

(d)
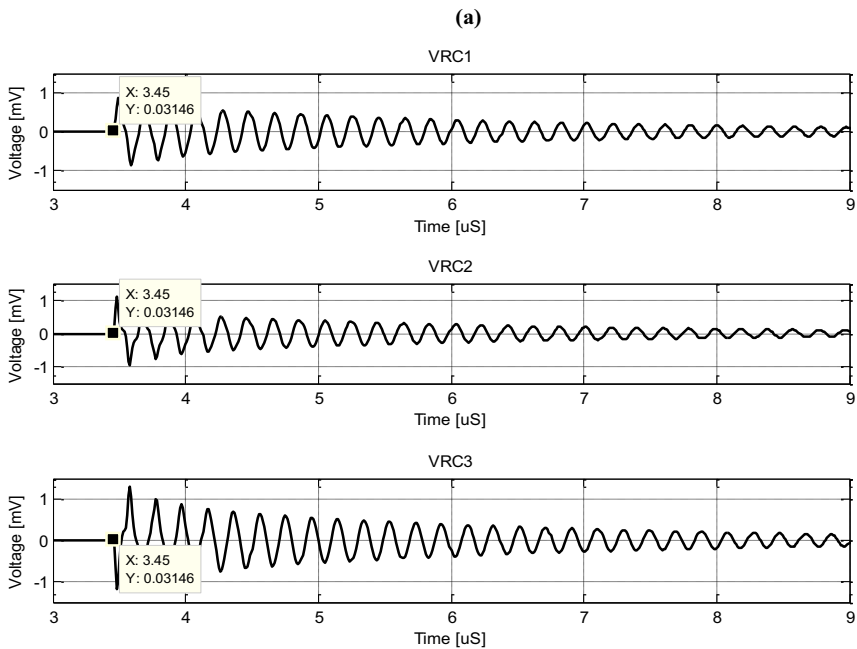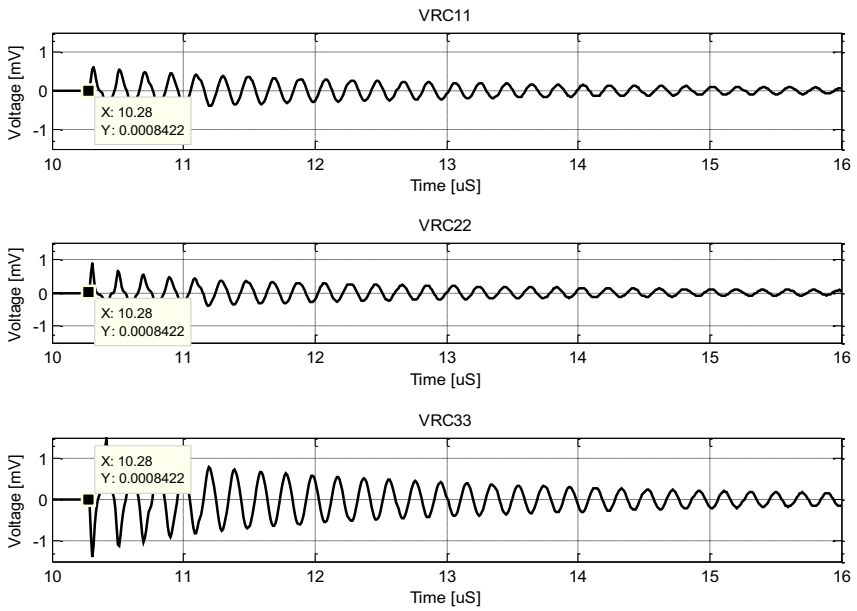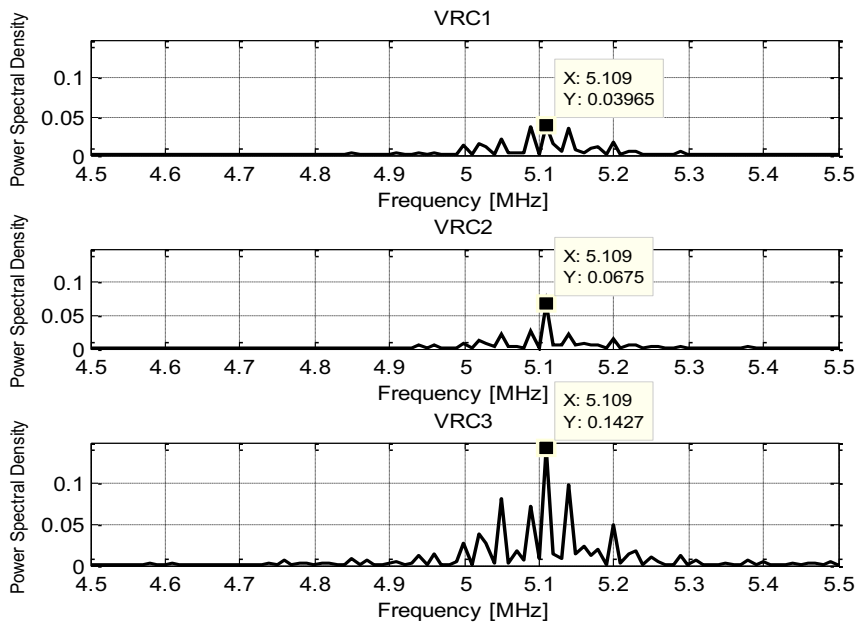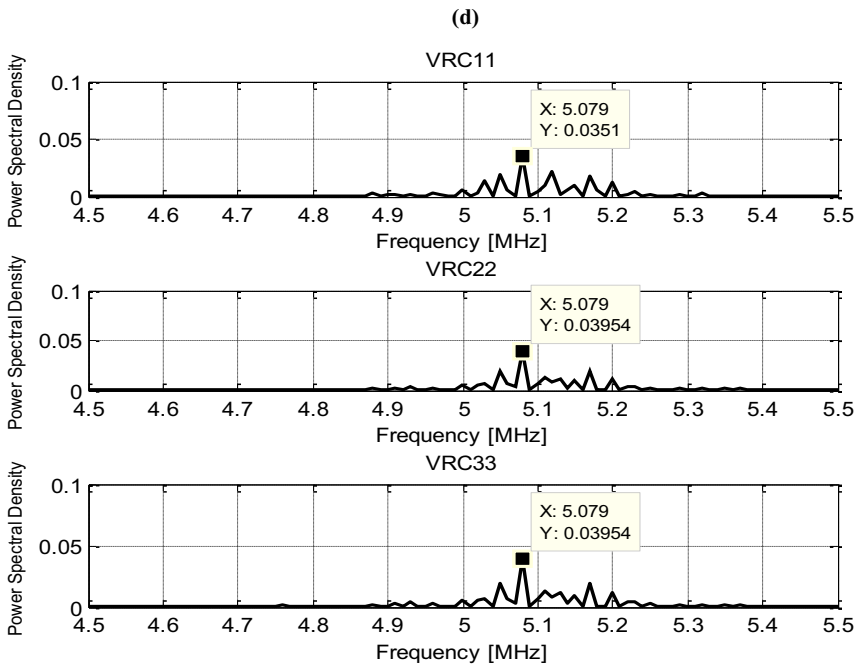
Fig. 4.5 Rogowski coils response for each phase resulting from the leaning of a tree at phases A, and B in time domain [(a), (b)], frequency domain [(c), (d)].

For case (iii), referring to Figs. 4.6 (a) and (b), the measured voltage signal by Rogowski coils at phase A, B, and C are similar with arrival of times of $t_1 = 3.43$ μs and $t_2 = 10.27$ μs. The distance of the PD source is 1.019 km from Rogowski coils RC_1, RC_2, and RC_3, and located at distance of 2.981 km from Rogowski coils RC_{11}, RC_{22}, and RC_{33}. It is clearly seen that the tree has fallen on all phases and are produced PDs. The FFT analysis in Figs.4.6 (c) and (d) show that the resonance frequency for this case occurs at 5.1 MHz.

(a)

VRC1

VRC2

VRC3

(b)

VRC11

VRC22

VRC33

40
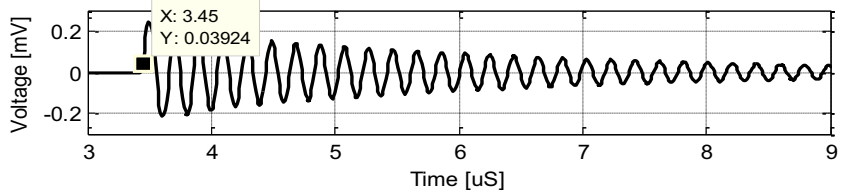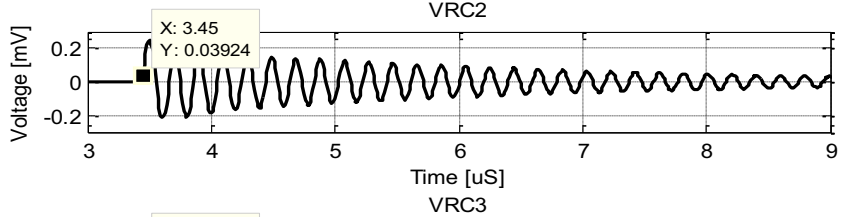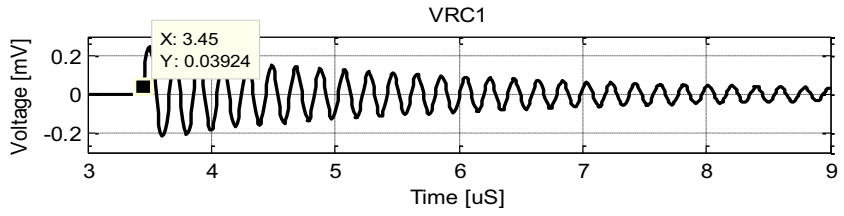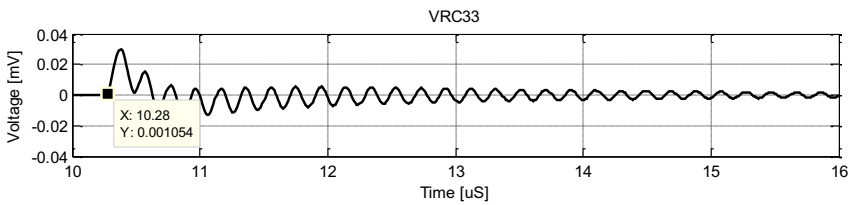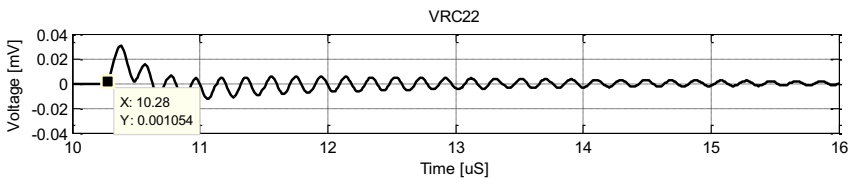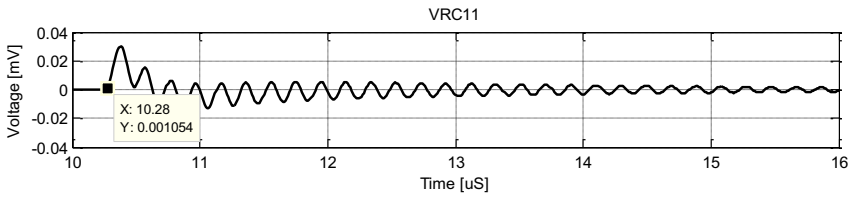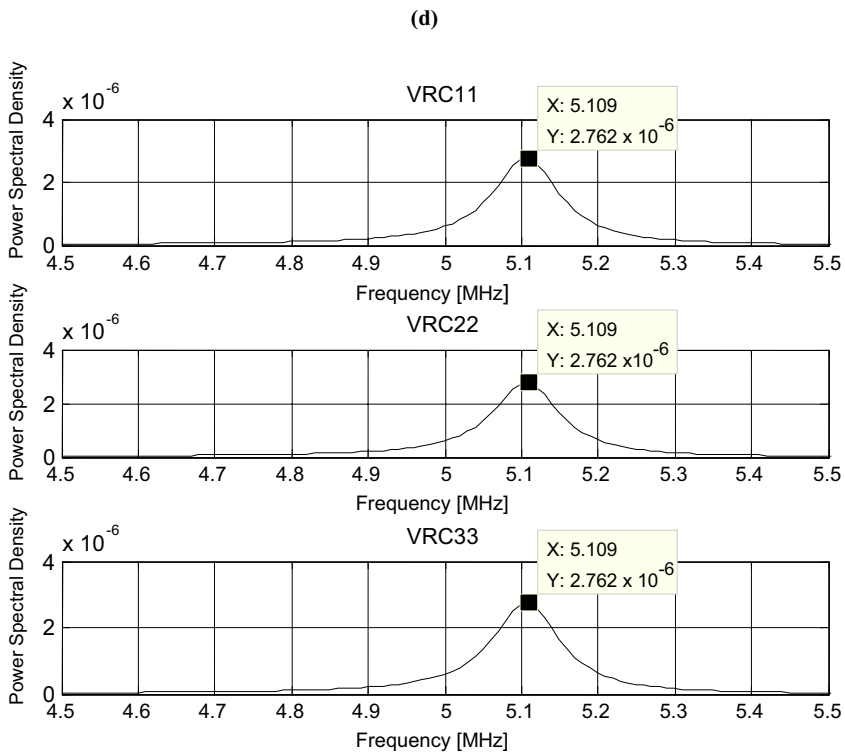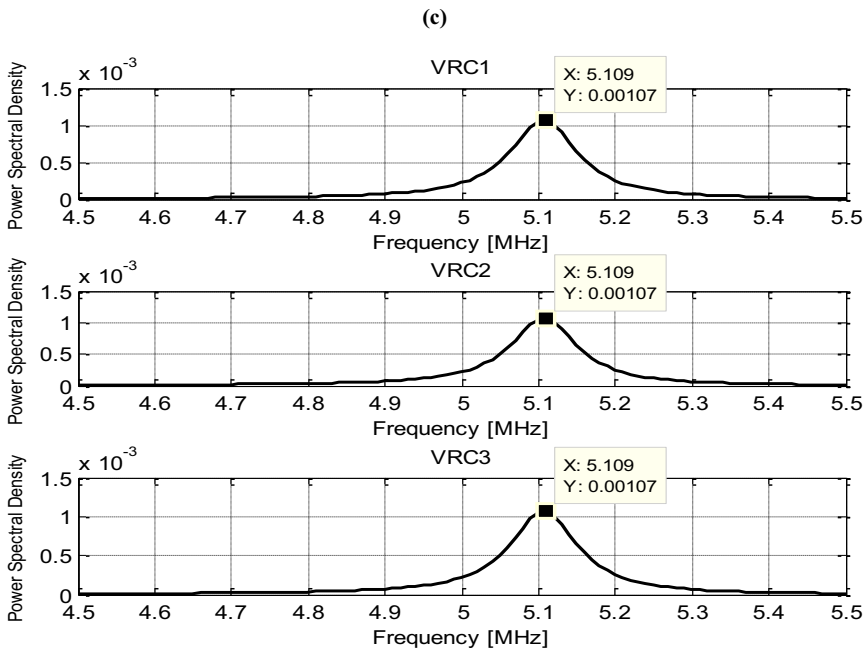
Fig. 4.6 Rogowski coils response for each phase resulting from the leaning of a tree on phases A, B, and C in the time domain [(a),(b)], the frequency domain [(c), (d)].
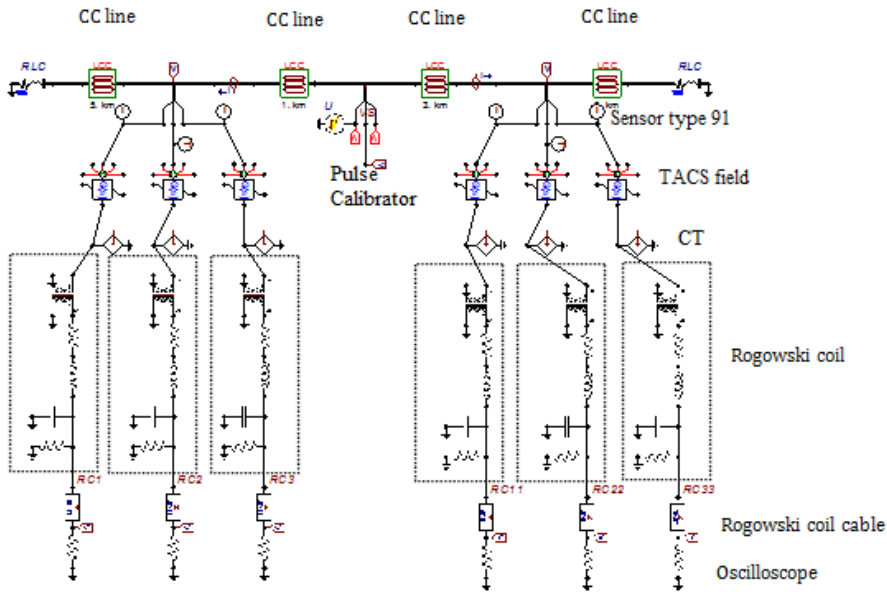
4.3 Discussion

An EMTP-ATP simulation environment is used to represent the online three-phase PD monitoring system for CC overhead distribution lines based on double-end measurement. The system is designed to detect and localize PD sources at different conditions and locations caused by a tree leaning on CC lines. Three such cases have been studied. Attenuation of the PD signal which defines its frequency band depends on the distance the signal has traveled. The attenuation is frequency-dependent and it increases by increased frequency of the propagated signals. As the PD pulse travels along the CC line, the higher frequency components of the pulse are heavily attenuated. The attenuation (and propagation velocity) in the CC line is strongly influenced by its location, i.e. the height of the conductor-core above the ground level. The attenuation decreases and propagation velocity increases by increasing the height of the CC line above ground level [23], [54], [102]. In addition, the PD signal amplitude measured by the Rogowski coil also depends on the number of leaning trees as described in Chapter 3, and the number of affected CC lines.

It is good to note that the main cause of pollution on the CC line in Finland is due to snow. The effect of snow on the wave propagation characteristics of the bare conductor has already been investigated in [54], [102]. It is revealed that the admittance is increased by the snow. The increase of the admittance depends on the depth, density, and temperature of the snow. The effect of snow on the attenuation constant increases and that on the propagation velocity and characteristic impedance decreases, as the frequency increases. The effect of snow on the wave propagation characteristics of a CC line are expected to be the same as the effects of snow as mentioned for bare conductor.

Based on previous results in [3], [5], and simulation works presented in this Chapter, 3.5 - 4 km is found to be the suitable distance to measure a PD pulse in CC overhead lines. This distance is selected to ensure the measured data to be useful in practice, especially in the multi-end measurement case which requires three measuring points (presented in the following chapters).

The disadvantage of the PD locator explained in this chapter is that its accuracy depends on the propagation velocity, v of the traveling wave and the time synchronization. The improvements in this simple PD locator algorithm are presented in the next chapters.

5- Three measuring points for PD location on CC overhead lines: experimental and algorithm evaluation

There are two important components in any online partial discharge (PD) measurement system. These are the sensors and the measurement system itself. The use of a correct sensor will greatly improve the PD detection because different sensors have their own strengths and weaknesses. There are reported experiments which investigate the high frequency characteristic of the Rogowski coil and represent the model of the coil [5], [6], [9], [14], [37], [63]-[65]. Such evaluation is not sufficient to test its enhancement in locating PD sources especially for covered-conductor (CC) overhead lines. Furthermore, the evaluation should be done by considering practical implementations, such as testing the performance with multi-measuring sensors and with the fundamental alternating current (AC) source.

An experimental analysis is performed to evaluate the PD measurement system performance and a locator algorithm for PD location on CC overhead distribution lines is developed. A multi-end measuring method with three measuring points is chosen as a technique to locate the PD source point on the line. A power transformer is used to energize one end of the CC line by the AC voltage source. The tests are carried out with different measurement conditions, such as offline and online PD measurement systems. For the offline measurements, the pulse similar to the characteristic of the PD signal is generated using a pulse calibrator where the CC line is not energized. Meanwhile for online measurements, two methods have been used to generate live PD signals with the CC line energized via a power transformer. The methods are by twisting a coil around the CC and by leaning a tree onto the CC line.

The physical geometrical size of Rogowski coil used in this work is listed in Table 5.1. The geometry and physical configuration of Rogowski coil can be seen in Fig. 2.2 and Fig. 2.3.

Table 5.1 Geometry of the Rogowski Coil

Geometrical Parameters	Specifications
Inner Diameter, d_1	101 mm
Outer diameter, d_2	109 mm
Transducer diameter, d_{rc}	8 mm
Number of turn, N_{rc}	1900

5.1 Experimental measurement set-up

The first experimental set-up shown in Fig. 5.1 was arranged in the high voltage (HV) laboratory at the School of Electrical Engineering, Aalto University, Finland. A, B, and C, are

measuring points of the Rogowski Coil, C_g is the terminating capacitance to the ground. L_{AB} is the distance between Rogowski coils A and B, L_{BC} is the distance between Rogowski coils B and C. Meanwhile L_A, L_B, and L_C are the distance from each Rogowski coil to the PD source point, respectively. A feeder with only two CC overhead lines is installed due to the shortage of the CC cable. As shown in Fig. 5.2, the CC overhead lines was laid at a height approximately 8 m above the ground level, and each feeder end was terminated with capacitor C_g, 500 pF to the ground. Rogowski coils A, B and C are looped around the CC and connected to the oscilloscope to measure the PD pulse propagation to both sides of the CC lines. A fast digitizing oscilloscope (DSO), model Lecroy 9384TM was used to capture the waveforms of the Rogowski coils. The sampling frequency used in the measurements was 2.5 GHz. An identical trigger value was used on the three measuring channels to order to synchronize the measured signals. The signals were displayed on the oscilloscope and the data was stored for further processing and features extraction.
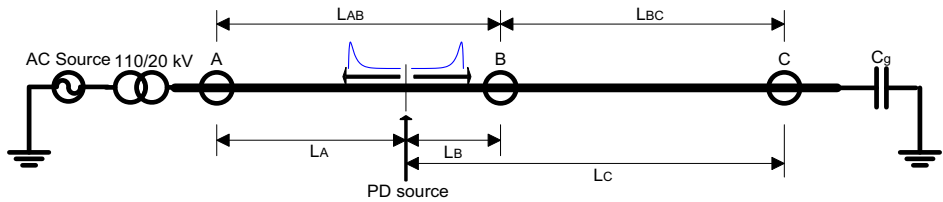
Fig. 5.1 The experimental configuration.

Two concepts were used to experimentally generate the PD signals. They are:

i)   Pulse calibrator, for calibrating the PD measurement system, and to inject a PD source into the CC line during offline measurement (without energized 11.5 kV AC voltage source),

ii)   Twisting a coil around the CC as shown in Fig. 5.3. The coil is connected to the ground via a 1000 pF capacitor to create a pulse like the PD source during online measurement (energized 11.5 kV AC voltage source). This idea of producing PD is based on the theory of two metallic electrodes having insulation between them with cavity towards the grounded electrode. The conductor inside the insulation (covered-conductor) is one electrode and the inductive coil is the second electrode. Insulation of CC is the insulation between the two electrodes while the air gap of the coil conductor and insulation can be considered as a gap or cavity. This cavity contains air as its insulating medium. The electric field collapses when the voltage stress between electrodes increases the inception voltage for this air gap to initiate high frequency pulses [66].

44
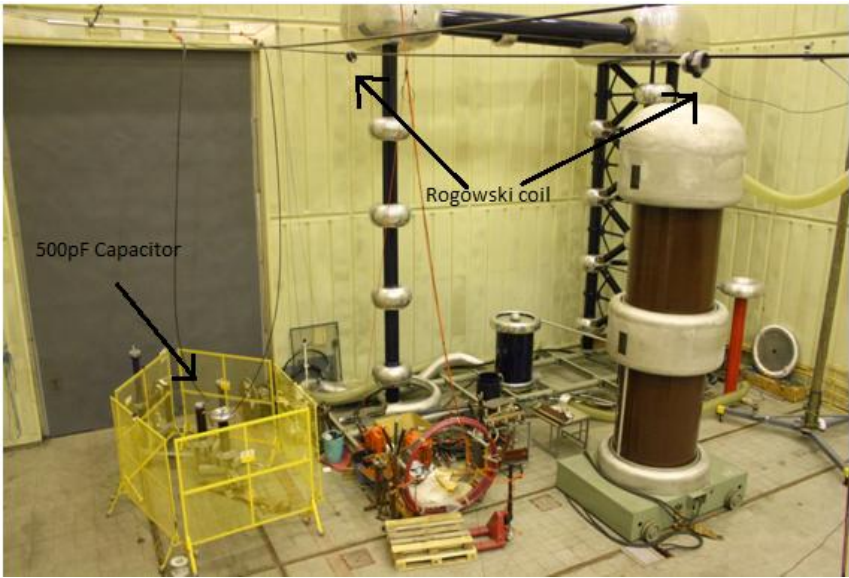
Fig. 5.2 500 pF capacitor used as terminating impedance to the ground, and the position of the Rogowski coil.
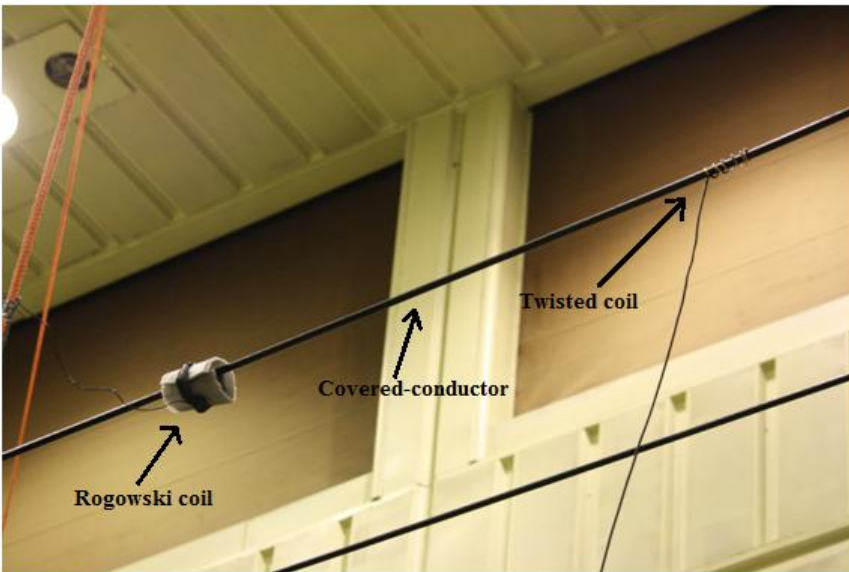
Fig. 5.3 The position of the Rogowski coil and twisted coil on the CC line.

Both concepts create two traveling waves which travel in opposite directions towards the power transformer and CC line end. Usually, the supply transformer end is not strictly an open circuit because of the shunt capacitance of the transformer windings. Therefore, the traveling wave is reflected from the transformer end with the surge impedance of the transformer as its termination. To avoid this reflection, a 1000 pF capacitor was inserted at the

end of the transformer. Fig. 5.4 shows the power transformer; 110/20 kV was used to energize the AC voltage up to 11.5 kV/phase (20 kV system). The experimental measurement has been tested in a noisy environment, the noise being generated using an energized three-phase power transformer 20 kV / 410 V AC, as shown in Fig. 5.4, where it was under certain test conditions to generate broadband interference white noises.
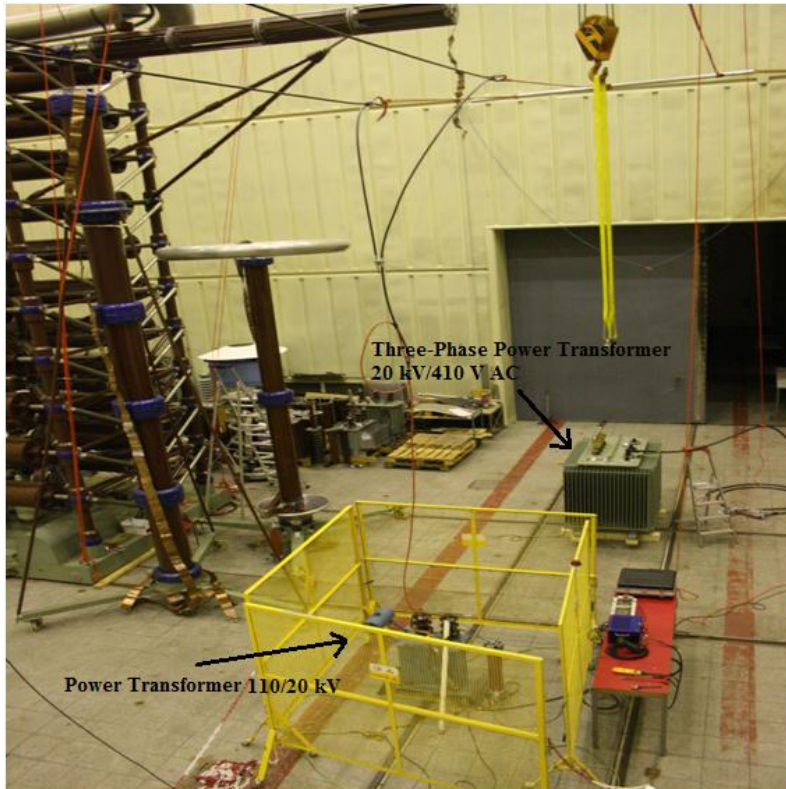
Fig. 5.4 Power Transformer used to generate AC voltage up to 11.5 kV/phase on the CC line.

As mentioned in Chapter 1, in practice PD is produced by a leaning tree which leads to the deteriorating of the conductors through chemical, thermal and electrical mechanisms after a certain period of time. However, based on [3] and [5], a real PD source due to surface discharge can be created instantly using a leaning tree on an energized CC line. In [3], an experimental measurement to study the characterization of PD signals due to the aforementioned reason has been done in HV laboratory measurement. In this measurement, only one measuring sensor was used to measure the PD signals and the PD was located using the single-end measurement technique.

The second online PD measurement in this work was performed with an Aspen (Populous Trimula) tree leaned on the CC line as shown in Fig. 5.5 (a, b, c), with the same experimental configuration as in Fig. 5.1. However, the CC line was installed at only 3 m above

the ground level compared to 8 m from the first experimental setup to make it suitable to use a leaning tree in the HV laboratory. The tree was earthed to the ground point. Its resistance which was measured at 3 m height from the ground level after 5 kV DC voltage source is applied was found equal to 600 MΩ. The sampling frequency used in this measurement was 2.0 GHz. There was no noise source generated during this measurement.

(a)

(b)
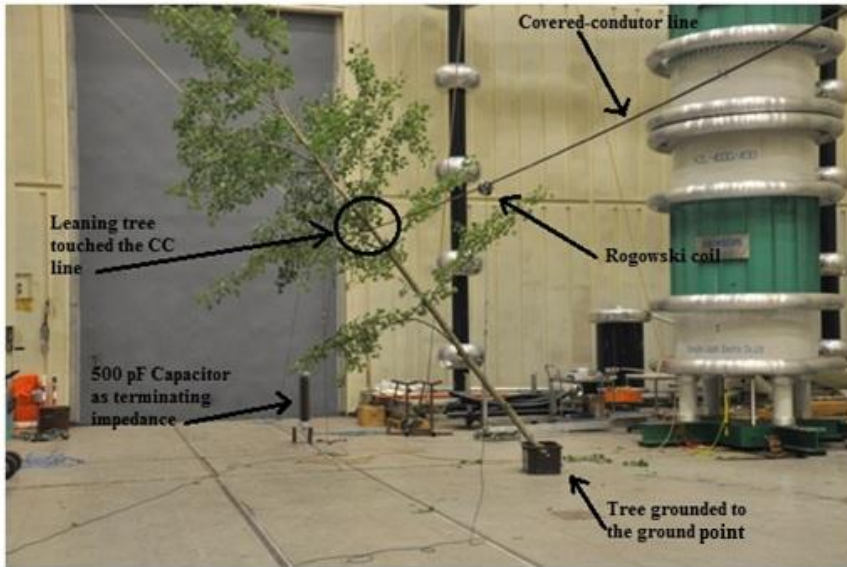
Fig. 5.5 (a), (b), (c) Experimental measurement set-up for PD detection and location resulting from a tree leaning on the CC line.

Fig. 5.6 shows that the PD diagnosis tool was used to measure the PD energy. The energy produced is found to be 3.93 nC after the CC line was energized by a 11.5 kV AC voltage source. There was no knife traces made on the insulator. This reveals that the PD could be produced immediately after a tree is leaning on the CC line in a real outdoor scenario. In [49], PDs produced due to a leaning pine tree on a 20 kV CC line in laboratory measurement were of magnitude around 3 nC. This amount could be higher in a real outdoor scenario, considering the larger scale and the potentially higher number of leaning trees on the line after heavy storms.
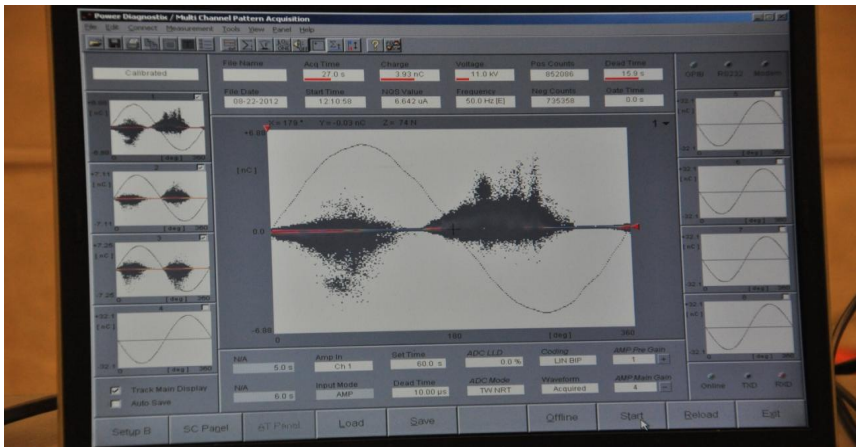
Fig. 5.6 Measurement of PD energy produced due to resulting from a tree leaning on the CC line.

5.1.1 Results of offline PD measurement system - PD produced by a pulse calibrator

This measurement was performed without energizing the AC power source on the CC line. The distances between each Rogowski coil is set as L_{AB} = 5.2 m and L_{BC} = 4.5 m (referring to the network shown in Fig. 5.1). The Calibrator signals for 5 nC, 10 nC, 20 nC and 50 nC pulses were injected at a distance of L_B = 0.9 m in section AB. Different values of calibrator signals were used in order to obtain reliable verification of PD measurement system performance response. The measured PD signals for each pulse calibrator value using Rogowski coils A, B, and C in the time and frequency domains are shown in Figs. 5.7 to 5.10.

From Figs. 5.7 to 5.10, the PD signals measured by the Rogowski coils for the injected 10 nC, 20 nC, and 50 nC pulse calibrator are clearly seen compared to the injected 5 nC pulse calibrator, both in the time and frequency domains. For the injected 5 nC pulse calibrator, the measured signal is corrupted by noise due to the low PD signal level. The amplitude of the PD signals measured by the Rogowski coils varies from 30 mV up to 700 mV depending on the injected pulse calibrator values. Referring to Figs. 5.7 to 5.10 (d, e, f), the frequency range for the PD signal is from 500 kHz up to 3 MHz. The other frequencies components are considered as noise. Even though this is an offline measurement, (without the CC line energized), the effect of noise due to the energized 20 kV / 410 V AC transformer can be seen. This can be explained as follows: after the PD pulse is injected, the CC line acts as a long antenna which then picks the noise from the transformer which then propagates along the CC line together with the PD pulse.
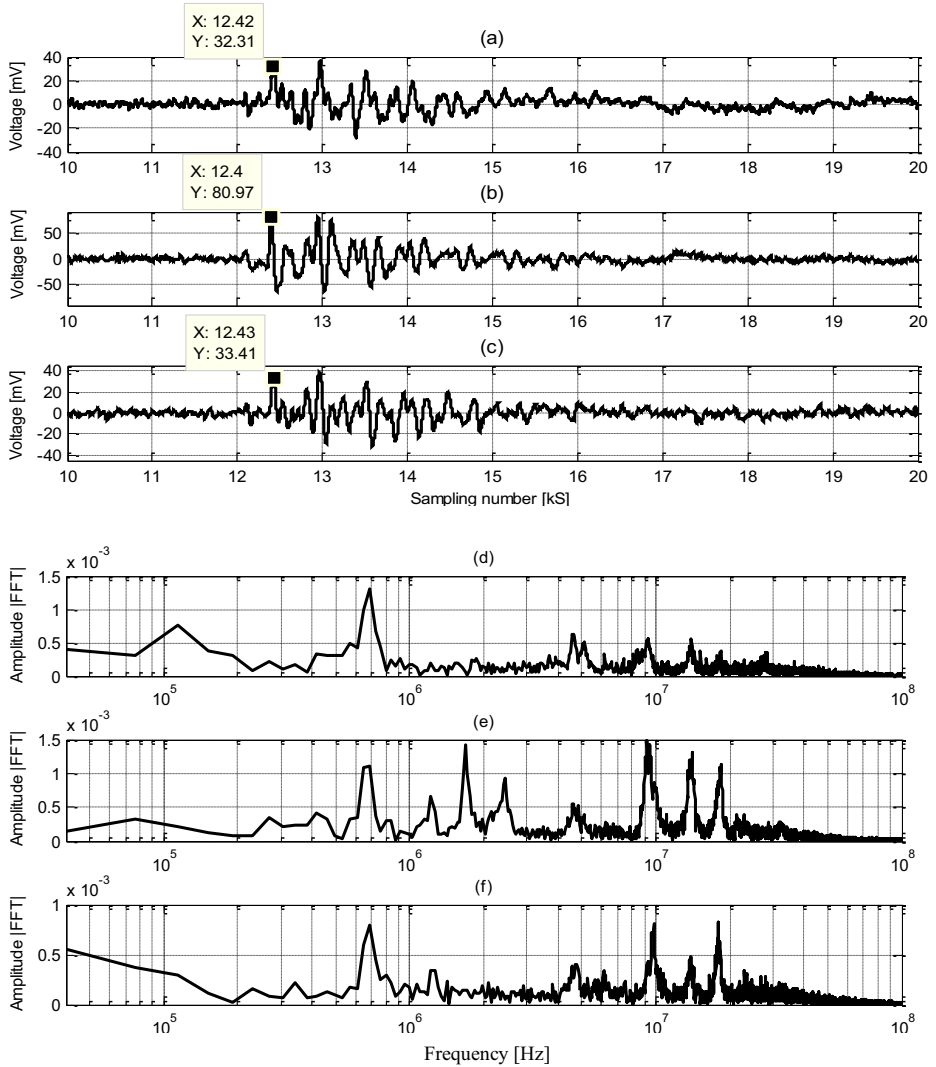
Fig. 5.7 Rogowski coil response for the injected 5 nC pulse calibrator; (a), (b), (c) in the time domain, (d), (e), (f) in the frequency domain for Rogowski coils A, B and C, respectively.
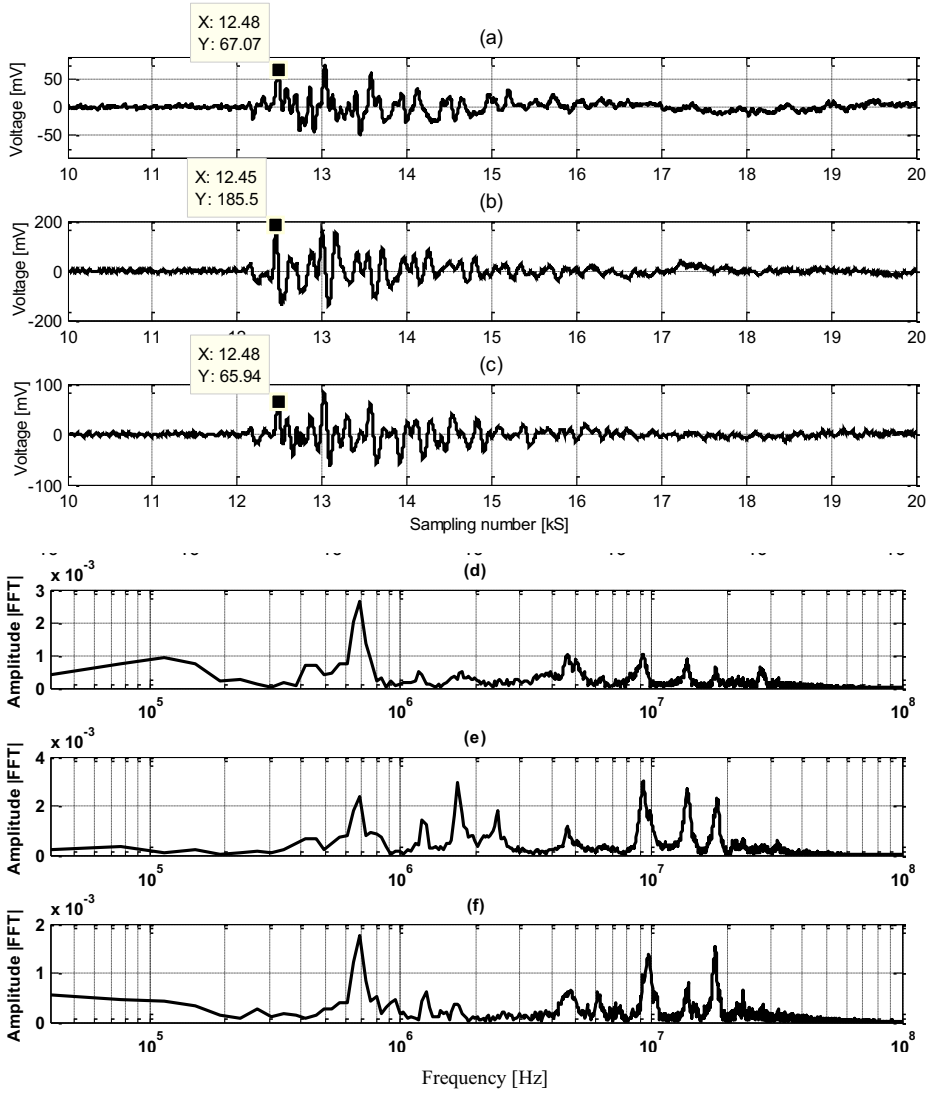
Fig. 5.8 Rogowski coil response for the injected 10 nC pulse calibrator; (a), (b), (c) in the time domain, (d), (e), (f) in the frequency domain for Rogowski coils A, B and C, respectively.
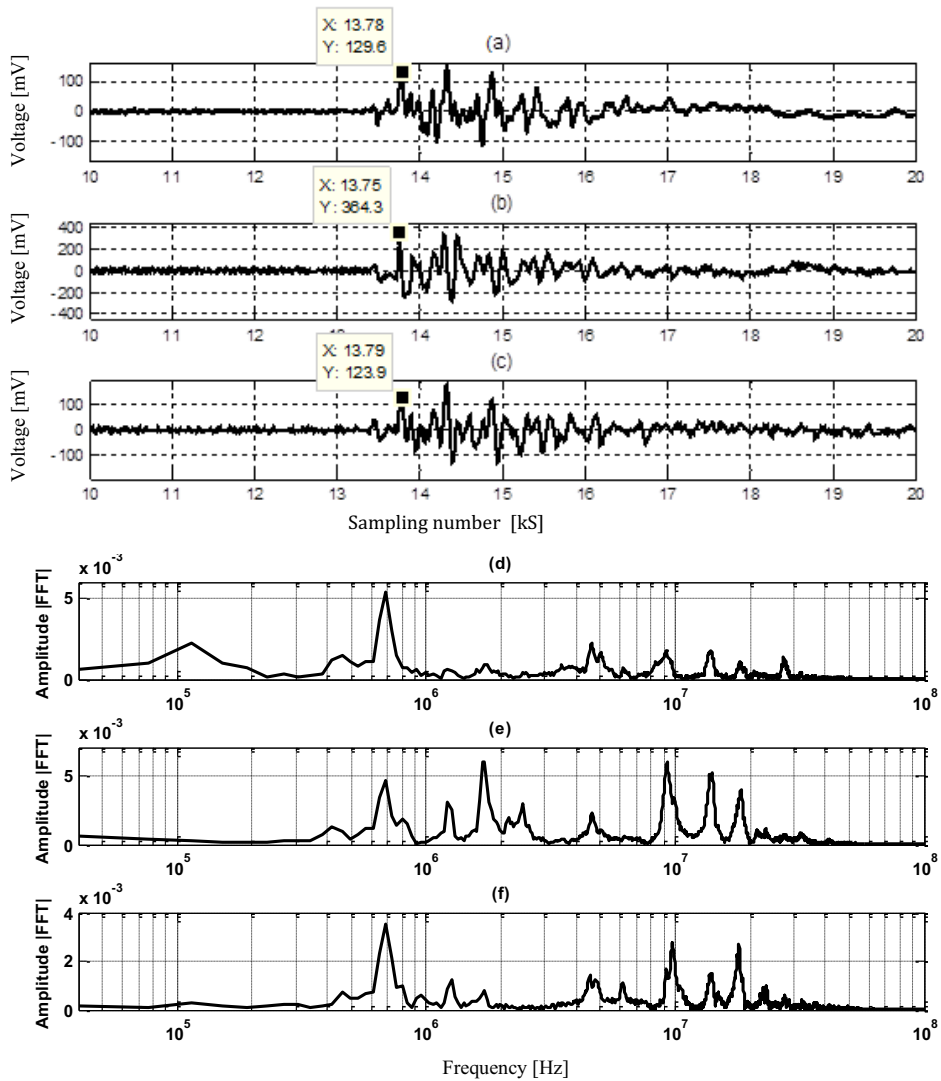
Fig. 5.9 Rogowski coil response for the injected 20 nC pulse calibrator; (a), (b), (c) in the time domain, (d), (e), (f) in the frequency domain for Rogowski coils A, B and C, respectively.
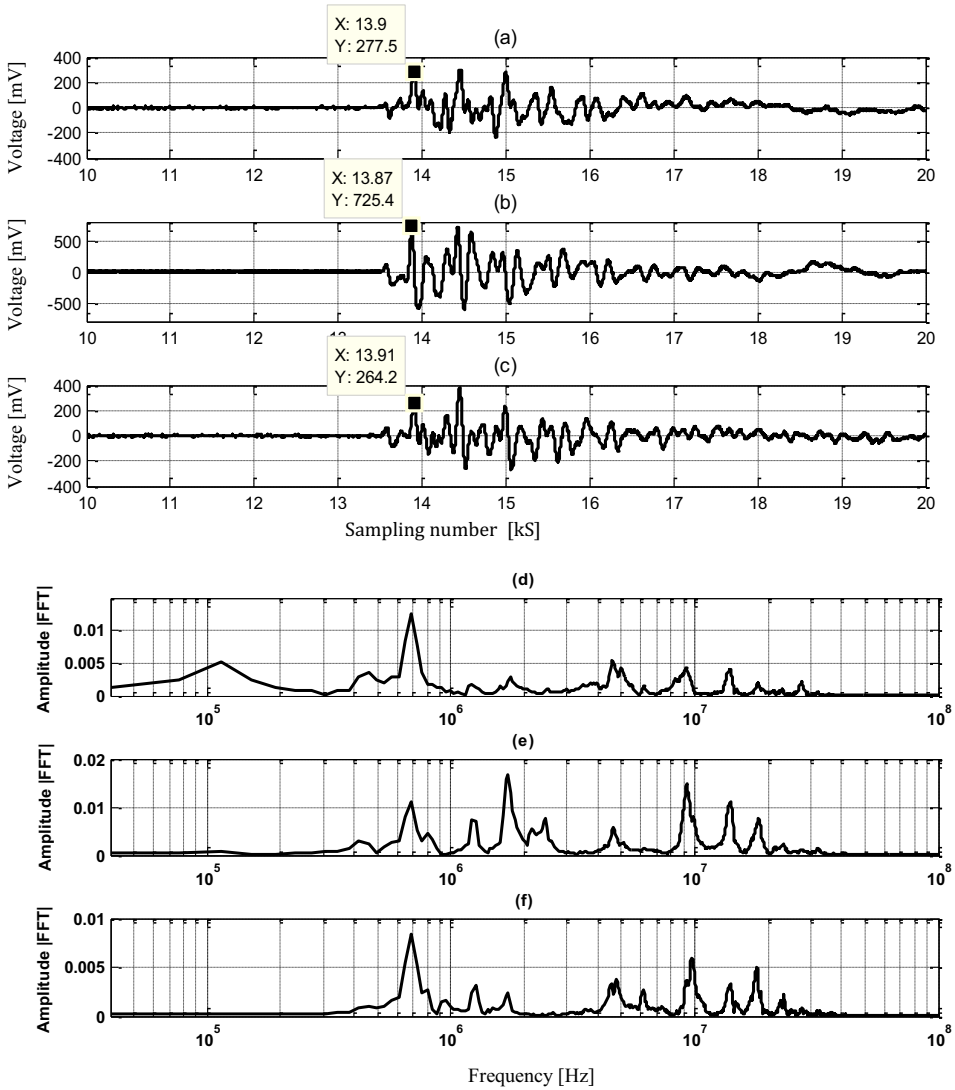
Fig. 5.10 Rogowski coil response for the injected 50 nC pulse calibrator; (a), (b), (c) in the time domain, (d), (e), (f) in the frequency domain for Rogowski coils A, B and C, respectively.

5.1.2   Results of online PD measurement system

5.1.2.1 PD produced by twisted-coil around the CC line

Referring again to Fig. 5.1, different distances between Rogowski coils considered for this set-up are L_{AB} = 4.7 m and L_{BC} = 5.0 m. The PD source is set at L_B = 2.5 m in section BC. The measured signals from the Rogowski coils in both time and frequency domains at points A, B, and C are shown in Fig. 5.11.
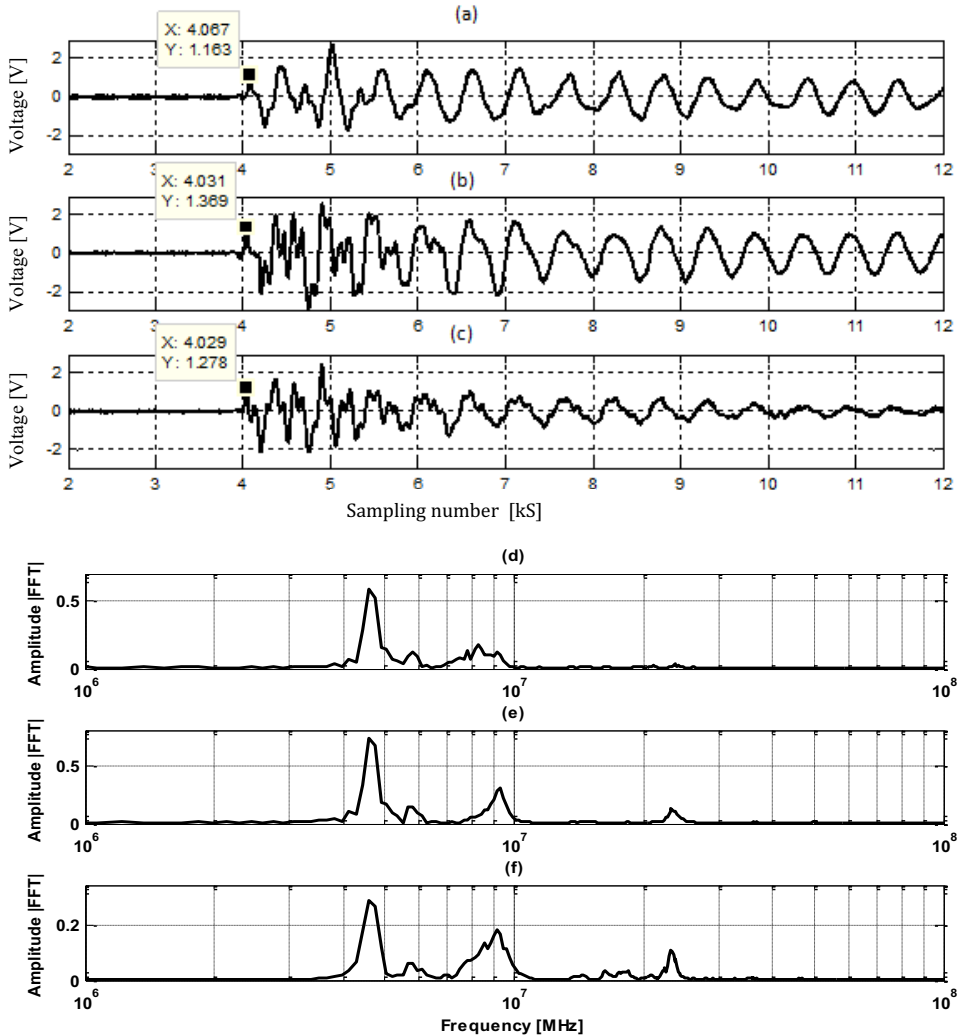
Fig. 5.11 Rogowski coil response for PD signals due to twisted-coil with energized AC power source; (a), (b), (c) in the time domain, (d), (e), (f) in the frequency domain for coils A, B and C, respectively.

It is revealed that the dominant frequency contents in this measurement are in the range of 3 MHz -10 MHz, which is slightly higher than the case of PD measurement using a pulse calibrator (offline measurement). The maximum amplitude of the PD signal measured in this setup is found to be 2.5 V which is almost 5 times higher than the PD signal measured after injecting the 50 nC calibrator pulse. The noise level for online measurement with the AC source is not clearly seen in the Fast Fourier Transform (FFT) plot due to higher PD amplitudes created in this set-up. Noise affected by the power line source and the energized 20 kV / 410 V AC transformer can be seen in the time domain plot.

5.1.2.2 PD produced by a tree leaning on the CC line

Fig. 5.1 is again referred to in this case. The distances between Rogowski coils were equally set to $L_{AB} = L_{BC} = 6.5$ m. The tree has been leaned at a distance of $L_B = 3.4$ m in section BC. The measured signals from the Rogowski coils in the time domain and frequency domain at points A, B, and C are shown in Fig. 5.12 (a - f). The maximum amplitude of the PD signal measured in this setup is found to be 7.6 mV. The dominant frequency content in this measurement is in the range of 3 MHz - 12 MHz.
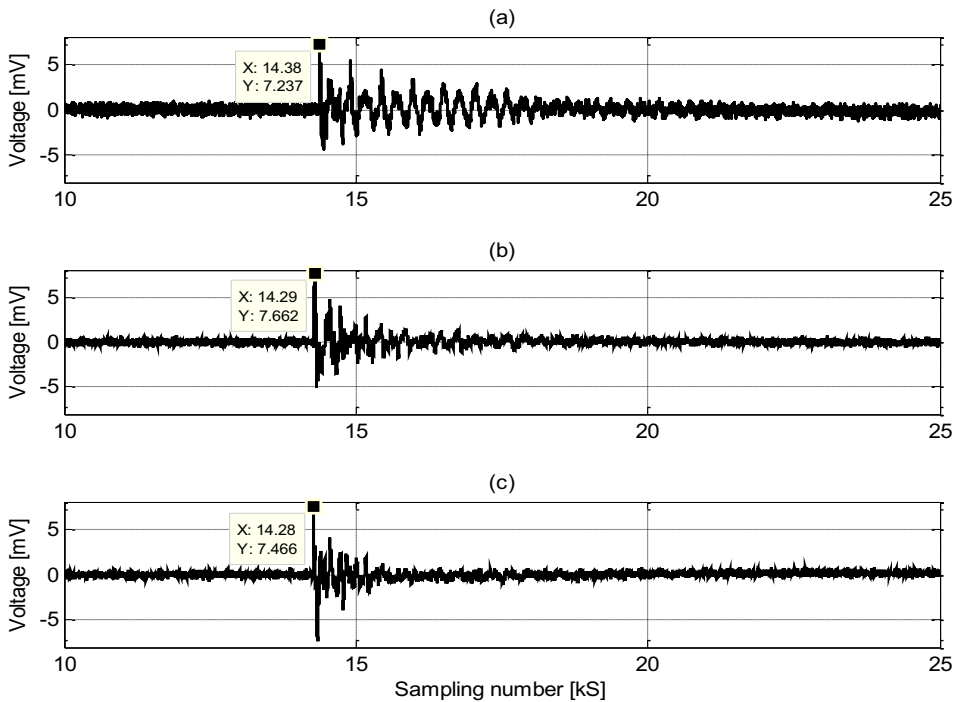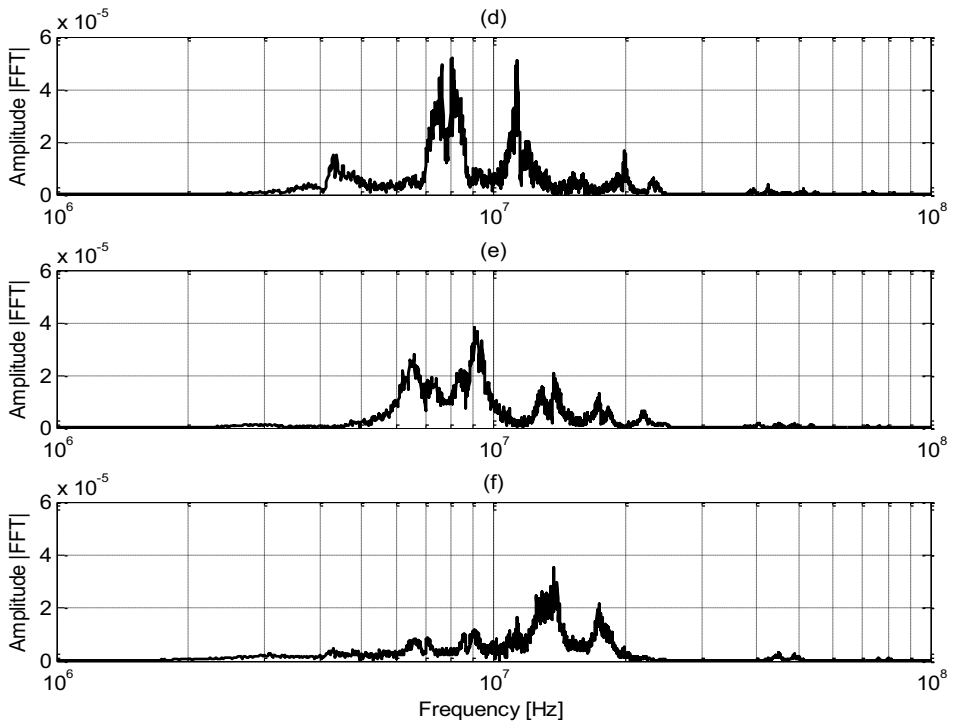
Fig. 5.12 Rogowski coil response for PD signals resulting from a tree leaning on the CC line; (a), (b), (c) in the time domain, (d), (e), (f) in the frequency domain for Rogowski coils A, B and C, respectively.

5.1.3   Discussions of the measurement results

For online measurement using a twisted-coil and a leaning tree, the ranges of PD signal frequency is a little higher (3 MHz - 12 MHz) compared to offline measurement using a pulse calibrator. These different PD signal frequency ranges produced by the two kinds of measurements are no surprise due to the different type of PD generator employed. However, the frequency range for the online measurement is acceptable for the PD source measurement caused by a leaning tree [3]. The Rogowski coil used in this measurement has a bandwidth from 500 kHz to 20 MHz. Therefore it does not respond to 50 Hz power signal. Output of Rogowski coil is linearly dependent on frequency of the measured current. The bandwidth of the Rogowski coil used was from 500 kHz to 20 MHz in which area it gives an accurate measurement result. Since the lower limit frequency of bandwidth is four decades above the fundamental frequency, 50 Hz is easy to filter out from the measured signals.

For the online measurement, the results obtained from the PD produced by a leaning tree is higher in magnitude compared to the result from the hand-made twisted coil. The magnitude of the PD pulse measured from the leaning tree is more realistic when compared to the real PD signal in a real outdoor scenario [3], [5]. Nevertheless, this difference does not

56

affect the main objective of the work, which is to develop and prove the efficiency of the PD locator algorithm.

From both offline and online measurements results, the PD source on the CC overhead line is possible to locate based on stamping time of arrival between the measured signals, using the locator algorithm presented in the next section. However, it is quite difficult to determine this accurately due to multiple signal peaks and the effect of noise appearance. In order to overcome this difficulty, a signal processing tool in the Matrix Laboratory (MATLAB) environment is employed which is explained below in Section 5.3.

5.2   Locator algorithm based on multi-end traveling wave-based PD location

Traveling wave principles have been used to locate faults in power networks and they are also suitable for locating PDs [67], [68]. However, there are aspects affecting the locator accuracy, such as the propagation velocity, identification of the arrival time of signals at the measuring points and the need for time synchronization for the multi-end locator type.

In fault location techniques, there are concepts used to eliminate the propagation speed needed for the locator function. One of these concepts applies simultaneously the principles of both single-end and multi-end locator functions [22]. However, such a concept cannot help to locate PD points where the single-end function is not appropriate for the PD signal detection. The other concept is by applying double-sided measurements with a minimum three measuring points [69], [100]. This concept can successfully help to locate the PD points.

From the network shown in Fig. 5.1, consider a PD which occurs in section AB of the conductor line. The PD source distances from sensors A, B and C can be calculated as follows:

$$L_B - L_A = (T_B - T_A)v \tag{5.1}$$

$$L_B - L_C = (T_B - T_C)v \tag{5.2}$$

$$L_A + L_B = L_{AB} \tag{5.3}$$

$$L_A + L_C = L_{AB} + L_{BC} \tag{5.4}$$

Where $(T_B - T_A)$ is the time difference of the PD arrivals between sensors B and A where its acronym is TD_{BA} and similarly $(T_B - T_C)$, TD_{BC}, is the time difference of PD arrivals between sensor B and sensor C. Solving the above equations yields:

$$L_B = \frac{1}{2}\left(L_{AB} - \frac{TD_{BA}}{TD_{BC}}L_{BC}\right) \tag{5.5}$$

$$L_A = L_{AB} - L_B \tag{5.6}$$

From Equations (5.5) and (5.6), the measured signal at the middle sensor B is considered the reference, to which the others are correlated. If the fault is in section BC, the locator equations

become:

$$L_B = \frac{1}{2}\left(L_{BC} - \frac{TD_{BC}}{TD_{BA}} L_{AB}\right)$$ (5.7)

$$L_C = L_{BC} - L_B$$ (5.8)

It is clearly seen from Equations (5.5) and (5.7) that the PD source locator algorithm proposed in this work does not depend on the value of the wave propagation velocity v, although the characteristic of propagation velocity v on CC line, still gives an impact on the arrival times stamped at measuring points. This locator algorithm is valid under circumstances that the measurements are synchronized and the PD faulty section is identified. The identification of the faulty section of the line can be based on the values of the arrival time and measured voltage at each Rogowski coil.

5.3 PD-time localization using chirp detector

Frequency Modulation (FM) is a technique that is used in communication systems to send information from one point to another by changing the instantaneous sinusoidal carrier frequency linearly with the message. In communication applications, the frequency modulation has the advantage of more robustness against the noise effect with increased bandwidth requirements. A frequency-modulated wave can be written generally in the form as:

$$s(t) = A\cos\left(2\pi f_0 t + 2\pi k \int_0^t m(\tau)d\tau\right)$$ (5.9)

where $m(.)$ is the message information that will cause frequency variations of the sinusoid, and k is a sensitivity factor. The instantaneous frequency of the waveform given above is as:

$$f_i(t) = f_0 + km(t)\,\text{Hz}$$ (5.10)

In [67], this transform has been used to evaluate the performance of chirp detector to localize earth faults in MV networks based on a traveling wave fault locator. Theoretically, a sudden frequency chirp or frequency modulation occurring in the measured signal at the Rogowski coil can be extracted using a frequency demodulator making it possible to identify an exact time of the chirp. In order to evaluate this information, the chirp detector is applied on the offline PD signal of the injected 20 nC pulse calibrator shown in Fig. 5.9 and the corresponding detected chirp is shown in Fig. 5.13. Fig. 5.14 shows the detected chirps of the PD signals due to the twisted-coil for the online measurements shown in Fig. 5.11. The noise impacts in Fig. 5.13 and Fig. 5.14 make it difficult to localize the PD signal source. Therefore, the measured signals are denoised before the chirp detector is applied and the corresponding results are shown

in Figs. 5.15 and 5.16 for offline and online measurements, respectively. The denoising is carried out using DWT as explained in the next chapter. After denoising the measured waveforms, the PD signals are more accurate to be localized.
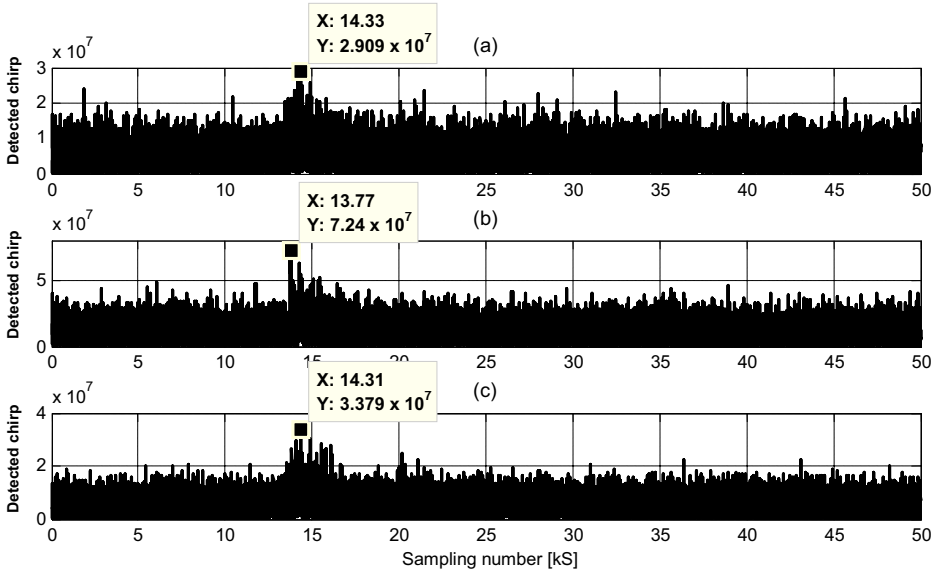
Fig. 5.13 Detected chirp of the PD signal without denoising measured at, (a) Rogowski coils A, (b) Rogowski coils B, and (c) Rogowski coils C, for the injected 20 nC calibrator pulse.
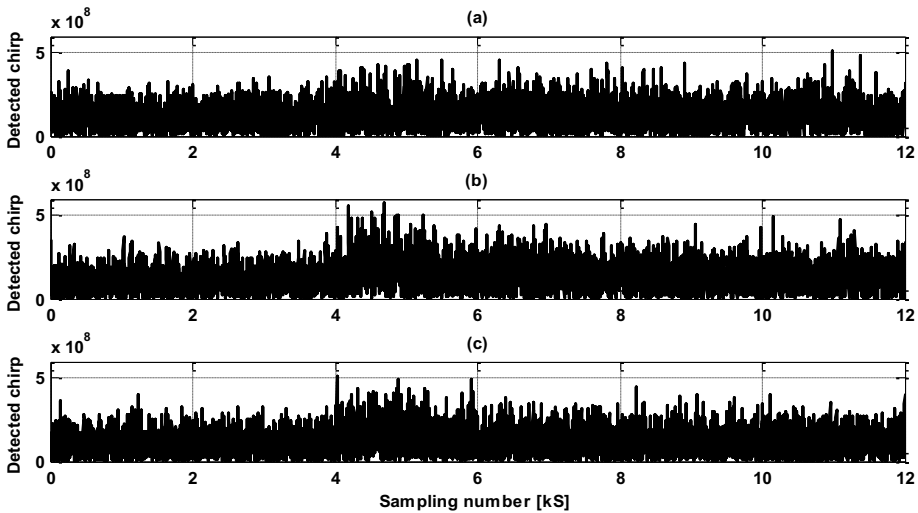
Fig. 5.14 Detected chirp of the PD signal without denoising measured at, (a) Rogowski coils A, (b) Rogowski coils B, and (c) Rogowski coils C, for PD signals due to the twisted-coil with energizing AC source.
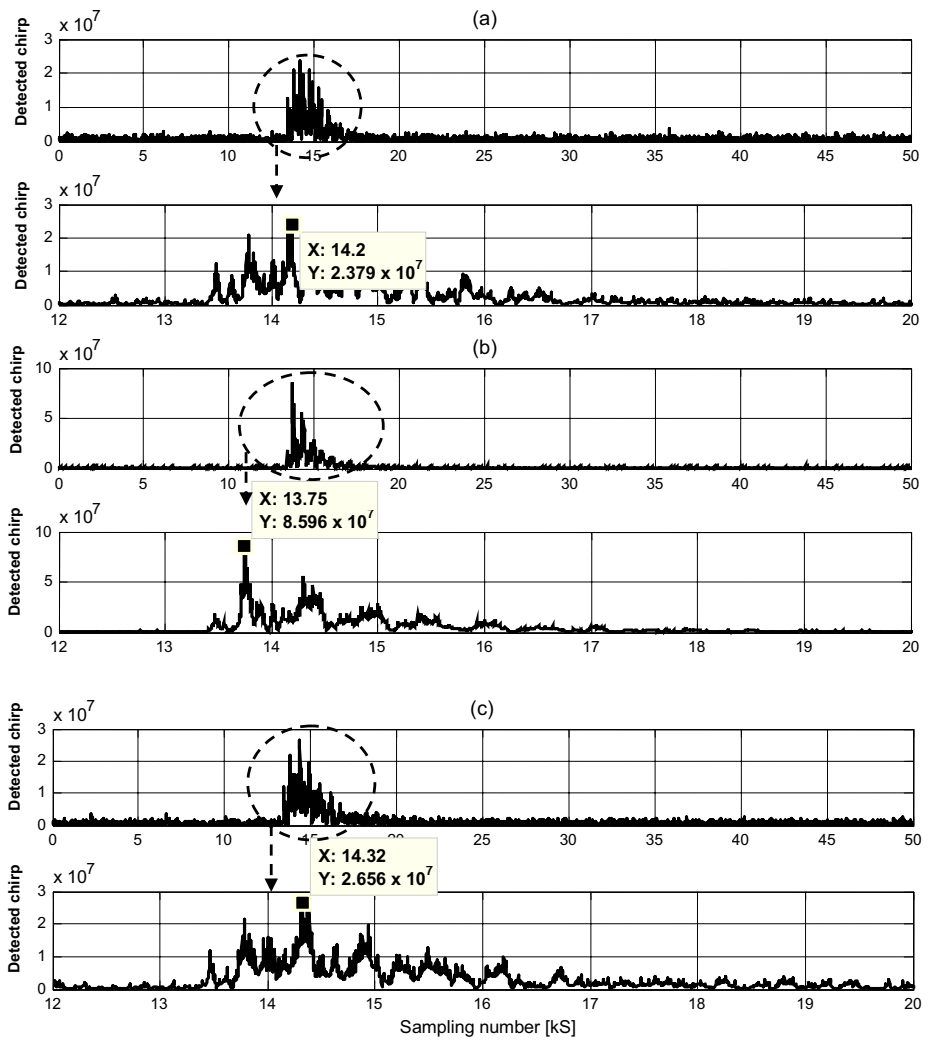
Fig. 5.15 Detected chirp of the denoised PD signal measured at, (a) Rogowski coils A, (b) Rogowski coils B, and (c) Rogowski coils C, for the injected 20 nC calibrator pulse.
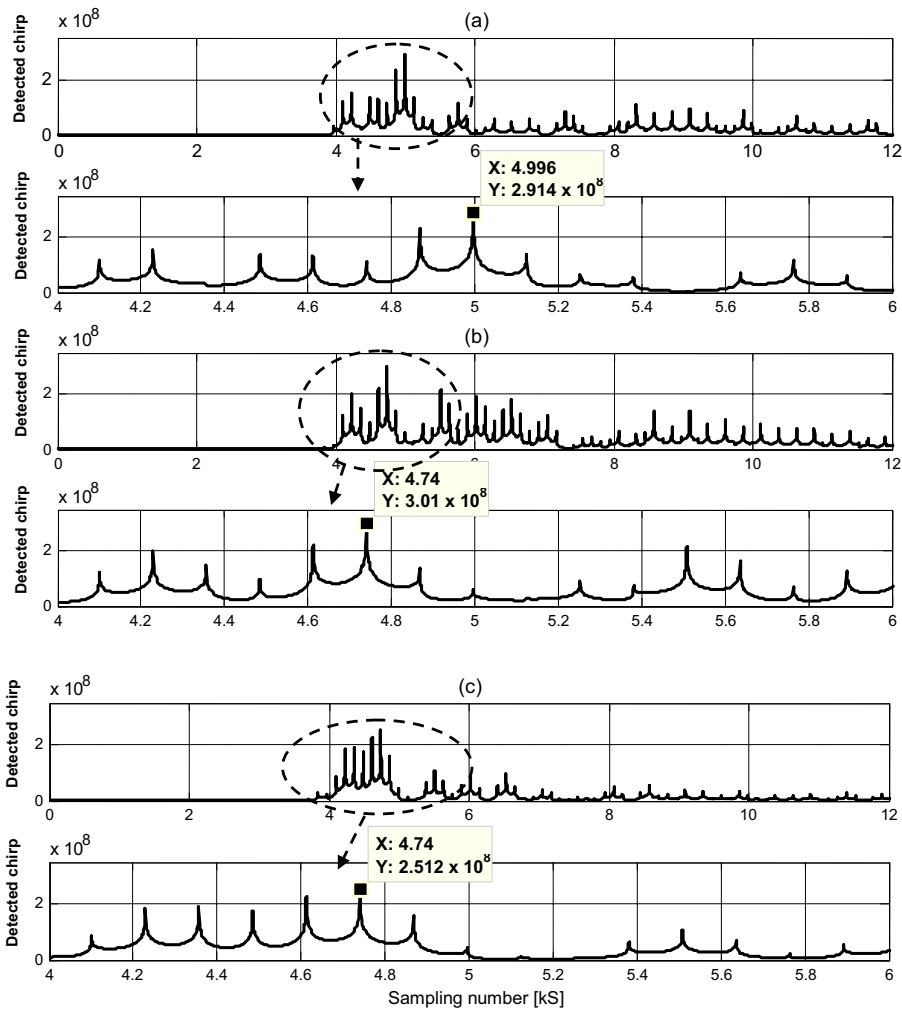
Fig. 5.16 Detected chirp of the denoised PD signal due to the twisted-coil measured at, (a) Rogowski coils A, (b) Rogowski coils B, and (c) Rogowski coils C, for online measurement with the energizing AC source.

Since there is no noise generated during the measurement of PD signals due to the leaning tree, no denoising processing is done to the measured signals in Fig. 5.12. Fig. 5.17 shows the detected chirp of the corresponding PD signals.
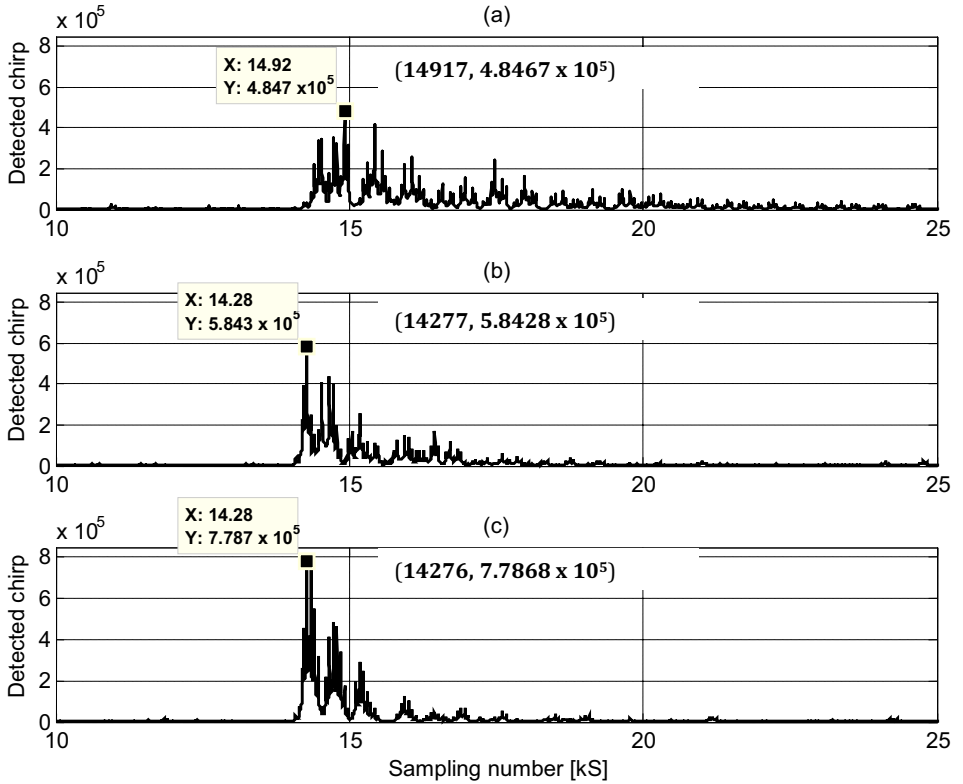
Fig. 5.17 Detected chirp of the PD signal caused by a leaning tree measured at, (a) Rogowski coils A, (b) Rogowski coils B, and (c) Rogowski coils C, for online measurement with the energized AC source.

Different from the previous time of arrival techniques which depend on the first peak of time stamping, the signal processing technique presented here identifies the arrival surge generated by the same PD source by taking the maximum value of the detected chirps signal. This criterion can help to overcome the denoising impacts on the signal without the chirp detector, where the low amplitude surges can be removed during the process. If the traveled PD surge is removed at one of the measuring nodes, it can produce an error because the locator will not be applied on signals of the same PD. Therefore, the highest PD surge of the chirp signal can help to select the time of arrival from the same PD surge source.

Referring to the result of the detector chirp in Figs. 5.15, 5.16 and 5.17, the distance of L_B for offline measurement is found to be 0.82 m using the locator (5.5) where the actual distance was 0.9 m in section AB. Meanwhile, the distances of L_B for online measurements are 2.5 m (for twisted-coil) and 3.24 m (for leaning tree) using the locator (5.7) where the actual

distances were 2.5 m and 3.4 m, respectively, in section BC. The results prove the validity of using a chirp detector as a signal processing tool in order to localize the PD source on a CC overhead line.

Due to the experimental limitations in the HV laboratory, the distances used in this work are clearly too short. In order to be able to use this algorithm to localize the PD in this compact experiment size, a good time resolution has been used where the sampling frequencies were 2.5 GHz and 2 GHz, which means that the sampling time is 0.4 ns and 0.5 ns respectively. At a wave velocity of 290×10^6 m/s, the distances covered between the two adjacent samples are 0.116 m and 0.145 m, which are acceptable with the networks size in meters as in the experiments. These sampling frequencies can be reduced when the algorithm is used in a real network, where the scale is in kilometers. In other words, a lower sampling frequency can be used in the field applications due to the long distances between the allocated sensors.

5.4 Discussion

The measurement analysis shows that the experimental measurement system and locator algorithm developed in this work performed well to detect and locate the PD signal source on the CC line. The PD signals initiated during offline and online measurements have different frequency ranges. These are due to the different source of PD signals created on the CC line. A pulse calibrator is used during offline measurement, while a twisted-coil and a leaning tree are used during online measurement. The results obtained from the laboratory measurements also confirm the capability of the Rogowski coil to measure the high frequency PD source on the CC line in consistency with the energized AC source.

For all the measured results, the high frequencies signals are extracted using a chirp detector. The performance of the chirp detector used as a signal-processing tool in this work gives good results in finding an accurate stamping time of arrival between the measured signals. The location of the PD signals source can be found using multi-end traveling wave fault locator principles. The multi-end traveling wave locator with the two-end synchronized measurements method gives in general a good accuracy for the PD location. However, it needs information about the wave propagation velocity over the feeder, which is a function of the feeder parameters, soil properties and tower configuration. In order to avoid the use of the propagation velocity, the multi-end fault locator of three synchronized measurements method can be applied. The algorithm of the PD source locator proposed in this work is advantageous since it does not need to know the propagation velocity of the traveling wave to locate the PD source. However, some improvements are still required for the PD locator algorithm and signal processing tool used, which is presented in the next chapter.

6- Multi-end correlation-based PD location technique for CC overhead distribution lines

6.1   Introduction to PD source location algorithm

Partial discharge (PD) measurements and the discharge location are of importance for the covered-conductor (CC) line, since the lifetime of the insulation material at any given voltages stress depends on the amount of discharges. The weakness of the insulation can be detected with the help of localization method. The cause of PDs, can in best case be removed before they result in an outage.

In this chapter, a multi-end correlation technique for locating PD sources on CC overhead lines is presented. The theory of maximum correlation factor is used in order to find the time differences between PD signal arrivals at three synchronized-measuring points. The location of the PD source is found using the same equation of locator algorithm in (5.5) and (5.7) which is based on the multi-end traveling wave technique.

This new proposed technique is a combination of three different stages of signal analysis: 1) denoising by applying discrete wavelet transform (DWT), 2) extracting the PD features using the absolute or windowed standard deviation (STD) and then, 3) locating the PD source by correlating the signals measured at the three Rogowski coils. Applying multi-end correlations between three measuring points as proposed in this chapter made it possible to identify the PD source location without knowing the exact propagation velocity of the signals. At the same time, this technique makes it is easier to identify the faulty section of line compared to the previous proposal explained in Chapter 5. The simulated study is performed using an Electromagnetic transient program-Alternative transient program (EMTP-ATP) environment with different use-cases and the algorithm is implemented in the Matrix Laboratory (MATLAB) signal processing toolbox. Afterwards locator technique is then verified using an experimental measurement signal.

The EMTP-ATP is used to implement and analyze a PD monitoring system model. The noise model is added to the simulated power network signals. The PD signals corrupted with noise are measured from a Rogowski coil which is utilized as a high frequency transducer. Then the DWT tool in MATLAB is used to implement the denoising process of the signals. The high frequency features from the resulting signals are extracted using the windowed STD before the multi-end correlation algorithm is employed. The algorithm outline developed and their derivatives are discussed in the next section.

6.2 Time difference of arrival (TDOA) estimation techniques

The time difference of arrival (TDOA) techniques are based on estimating the difference in the arrival times of the signals from the source at multiple sensors. This is usually accomplished by taking a snapshot of the signal at a synchronized time period at multiple sensors. Two general methods can be used to estimate the TDOA. The methods are by subtracting time of arrival (TOA) measurements from two measuring sensor terminals to bring into being a relative TDOA, or the use of correlation techniques, where the received signal at one measuring sensor is correlated with the signal received at another measuring sensor terminal [70], [100].

The first method is applicable if we have absolute TOA measurements. Superficially, there does not seem to be any advantage in converting TOA measurements into TDOA measurements, as we can localize the PD source location using the TOA measurement directly. However, using a TDOA technique may give us some increased accuracy when errors due to multiple signal reflections in pairs of TOA measurements are positively correlated because of having a common signal reflector. The more similar the errors in pairs of TOAs are, the more we can gain by changing them into TDOAs. However, this is practical only when we can estimate the TOA by having knowledge of the time of transmission. If we have no timing reference at the transmitter, then this method for estimating TDOAs cannot be used.

Because of the absence of a timing reference on the PD source to be located, the most commonly used technique for TDOA estimation is the correlation technique. The timing requirement for this method is the synchronization of all the sensors contributing in the TDOA measurement, which is more practical to achieve in most PD location applications. Because of these factors, we will discuss in detail only the correlation technique for estimating TDOAs.

Generally, a correlation method is a matching process showing the strength of relationship between any pair of variables through an appropriate mathematical formulation [27]. It is a measure of self similarity of a signal with its delayed version. The general model for the time-delay estimation between measured signals at two sensor terminals, $x_1(t)$ and $x_2(t)$, is given by [71]:

$$x_1(t) = A_1 s(t - d_1) + n_1(t) \qquad\qquad (6.1)$$
$$x_2(t) = A_2 s(t - d_2) + n_2(t) \qquad\qquad (6.2)$$

where A_1 and A_2 are the amplitude of the signal, $n_1(t)$ and $n_2(t)$ are the noise and interfering signals and d_1 and d_2 are the arrival times for the signal. Referring to the shortest time arrival and amplitudes to the signal, assuming $d_1 < d_2$, the models of (6.1) and (6.2) can be rewritten as:

$$x_1(t) = s(t) + n_1(t) \qquad\qquad (6.3)$$
$$x_2(t) = As(t - D) + n_2(t). \qquad\qquad (6.4)$$

A is the amplitude ratio and $D = d_2 - d_1$ = TDOA. The use of time delay estimation techniques

65

which provide resistance to noise and interference, and also the ability to resolve multipath signal components are required to achieve an accurate TDOA. Several techniques with varying degrees of accuracy and robustness have been developed to estimate TDOA. This includes the correlation technique [71].

Generalized cross-correlation (GCC) methods are referred as a conventional correlation technique that has been used to solve the problem to estimate the TDOA [71]-[78]. These methods cross-correlate pre-filtered versions of the received signals at two measuring sensor terminals, then estimate the TDOA between the two terminals as the location of the peak of the correlation. Pre-filtering is intended to accentuate frequencies for which the signal to noise ratio (SNR) is the highest and attenuate the noise power before the signal is passed to the correlator. As shown in Fig. 6.1, each signal $x_1(t)$ and $x_2(t)$ is filtered through $H_1(f)$ and $H_2(f)$, then correlated, integrated and squared. This is performed for a range of time shifts, τ, until a peak correlation is obtained.
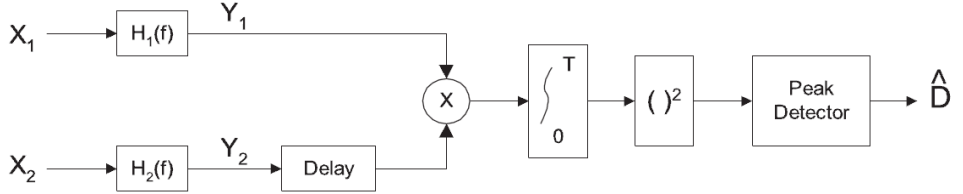
Fig. 6.1 The generalized correlation method for estimate the TDOA [71].

An estimate of the cross-correlation is given by [71]:

$$R_{x2x1}(\tau) = \frac{1}{T}\int_0^T x_1(t)x_2(t-\tau)dt \qquad (6.5)$$

where T represents the observation period. Equation (6.5) proposes the use of an analogue correlator. An integrated and dump correlation sensor of this form is one realization of a matched filter sensor [78]. The correlation process can also be implemented digitally, if sufficient sampling of the waveform is used. The output of a discrete correlation process using digital samples of the signal is given by [71]:

$$R_{x2x1}(m) = \frac{1}{N}\sum_{n=0}^{N-|m|-1} x_1(n)x_2(n+m)dt . \qquad (6.6)$$

These TDOA estimation methods have been shown to be effective in reducing the effect of noise and interference [74]. Nevertheless, if the noise and interference $n_1(t)$ and $n_2(t)$ in (6.3) and (6.4) are both temporally and spectrally coincident with $s(t)$, there is little that correlation methods can do to reduce the undesirable effects of this interference. In this situation, correlation methods encounter two problems. First, correlation methods experience a resolution problem. These methods require the differences in the TDOAs for each signal to be greater than the widths of the correlation functions so that the peaks can be resolved. Consequently, if the TDOAs are not sufficiently separated, the overlapping of correlations can introduce significant

errors in the TDOA estimation. Second, if $s(t)$, $n_1(t)$ and $n_2(t)$ are resolved, correlation methods must still identify which of the multiple peaks is due to the signal of interest and interference. These problems arise because the methods are not signal selective and produce TDOA peaks for all signals in the measured data, unless they are spectrally disjoint and can be filtered out [73].

6.3   Multi-end correlation-based technique for PD location

Considering a multi-end locator algorithm (5.5) or (5.7), as discussed in Section 5.2 in Chapter 5, a new PD source location technique is proposed based on multi-end correlation of high frequency impulse signals measured using three allocated Rogowski coils. The GCC method is used as a correlation function. The wavelet function is used to extract and denoise the high frequency response from the voltage signals measured by the sensors. The algorithm based on the maximum correlation factor of the respective signals is developed to determine the time differences, TDOA between PD arrivals at different points [87].

Referring back to the network shown in Fig. 5.1, for a PD occurring in section AB of the conductor line, this locator algorithm, (5.5) or (5.7), is valid if the measurements are synchronized. In order to implement the proposed algorithm, the PD faulty section of the line and the time differences TD_{BA} and TD_{BC} have to be known. The time differences TD_{BA} and TD_{BC} are found using the proposed multi-end correlation algorithm. Towards identifying the faulty section, the information of the time differences TD_{BA} and TD_{BC} can be helpful. For example, if the PD is in section AB, TD_{BC} represents the traveling time over section BC and therefore TD_{BC} is close to L_{BC} / v; however, TD_{BA} is lower than and not close to L_{AB} / v, with a difference depending on the PD location. Similarly, if the PD point is in section BC, TD_{BA} is close to L_{AB} / v; however, TD_{BC} is not close, with a lower value than L_{BC} / v. The propagation velocity does not contribute in calculating the PD distance but it is used only and simply for identifying the PD faulty section.

In this work, the correlation process between measurements is exploited to accurately identify the time differences which are going to be used in the aforementioned traveling wave locator. The benefit of using the correlation is to overcome the complexity of identifying the arrival times of PD signals, where such difficulties can be due to the level of noise and irregular signals appearance of the PD signal [100].

In a digital form, the correlation formula, CR that is used between two vectors WF_B and WF_A is a multiplication and then summation process of n samples of these two sampling windows WF_B, and WF_A, as in [87]:

$$CR_{BA} = \sum_{j=1}^{n} WF_B(j).WF_A(j) \qquad (6.7)$$

where $WF_B(.)$ and $WF_A(.)$ are the two synchronized windows of n samples measured at nodes B and A, respectively. Rogowski coils are located at these nodes, as shown in Fig. 5.1. This correlation factor is not the maximum one because the signals do not usually arrive simultaneously. In certain circumstances, where the PD location is at the middle point in section AB, the correlation between $WF_B(.)$ and $WF_A(.)$ is the maximum, because the PD signal arrives at the same time at the measuring nodes A and B. In other circumstances, the computed CR_{BA} is not the maximum one as mentioned above. In order to compute the maximum correlation factor CR_{BA}, the window $WF_A(.)$ is rotated in increments of one sample. $WF_B(.)$ is fixed as it is taken to be the reference. The CR_{BA} is computed by considering each increment until the nth shifting degree is reached. The maximum rotating degree is n because there are n number of samples of the window $WF_A(.)$. After computing the correlation factor CR_{BA} against the rotating degree, the corresponding degree that gives the maximum correlation factor can be identified. This degree represents the time difference TD_{BA} between the arrivals at measurement points B and A. The advantage of using the maximum correlation factor is that there is no need to use a certain function in order to identify the arrival instants at the measuring nodes. Similarly, the time difference TD_{BC} between nodes B and C can be computed by estimating the shifting degree that corresponds to the corresponding maximum correlation between the Rogowski measurements at nodes B and C.

Fig. 6.2 shows the proposed algorithm implementation, where the Rogowski coil measurements are loaded in windows of n samples, $WS_A(.)$, $WS_B(.)$ and $WS_C(.)$. The number of samples n in the window can be selected based on the distance between allocated Rogowski coils because the window size n is a time length and it should be suitable to extract the time differences between the arrival signals. It is assumed the Rogowski coils are separated by distances of 4 km as discussed in [5]. Then, the denoising process can be applied on the window samples using discrete wavelet transform (DWT) tools and discussed in Section 6.5.2. The windows $WF_A(.)$, $WF_B(.)$ and $WF_C(.)$ of the suitable features are used to apply the multi-correlation principles and therefore to estimate the time differences TD_{BA} and TD_{BC} by finding the maximum correlation degree. Evaluating TD_{BA} and TD_{BC} helps to identify the faulty section and therefore apply the suitable locator algorithm (5.5) or (5.7).

One of the features of the PD sources is that the PD signal generation is repeated as soon as there is an active PD fault. This makes it a challenge to apply the traveling wave locators by identifying the arrival times of the corresponding PD pulses at different measuring points. However, more than one PD signal in the synchronized windows increases the correlation factor, CR and therefore supports its maximum finding. Meanwhile, the accuracy of the TDOA estimates which are calculated by multi-end correlation procedures also depends on the sampling rate of the signals. Usually, the higher the bandwidth of the incoming signals the higher the sampling rate of the system. However, even a signal with a comparatively narrow

bandwidth can give more accurate TDOA estimates, if its sampling rate is increased. The reason is that as we increase the sampling rate of the system, the time quantization error in TDOA decreases. In this work, the sampling rate at 100 MHz is used in the simulated study, and 2.5 GHz is used in the laboratory measurements. Low sampling rate is chosen in simulation to avoid long execution times taken for each of the fault cases.
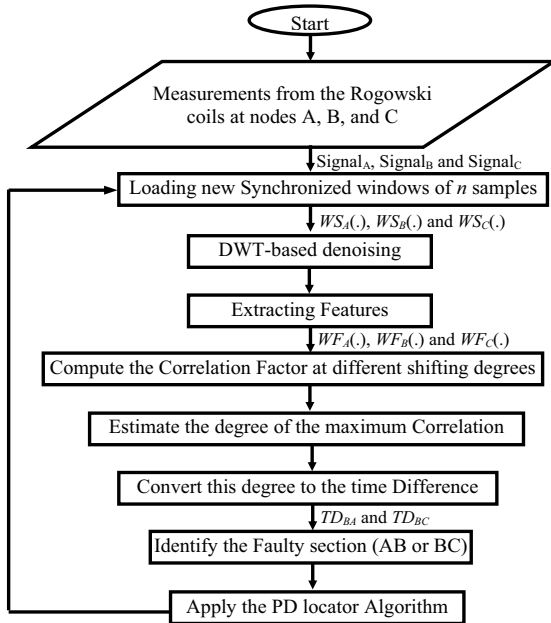
Fig. 6.2 An algorithm developed for PD source location technique [87].

Towards implementing sliding windows, there is no need to load any sample to slide windows $WS_A(.)$, $WS_B(.)$ and $WS_C(.)$. However, loading completely new windows exactly measured after the previous window can be implemented. For example:

$$WS_B(1:n) = \text{Signal}_B(k+1:k+n)$$
(6.8)

where k is a constant and equals $0,1,2,\ldots$ and Signal_B is the signal measured from the Rogowski coil at node B.

6.4   Simulated study

A three-phase PD monitoring system for CC overhead in distribution lines has been modeled using the EMTP-ATP simulation environment, where ATPDraw is used as a preprocessor [56]-[60], [63], [64]. As shown in Fig. 5.1, the CC overhead line feeder is energized by AC sinusoidal waveforms via a 110/20 kV, delta/star transformer. The CC overhead lines is represented using a JMarti frequency model, where the feeder configuration is:

8 m height, 0.4 m distance between the CC, 9.7 mm diameter over the conductor, 14.3 mm diameter over the covered conductor, 0.493 Ω/km conductor resistance and 200 Ω.m soil resistivity.

The Rogowski coils are located on the CC lines at distances of 4 km ($L_{AB} = L_{BC} = 4$ km). The Rogowski configuration and its equivalent simulated circuit are shown in Figs. 2.2 and 2.3, where the number of turns is 1900 with an inner diameter of 101 mm and an outer diameter of 109 mm as shown in Table 5.1. The corresponding equivalent circuit is $R_l = 63$ Ω, $L_l = 0.191$ mH and $C_l = 51.6$ pF, with a terminating impedance of $Z_{out} = 3$ kΩ. This trial model and its parameters have been experimentally verified where the model showed good performance up to 29 MHz [70], [100].

Based on the PD pulse shape produced and its characteristic caused by the tree leaning on the CC overhead line as presented in [3], [5], [55], two methods to generate the PD pulse have been employed during the simulation work in this thesis. For the simulation work in Chapters 3 - 4, the pulse calibrator has been used to create the PD pulse in the CC line. This method, however can produce only one PD pulse at a time during the simulation.

But for the simulation work in this and the following chapter, the PD signal has been numerically modeled and simulated using the function of damped exponential pulse (DEP) in order to generate multiple PD pulses in the CC line. This current source function is given by [62]:

$$i(t) = A[10^{-1.3(t-t_o)/\tau} - 10^{-2.2(t-t_o)/\tau}]. \tag{6.9}$$

The Fortran expressions were exploited to implement (6.9) and then interacted with the feeder as a transient analysis control system (TACS) controlled current source type 60 as shown in Fig. 6.3. A is the amplitude of the PD pulse, t_o is the time of PD occurrence, and τ is the damping factor of the PD pulse. A set of three PD pulses is adopted in this work where their parameters are listed in Table 6.1.

Table 6.1 Parameters of 3 PD pulses

No.	$A(mA)$	$t_0(\mu s)$	$\tau(\mu s)$
1	14.83	30	0.08
2	13.50	60	0.08
3	12.75	90	0.08

Damped exponential pulse (DEP) as PD signal

TACS controlled current source type 60

Fortran expressions
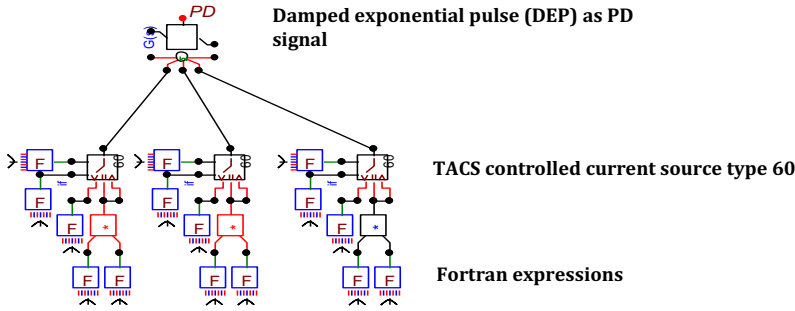
Fig. 6.3 EMTP-ATP simulated PD pulse using TACS expression in ATPDraw.

Concerning the fault point in section AB shown in Fig. 5.1, where its location is 2.5 km from point B, the corresponding waveforms taken are depicted in Fig. 6.4, where Fig. 6.4(a) shows the PD signals and Figs. 6.4(b), (c) and (d) show the Rogowski coil responses for the PD signal traveling from the source in both directions along the CC lines. These three signals are $Signal_A$, $Signal_B$ and $Signal_C$ measured at nodes A, B and C, respectively. Directly applying the correlation function (6.7) on the synchronized windows of these signals $(WS_A(.), WS_B(.)$ and $WS_C(.))$ cannot help. Therefore, computing the absolute values of the samples of these windows is considered before calculating CR_{BA} and CR_{BC}, where the new windows are called $WF_A(.),$ $WF_B(.)$ and $WF_C(.)$. The corresponding results are shown in Fig. 6.5. In Fig. 6.5(a), the maximum CR_{BA} value is at correlation degree 343, which means that window $WF_A(.)$ is rotated by 343 samples in order to get the maximum CR_{BA}. Accordingly, TD_{BA} is 3.43 μs where the sampling frequency is 100 MHz. In Fig. 6.5(b), the maximum correlation between $WF_B(.)$ and $WF_C(.)$ is at shifting degree of 11130, which means $WF_C(.)$ is rotated by 11130 samples or 111.30 μs to find the maximum correlation. Such a rotation is greater than half of the window length and therefore the time difference is negative and is computed as $TD_{BC} = 111.3 - 125 = -$ 13.7 μs. In order to understand what a negative TDOA implies, the implementation of the phasors in polar form can be helpful. If the phasor is shifted by zero time with respect to a reference phasor, the angle is zero. If the phasor is shifted by a quarter of the phasor time constant with respect to the reference, the phasor angle is $\pi/2$. If the phasor is shifted by three quarters, the angle is $-\pi/2$. Therefore, the negative means that the rotating time is greater than half of the signal time constants. In the present study, the maximum rotation can be the window length, which is considered to be 12500 samples. Therefore, if the time difference TDOA is greater than a half of the window size, it is presented as a negative value, as it is done in Fig 6.5(b).

Evaluating $TD_{BA} = 3.43$ μs and $TD_{BC} = -13.7$ μs with respect to the traveling time over the section in turn, TD_{BA} is very low while TD_{BC} is very close. Therefore, the faulty section is AB and then the locator function in (5.5) is used. It is found that $L_B = 2.501$ km and therefore L_A

71

= 1.499 km.
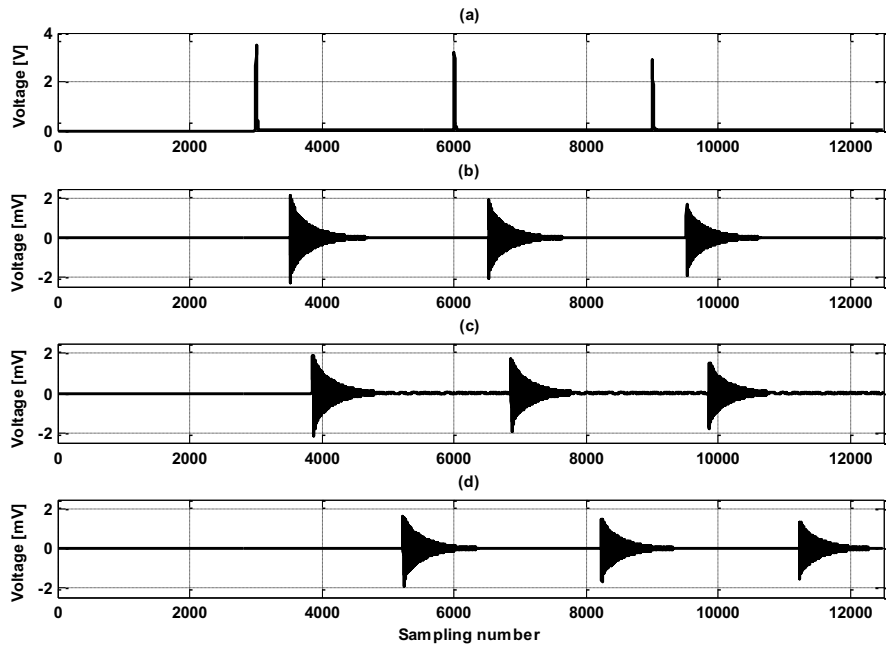
Fig. 6.4 Results from simulation. (a) PD pulse source at the fault point, (b) Rogowski coil responses at sensor A, (c) at sensor B, and (d) at sensor C.
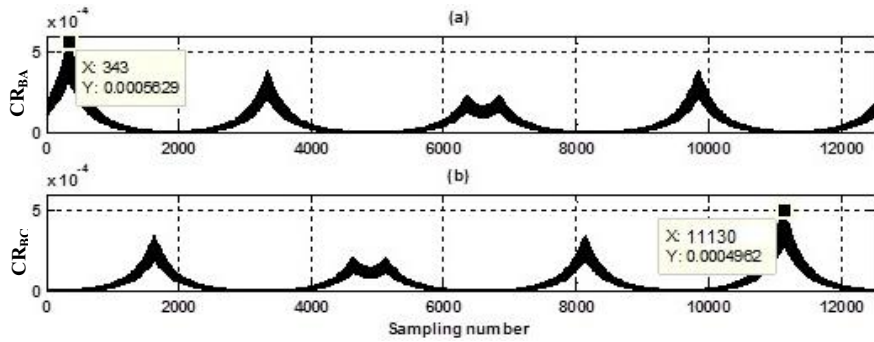
Fig. 6.5 Correlation results. (a) Between sensors B and A, (b) between sensors B and C.

6.5   PD with noise modeling

For online PD measurement, the denoising technique is one of the most important things to consider. Different types and levels of noise all produce an effect on the signals that are measured. There are two noise types which are mostly observed during online PD measurement. These types are the narrowband noise spectrum and the broadband noise spectrum. Narrowband noise interferences are such as discrete spectral interference (DSI) caused by a radio broadcast signal, periodical pulse shaped disturbances from power electronics equipment and stochastic pulse shaped disturbance due to lightning or switching operations. Meanwhile, white noise which is caused by the measuring instrument itself is known as broadband interference. In the published literature, DWT has shown good performance when denoising online measured PD signals [3], [79]-[82].

6.5.1   Noise modeling

The performance of the proposed locator was tested with different noise conditions and types. Detection and location of online or on-site PD signals are not free from strong coupling of external noise. Therefore, two noise models are used, the DSI and Gaussian white noise (GWN) models, in order to evaluate the proposed locator. Their implementation is carried out by exploiting facilities of the TACS expressions in the EMTP-ATP. DSI is generated at four different frequencies from 500 kHz to 1.5 MHz, as reported in [81]. GWN is generated using the model addressed in [83]. A brief illustration of these noise models is presented as below.

All noise was simulated with the DSI and GWN mathematical models. DSI was generated at four different frequencies, 500 kHz, 800 kHz, 1 MHz and 1.5 MHz. The maximum magnitudes were 3 mV using the sinusoidal equation as in [81]:

$$DSI(t) = A_{max} \sum_{i=1}^{N} \sin 2\pi f_i t \qquad (6.10)$$

where f_1 = 500 kHz, f_2 = 800 kHz, f_3 = 1 MHz, and f_4 = 1.5 MHz. GWN was generated using the proposed mathematical equation as in [83]:

$$S_n = \sigma_n \sqrt{-2 \log(A)} \times \cos(2\pi B) \qquad (6.11)$$

where A and B are random numbers, which are independent and are distributed uniformly from 0 to 1. These random numbers are implemented in an ATPDraw environment using the TACS expression (RAN) with two different seeds. σ_n is the estimated noise standard deviation. The magnitude for this noise was 1.8 mV.

Both of these noise models were used because they are regularly found in conducted PD measurements [3]. They and their frequency spectrums are shown in Fig. 6.6.

73
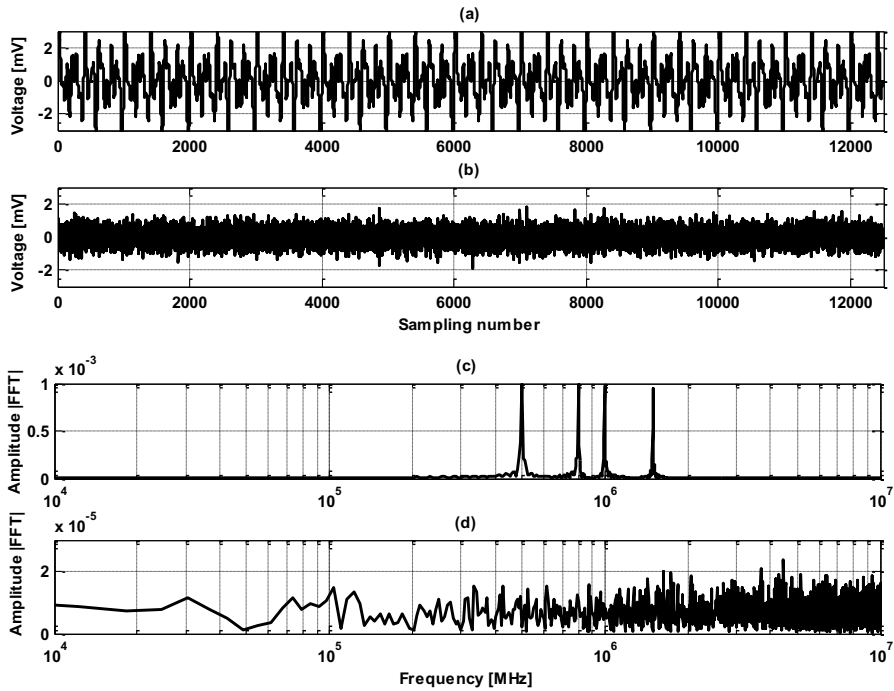
Fig. 6.6 Simulated noises and their spectra, (a) DSI, (b) GWN, (c) DSI frequency spectrum, (d) GWN frequency spectrum.

These noise signals were used to corrupt the primary currents in the Rogowski coils. Accordingly, four different cases are generated as following. Case 1 is the performance without considering the noise impact, as in the aforementioned test case shown in Fig. 6.4. Case 2 is when the noise is simulated using a DSI model, and the corresponding Rogowski coil waveforms at points A, B and C are shown in Fig. 6.7. Case 3 is when the noise is simulated using a GWN model, where the corresponding waveforms are shown in Fig. 6.8. Case 4 is when DSI and GWN are both added, for which the waveforms are shown in Fig. 6.9.
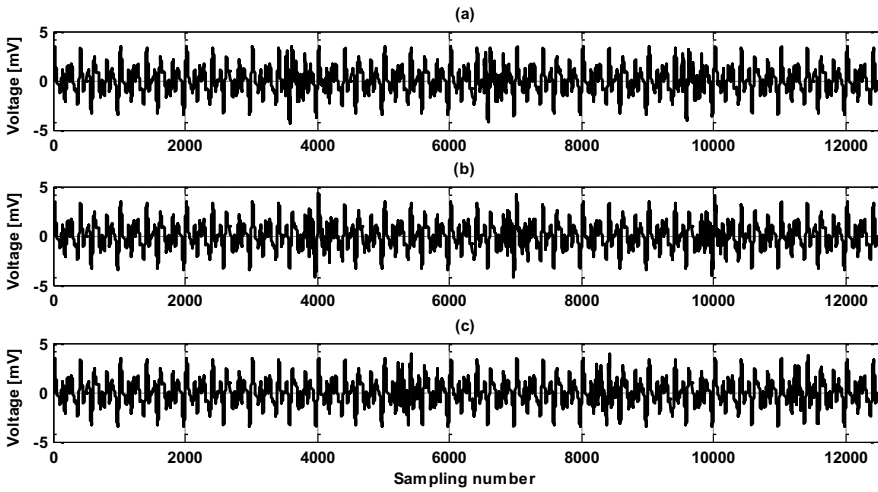
Fig. 6.7 Simulated original PD signal corrupted with DSI noise model measured. (a) Signal$_A$ at sensor A, (b) signal$_B$ at sensor B, (c) signal$_C$ at sensor C.
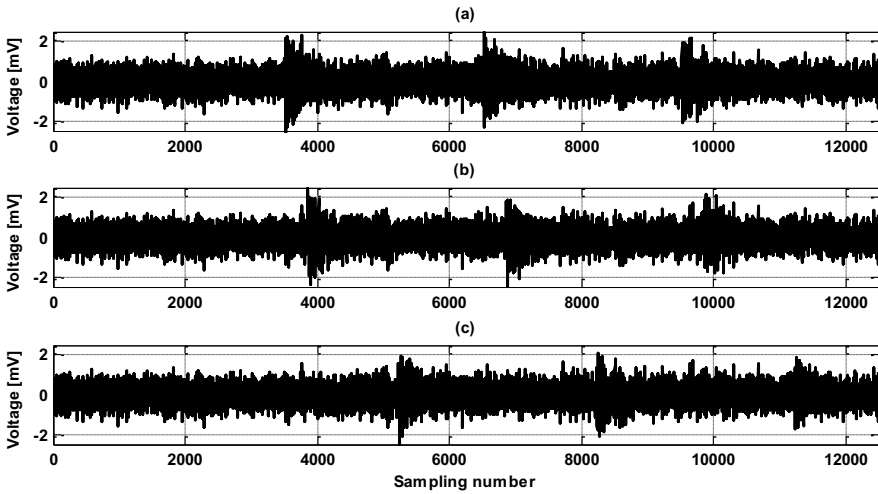
Fig. 6.8 Simulated original PD signal corrupted with GWN measured. (a) Signal$_A$ at sensor A, (b) signal$_B$ at sensor B, (c) signal$_C$ at sensor C.
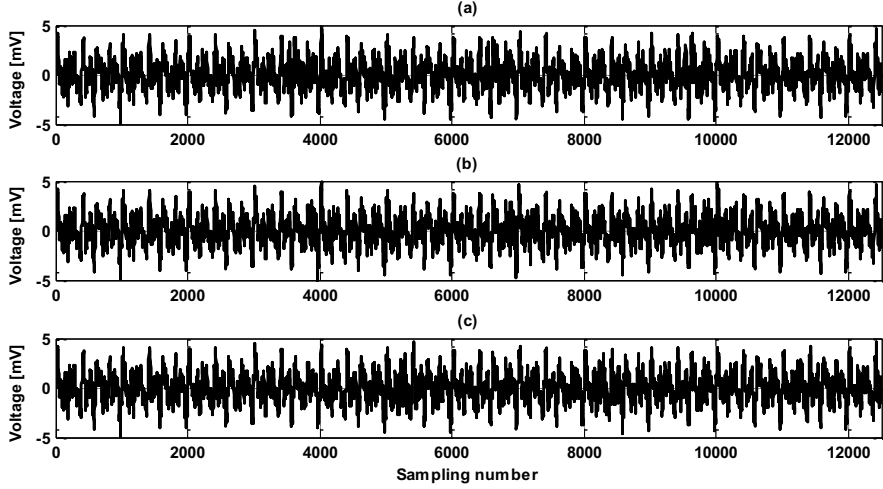
Fig. 6.9 Simulated original PD signal corrupted by both DSI and GWN measured. (a) Signal$_A$ at sensor A, (b) signal$_B$ at sensor B, (c) signal$_C$ at sensor C.

From Figs. 6.7 to 6.9, the noises obviously make it challenging to locate the PD signals. The denoising technique is performed before evaluating the PD source locator. The denoising and extraction of noisy PD signals were performed using DWT-based feature extraction. A brief summary on DWT is given in the next section.

6.5.2 DWT-based denoising

Since the PD signals are non-stationary and transient in nature, their energy spreads over the whole band and merges with noise if extracted using continuous and periodic base (sine and cosine) functions [84]. Furthermore, it is difficult for conventional numerical algorithms, such as Fast Fourier Transform (FFT), to achieve both high frequency resolution and accurate time location. Therefore, DWT techniques are viable and superior in rejecting different kinds of interference from the noisy signal [85].

Wavelets are families of functions generated from one single function, called the mother wavelet, by means of scaling and translating operations. The scaling operation is used to dilate and compress the mother wavelet to obtain the respective high and low frequency information of the function to be analyzed. Then the translation is used to obtain the time information. In this way a family of scaled and translated wavelets is created and it serves as the base for representing the function to be analyzed [79]. The DWT is in the form as:

$$DWT_\psi f(h,k) = \frac{1}{\sqrt{a_o^h}} \sum_n x(q)\psi(\frac{k - qb_o a_o^h}{a_o^h})$$

(6.12)

76

where $\psi(.)$ is the mother wavelet that is discretely dilated and translated by a_o^h and $q b_o a_o^h$, respectively. a_o and b_o are fixed values with $a_o > 1$ and $b_o > 0$. h and q are integers. In the case of the dyadic transform, which can be viewed as a special kind of DWT spectral analyzer, $a_o = 2$ and $b_o = 1$. DWT is implemented using a multi-stage filter with down sampling of the output of the low-pass filter.

Three steps using the general wavelet procedure have been performed for denoising the PD signal. These steps are wavelet decomposition, manipulating wavelet coefficients, and wavelet reconstruction. Fig. 6.10 shows the proposed algorithm implementation in the denoising process.
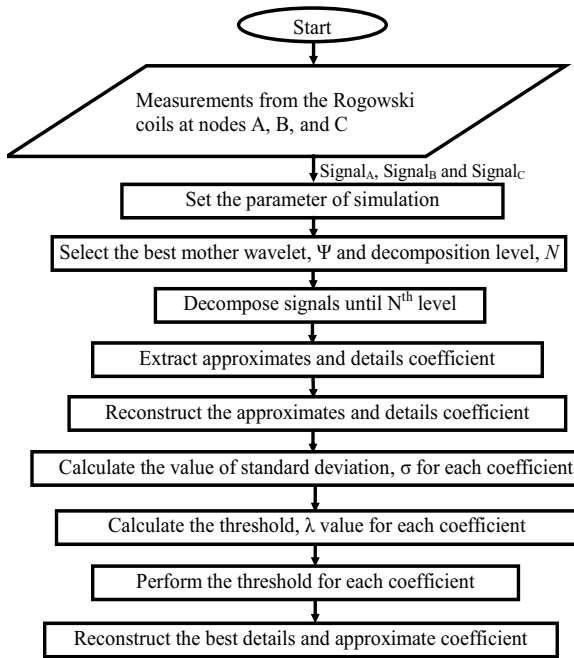
Fig. 6.10 An algorithm developed for denoising of PD signals [87].

6.5.2.1 DWT decomposition

The DWT is a tool that divides up data, functions or operators into different frequency components, and then studies each component with a resolution matched to its scale. The number, N, of decomposition levels selected should ensure that the DWT decomposition has enough frequency resolution to distinguish PD-associated coefficients from the noise at a certain scale. The maximum number of decomposed levels for a signal is as determined by [85]:

$$N = fix(\log 2n) \qquad (6.13)$$

where n is the length of the signal and N is rounded up to its nearest integer. In this work, six

and nine levels of wavelet decomposition have been selected for the simulation studies and for the laboratory measurements, respectively. Biorthogonal 2.4 (bior 2.4) has been found to be the appropriate mother wavelet as it produced the best performance for the correlation task. The smallest error between the original signal and the reconstructed signals was the criterion considered for selecting this wavelet, as mentioned in [68].

6.5.2.2 Threshold determination

The threshold value must have the ability to discard the coefficients related to noise and store the PD related ones for signal reconstruction. Therefore, its selection plays an important role in the denoising process, especially for online PD detection and measurement. In this work, the automated threshold technique addressed in [79] was modified to estimate the level of noise in the processed PD signal. The threshold value for each level is determined using:

$$\lambda_j = \frac{\sigma_j}{0.6745 j} \sqrt{2 \log_2 n_j}$$

(6.14)

where λ_j is the threshold value at level j, σ_j is the standard deviation of the wavelet coefficients and n_j is the length of the wavelet coefficients. Normally, the first level detail coefficient in the DWT contains higher information of the noise level for a noisy PD signal. The automated threshold is implemented in MATLAB using the Hard Threshold function as it shows better performance for PD signal processes than the Soft Threshold function.

6.5.2.3 Reconstruction

The PD signals were reconstructed after applying the automated threshold concept on each coefficient detail up to $N = 6$ levels. The reconstructed PD waveforms, after the denoising process of the PD signals depicted in Figs. 6.7, 6.8 and 6.9, are shown in Figs. 6.11, 6.12 and 6.13, respectively. From these Figures, the PD signals are more obvious and they can be used for applying the correlation and then the locator. The performances of the DWT-based denoising were evaluated by comparing the signal to noise ratio (SNR) before and after the denoising (SNR$_{den}$) process, as summarized in Table 6.2. The SNR is calculated using Equations (6.15) and (6.16), which is used in [79], and it is significantly reduced after the denoising process.

$$SNR = 10 * \log \frac{\max(signal)}{\max(noise)}$$

(6.15)

$$SNR_{den} = 10 * \log \frac{\max(signal_{den})}{\max(noise)}$$

(6.16)
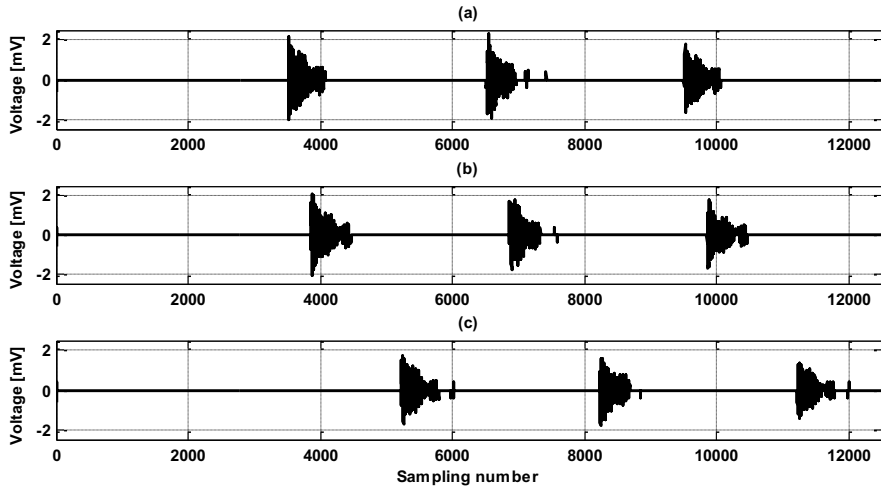
Fig. 6.11 Extracted denoised PD signals of Fig. 6.7. (a) Signal$_A$ at sensor A, (b) signal$_B$ at sensor B, (c) signal$_C$ at sensor C.
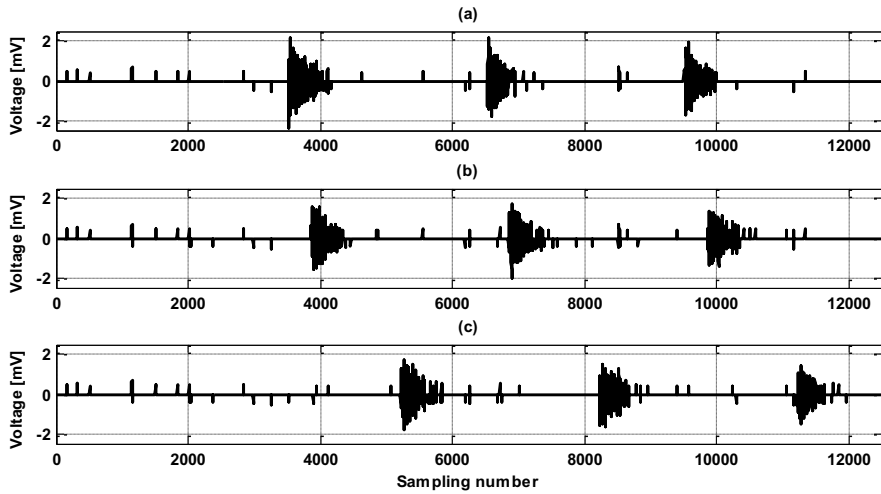
Fig. 6.12 Extracted denoised PD signals of Fig. 6.8. (a) Signal$_A$ at sensor A, (b) signal$_B$ at sensor B, (c) signal$_C$ at sensor C.
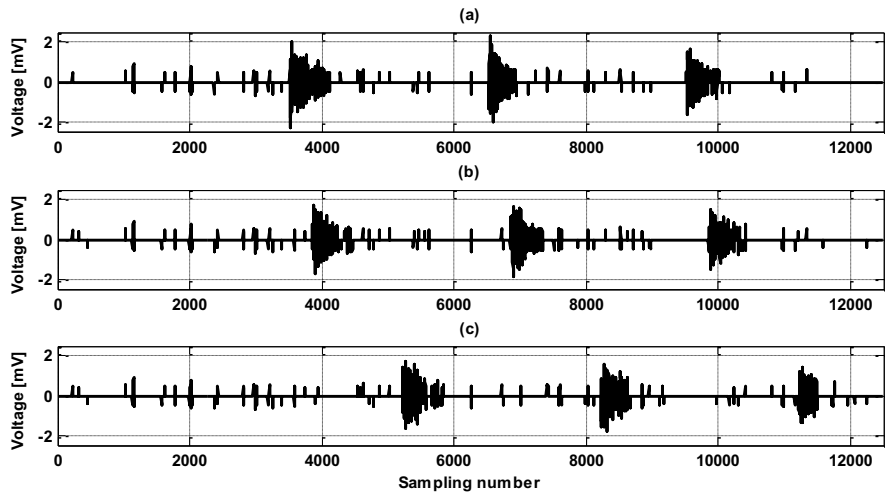
Fig. 6.13 Extracted denoised PD signals of Fig. 6.9. (a) Signal$_A$ at sensor A, (b) signal$_B$ at sensor B, (c) signal$_C$ at sensor C.

Table 6.2 Details of DWT denoising performance

PD Signal		SNR (dB)	SNR$_{den}$ (dB)
Comparing Figs. 6.7 and 6.11	Signal$_A$	-17.27	-0.022
	Signal$_B$	-16.57	-0.024
	Signal$_C$	-16.19	-0.793
Comparing Figs. 6.8 and 6.12	Signal$_A$	-7.33	-0.667
	Signal$_B$	-6.62	-0.203
	Signal$_C$	-6.25	-0.959
Comparing Figs. 6.9 and 6.13	Signal$_A$	-17.71	-0.724
	Signal$_B$	-17.01	-0.241
	Signal$_C$	-16.63	0.925

Although in this denoising evaluation, the periodical pulse shaped disturbances (pulse-noise-like PD), for example from power electronics equipment and telecommunication signals and stochastic pulse shaped disturbance due to lightning or switching operations have not been evaluated, there is already published work related to this matter which can be consulted in [62], [82].

6.6   Algorithm evaluation after DWT-based denoising

Figs. 6.14, 6.15 and 6.16 show the correlation factors CR_{BA} and CR_{BC} using the denoising waveforms shown in Figs. 6.11, 6.12 and 6.13, respectively. From these figures, the time differences CR_{BA} and CR_{BC} are determined and summarized in Table 6.3. This table shows

the corresponding performance of the proposed locator. The error is increased to 0.3725 % due to the effects of the noise and its removal. This error is computed by:

$$\varepsilon_B \% = \frac{\text{Actual } L_B \text{ - Computed } L_B}{L_{AB}} \times 100\% \tag{6.17}$$

Table 6.3 The algorithm performance after denoising

	Case 1: Without Noise	Case 2: DSI Noise	Case 3: WGN Noise	Case 4: DSI and WGN Noises
TD_{BA}	3.43 us	3.52 us	3.53 us	3.53 us
TD_{BC}	-13.7 us	-13.7 us	-13.7 us	-13.7 us
L_B	2.5004 km	2.5135 km	2.5149 km	2.5149 km
Error, ε_B %	-0.01	-0.337	-0.3725	-0.3725
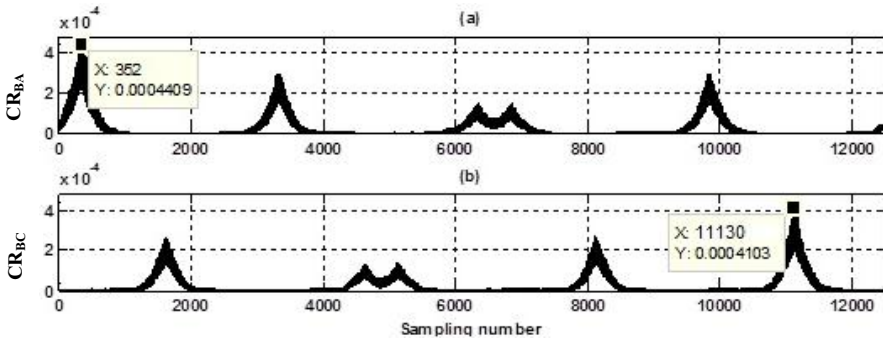
Fig. 6.14 Correlation results applied on the sample-absolutes of Fig. 6.11. (a) Between sensors B and A, (b) between sensors B and C.
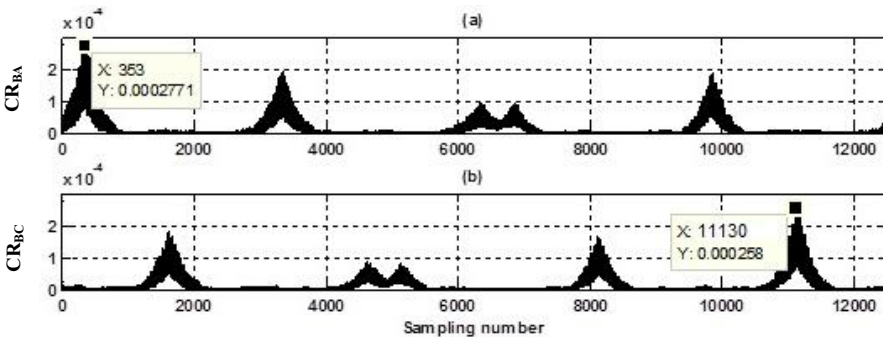
Fig. 6.15 Correlation results applied on the sample-absolutes of Fig. 6.12. (a) Between sensors B and A, (b) between sensors B and C.

81
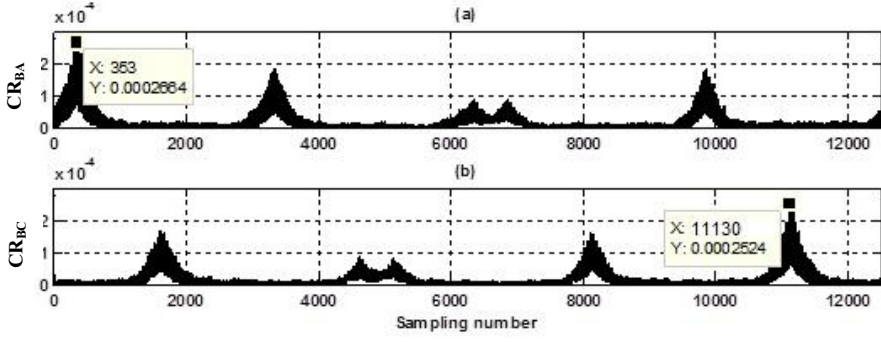
Fig. 6.16 Correlation results applied on the sample-absolutes of Fig. 6.13. (a) Between sensors B and A, (b) between sensors B and C.

6.7 Improvement using windowed standard deviation

Windowed STD-based feature extraction is used as an alternative technique to extract the transient PD pulse from the measured signal. The STD is in the form as:

$$STD = \sqrt{\frac{1}{m}\sum_{j=1}^{m}(x_j - \bar{x})^2} \tag{6.18}$$

$$\bar{x} = \frac{1}{m}\sum_{j=1}^{m}x_j \tag{6.19}$$

where STD is the standard deviation and m is the number of samples per a small sliding window of the input vector, x. The frequency information extracted by the STD depends on the m value or the window size. If the window size is 0.5, 1.0 or 2.0 ms, the frequencies higher than 2000, 1000 or 500 Hz can be correctly extracted, respectively [86]. This means that there is an inversely proportional ratio between the window size and the extracted frequencies. Therefore, if we are interested in extracting a certain frequency, the window size should be greater than the inverse value of this frequency. In the simulated network, the resonant frequency of the PD measurement is found to be 5 MHz and therefore a 1 μs window size is used to extract the simulated PD signals, as it can extract frequencies higher than on equal to 1 MHz. One of the advantages of STD is its ability to extract non-stationary signals such as PD pulses.

Considering the worst noise case illustrated in Fig. 6.9 and the corresponding denoised signal depicted in Fig. 6.13, Fig. 6.17 shows the extracted signal using the windowed STD. The corresponding correlation curves are shown in Fig. 6.18. They are better than those in Fig. 6.16, containing correlation curves using the absolute values of the denoised signal in Case 4. Table 6.4 summarizes the performance with the windowed STD-based extraction of the PD pulses and considering the same noise cases as depicted in Table 6.3. By comparing the results of these two Tables, the error is reduced using the windowed STD. Table 6.5 shows the accuracy,

82

considering different PD locations where the signals are noised by the DSI and GWN models.
These PDs are correctly located with an error less than 0.5 %.
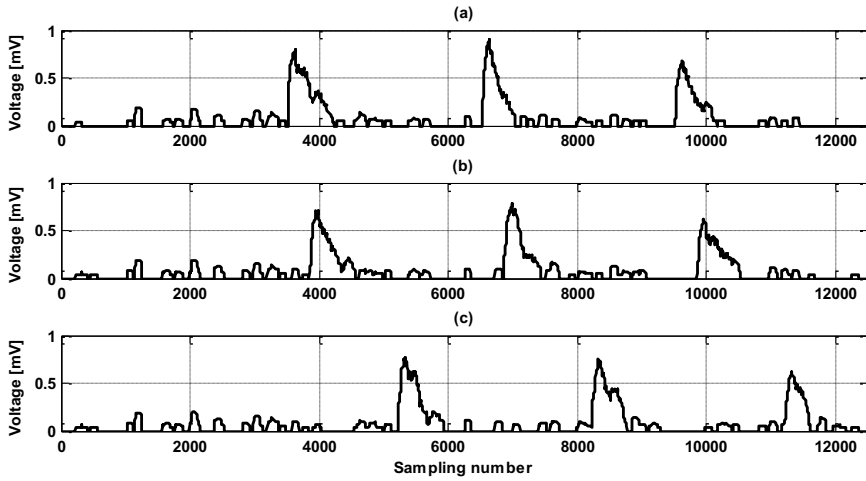
Fig. 6.17 STD of denoised PD signal in Fig. 6.13. (a) At sensor A, (b) at sensor B, (c) at sensor C.
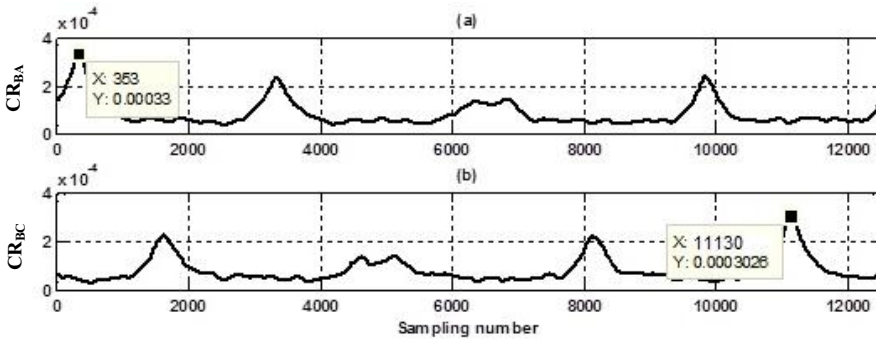
Fig. 6.18 Correlation results applied on waveforms shown in Fig. 6.17. (a) Between sensors B and A, (b) between sensors B and C.

Table 6.4 Accuracy of localization considering windowed STD

	Case 1: Without Noise	Case 2: DSI Noise	Case 3: WGN Noise	Case 4: DSI and WGN Noises
L_B	2.5004 km	2.5018 km	2.512 km	2.5137 km
Error, ε_B %	-0.01	-0.045	-0.30	-0.3425

Table 6.5 Accuracy of localization at different PD locations

	Actual L_B in section AB (km)				Actual L_B in section BC (km)			
	0.5	1.0	1.5	2.5	0.5	1.0	1.5	2.5
L_B	0.5047	1.0051	1.4953	2.5197	0.5040	1.0108	1.4927	2.4956
Error, ε_B %	-0.1175	-0.1275	0.1175	-0.4925	-0.1	-0.27	0.1825	0.11

6.8 Algorithm evaluation based on experimental measurement

An experimental set-up was arranged in the high voltage (HV) laboratory at Aalto University, Finland, as explained in Chapter 5. This was similar to the network shown in Fig. 5.1.

6.8.1 Algorithm evaluation based on PD produced by a pulse calibrator

The first experimental test case of a PD source on the CC line was injected using the PD calibrator. This measurement was performed without energizing the AC power source on the CC line. Different lengths were considered, L_{AB} = 5.2 m and L_{BC} = 4.5 m corresponding to the network shown in Fig. 5.1. Calibration signals of 20 nC pulse were injected at a distance of L_B = 0.9 m in section AB. The measured PD signals using Rogowski coils A, B, and C are shown in Fig. 6.19. The corresponding windowed STDs are shown in Fig. 6.20 and then the correlation results for determining the time differences are shown Fig. 6.21, where it is found that TD_{BA} = -383 and TD_{BC} = -505 samples. The sampling frequency of the experimental measurements was 2.5 GHz. The calculated distance, L_B = 0.8891 m with an error of 0.203 %. Further magnitudes of pulse from the calibrator, such as 5 nC, 10 nC and 50 nC, were injected at the same point and the results are summarized in Table 6.6. The highest error is in the lower PD signal. However the locator accuracy was attained.
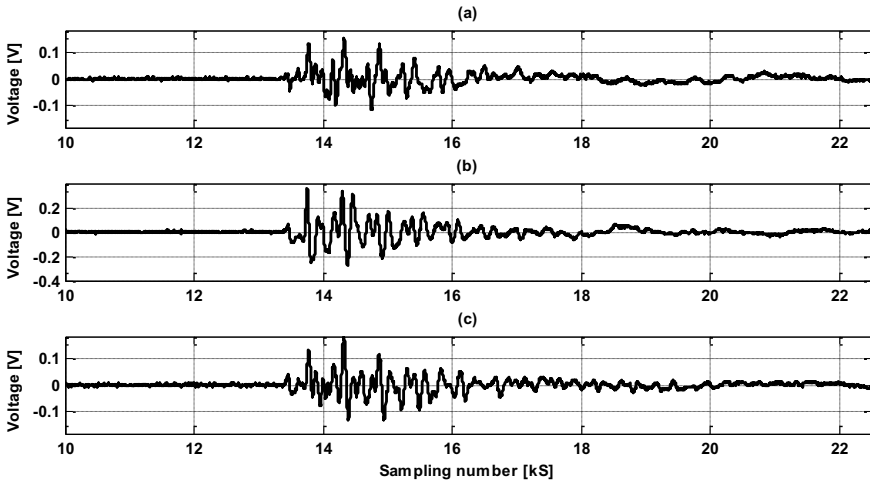
Fig. 6.19 The Rogowski coil responses from an injected 20 nC PD from the pulse calibrator.
(a) Rogowski coil A, (b) Rogowski coil B, and (c) Rogowski coil C.
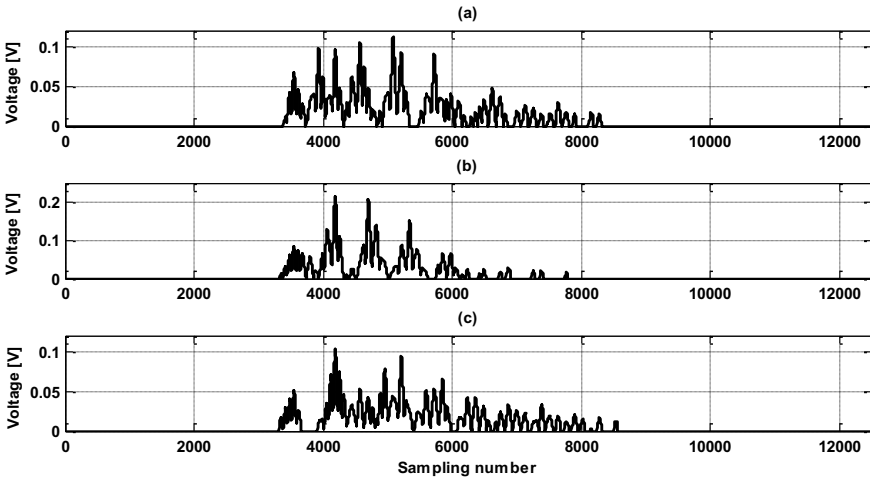
Fig. 6.20 Windowed STD of the measured PD signals from the pulse calibrator in Fig. 6.19. (a) Sensor A,
(b) sensor B, (c) sensor C.
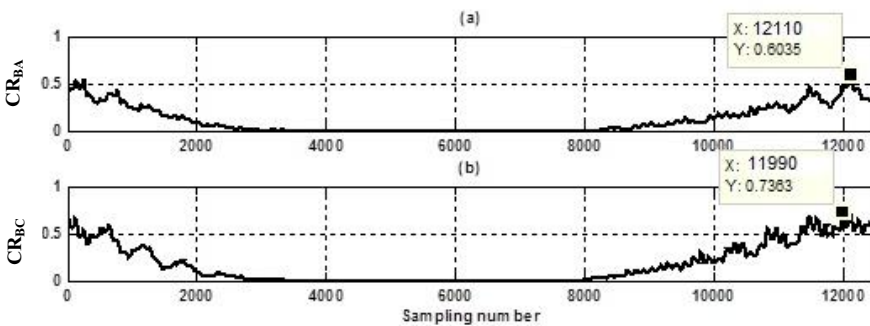
Fig. 6.21 Correlation results applied on the windowed STD of the measured PD signals from the pulse
calibrator in Fig. 6.20. (a) Between sensors B and A, (b) between sensors B and C.

Table 6.6 Accuracy of localization for injecting different PD calibration pulses

	5 nC	10 nC	20 nC	50 nC
Computed L_B (m)	0.7753	0.8894	0.8891	0.8972
Error, ε_B %	2.393	0.204	0.203	0.054

6.8.2 Algorithm evaluation based on PD produced by a hand-made twisted coil

Referring again to Fig. 5.1, different lengths were considered, with L_{AB} = 4.7 m and L_{BC} = 5.0 m. The PD source was at L_B = 2.5 m in section BC. The Rogowski coils measured signals at points A, B, and C, are shown in Fig. 5.11. The windowed STD-based feature extraction on each measured signal after denoising using DWT is shown in Fig. 6.22 and the corresponding correlation results are shown in Fig. 6.23. The distance of the PD source location was found to be L_B = 2.518 m. This ascertains the algorithm accuracy. Measurements at two PD distances were accomplished and the locator performance is summarized in Table 6.7, where the average and maximum errors are illustrated. This table statistically confirms the locator accuracy.

Table 6.7 Average and maximum errors for different testing on PD produced by a hand-made twisted coil

	L_B (m) = 2.5 m	L_B = 3.9 (m)
Number of tests	8	8
Average error, ε_B %	-0.306	-0.317
Maximum error, ε_B %	-0.378	-0.346
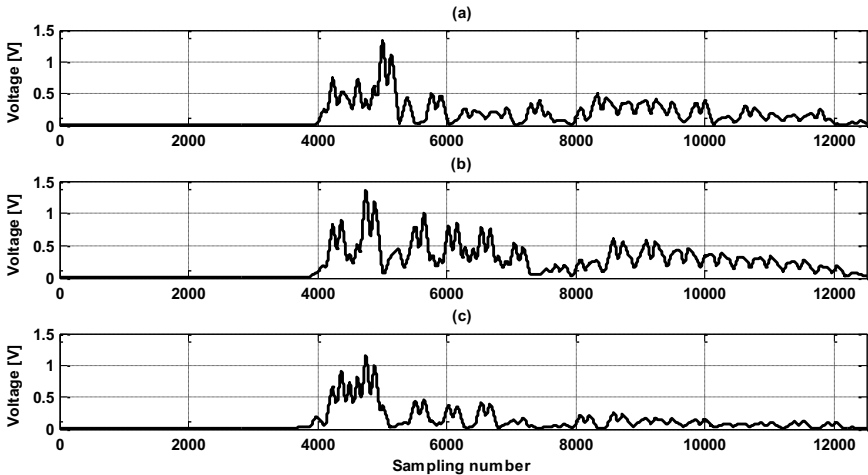
Fig. 6.22 Windowed STD of the measured PD signals due to the twisted-coil at (a) sensor A, (b) sensor B, (c) sensor C.
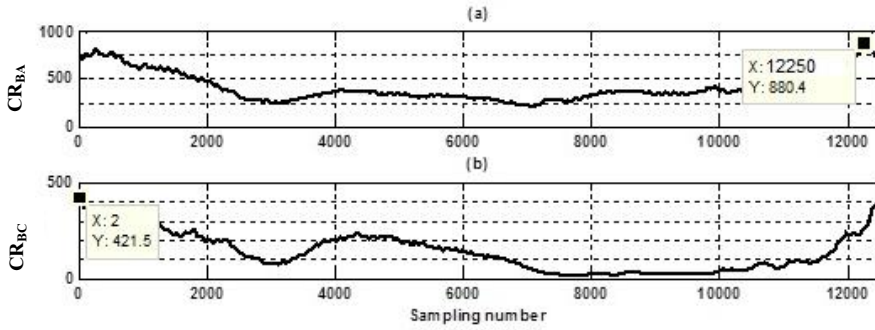
Fig. 6.23 Correlation results applied on the windowed STD of the PD signals due to the twisted-coil at (a) between sensors B and A, (b) between sensors B and C.

6.8.3   Algorithm evaluation based on PD produced by a tree leaning on the CC line

Referring again to Fig. 5.1, the distances between Rogowski coils were equally set to $L_{AB} = L_{BC} = 6.5$ m. The PD source was at $L_B = 3.4$ m in section BC. Fig. 5.12 shows the Rogowski coils measured signals at points A, B, and C and the corresponding windowed STD-based feature extraction on each measured signal after denoising using DWT is shown in Fig. 6.24. The correlation results are shown in Fig. 6.25. The distance of the PD source location was found to be $L_B = 3.46$ m, with only an error of 1.76 % in this compact measurement setup. The short line caused some distortion which is not present in real outdoor scenario.
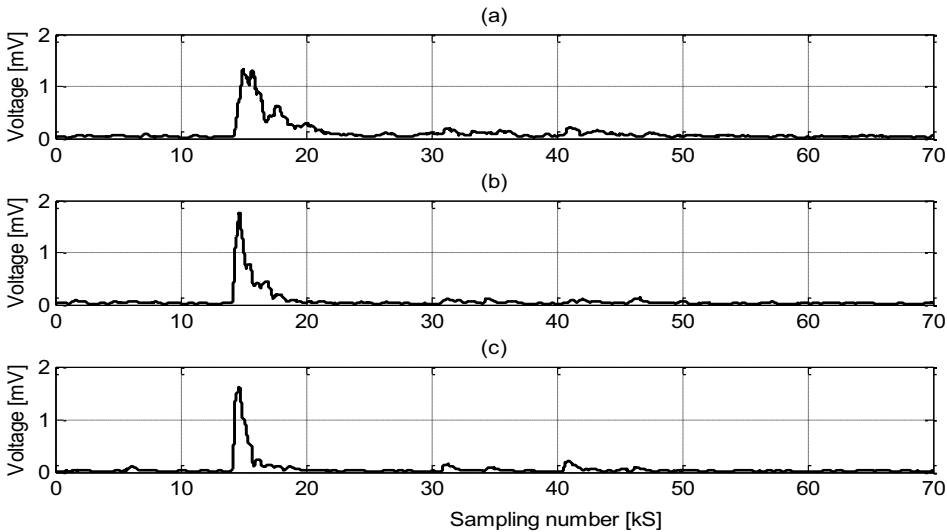
Fig. 6.24 Windowed STD of the measured PD signals caused by a tree leaning on the CC line. (a) Sensor A, (b) sensor B, (c) sensor C.
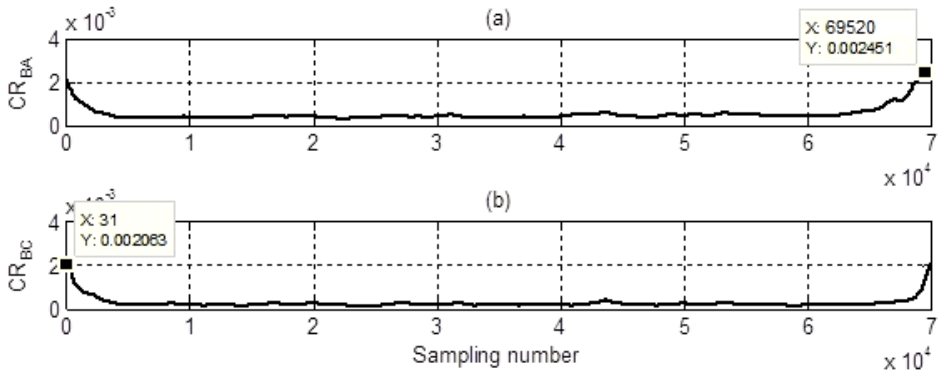
Fig. 6.25 Correlation results applied on the windowed STD of the measured PD signals caused by a tree leaning on the CC line. (a) Between sensors B and A, (b) between sensors B and C.

6.9   Discussion

A multi-end correlation-based PD source location technique for CC overhead lines has been proposed and experimentally verified. The time differences have been calculated by identifying the maximum correlation between signals measured from the Rogowski coils. Using this technique, the first arrival time for each measured signal and propagation velocity are not needed anymore in the PD source locator. Furthermore, this technique overcomes the difficulty of identifying a faulty section for multi-end measurement from the previous technique as discussed in chapter 5. The proposed algorithm yielded remarkably accurate results on locating PD sources provided the measured signals are synchronized. As proposed in [68], to achieve an accurate time tagging of the event, the sensors are synchronized to a Global positioning system (GPS) clock that provides time synchronization accuracies of less than 1 µs over the entire surface of the earth under all weather conditions. Telecommunication can be used through any convenient channel including microwave, optical fiber, or a supervisory control and data acquisition (SCADA) network. The timing accuracy of less than 1 µs is in fact not very accurate considering that other location error sources (such as the changes in propagation velocity and the effects of noise) will be minimized in this application (1 µs corresponds to a PD pulse traveling distance of almost 300 m on CC lines).

7- Correlation evaluation of unsynchronized two-end windows for PD location on CC overhead lines

Active research in highly distributed systems of small, wireless, low-power, unattended sensors and actuators are results of recent advances in efficiency and low-cost, low-power design [88], [89]. Researchers aim to invent 'smart-environments' with deployment of thousands of sensors. Each sensor comes possibly with a short-range wireless communication channel and is capable of detecting ambient conditions such as temperature, movement, sound, light, or the presence of certain objects.

In multi-end measuring such as in a multiple sensor networks set-up, time synchronization is an important issue. The local clocks of sensor nodes need to be synchronized, which are needed in many applications of sensor networks. First and foremost, sensor nodes need to coordinate their operations and collaborate to achieve a complex sensing task. An example of such coordination is data fusion in which data collected at different nodes is aggregated into a meaningful result. For example, in a vehicle tracking application, sensor nodes report the location and time that they sense the vehicle to a sink node which in turn combines this information to estimate the location and velocity of the vehicle. The estimation will be clearly inaccurate if the sensor nodes lack a common timescale.

Synchronization means two items are adjusted to do the same thing. Distributed wireless sensor networks make use of synchronized time extensively, for example, to integrate a time-series of proximity detections into a velocity estimate, to measure the time-of-flight of sound for localizing its source, to distribute a beam forming array, or to suppress redundant messages by recognizing that they describe duplicate detections of the same event by different sensors [90]-[92]. Sensor networks also have many of the same requirements as traditional distributed systems. For example, accurate timestamps are often needed in cryptographic schemes, to coordinate events scheduled in the future, and for ordering logged events during system debugging.

Time synchronization is a critical infrastructure for any distributed system. The main error sources of synchronization are from Global positioning system (GPS) timing errors. The accuracy of the GPS received signal is a function of the error and interference on the GPS signal and the processing technique used to reduce and remove these error. The GPS signals are also affected by the same types of phenomena as found in microwave-range systems. Both types of systems are highly affected by humidity and multi-path. Humidity can delay a time signal up to approximately 3 m. Satellites low on the horizon will be sending signals across the face of the earth through the troposphere. Satellites will directly transmit through much less troposphere. Sunspots and other electromagnetic phenomena cause errors in GPS range measurements of up

to 30 m during the day and as high as 6 m at night. Such errors can be estimated, although they are not predictable [68].

In this chapter, a correlation of the unsynchronized two-end windows technique is used for locating the partial discharge (PD) source on covered-conductor (CC) overhead lines. The maximum correlation factor between signal arrivals at two-end measuring points is used in order to find the ratio of correlation. Then the ratio of correlation signals is plotted against its ratio of difference distance. The graph is plotted using curve fitting (LAB Fit) software. The algorithm is developed and tested by means of simulation. The Electromagnetic transient program-Alternative transient program (EMTP-ATP) is used to implement and analyze a PD monitoring system. The proposed algorithm performance is evaluated by extracting the high frequency features using windowed standard deviation (STD).

7.1 Correlation of unsynchronized two-end windows

The opportunity to improve the PD location accuracy emerges since the rapid development of effective means of communication between the line terminals. The first solution appeared is unsynchronized sampling at the line terminals while the synchronized sampling, provided with the GPS, is also coming into applications as well. This section deals with two-end PD location based on unsynchronized measurements.

In unsynchronized measurement cases at the line terminals, the gathered measurement data is generally shifted in time. This can be caused by the detection of fault at both the line terminals at slightly different instants, no synchronization of the clocks which are controlling the sampling at the line ends and different sampling rates and/or the phase shifts introduced in the measurement channels.

In Chapter 6, the localization of PD source location on CC overhead lines using multi-end correlation technique based on three measuring points has been successfully presented. The technique has shown a good result in the localization of PD source, providing that the synchronization of measured data signal is assured for the correlation windows, *CR*. The locator accuracy depends on the time synchronization. In order to avoid the dependency on the time synchronization of the measured signals, a correlation of unsynchronized two-end windows technique is introduced.

Based on the difference location of the PD source on the CC line between sensors A and B, the theory of maximum correlation factor is used in order to find the ratio of correlation between two-end unsynchronized-measuring points. The ratio of correlation, *ROC* is plot against its ratio of difference distance, *LR* [101]. Referring to Fig. 7.1:

Ratio of correlation, $ROC = \frac{(|MCR_{AA} - MCR_{BB}|)}{MCR_{AB}}$ (7.1)

Ratio of difference distance, $LR = \frac{(|L_A - L_B|)}{L_{AB}}$ (7.2)

$L_A + L_B = L_{AB}$ (7.3)
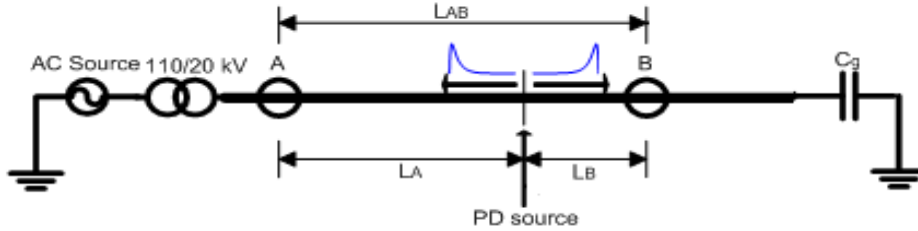
Fig. 7.1 Simulated three-phase system. A and B, are measuring points of the Rogowski Coil, C_g is the terminating capacitance to the ground [101].

Windowed STD-based feature extraction is used as the technique to extract the transient PD pulse from the measured signal. This extraction technique has been presented above in Chapter 6. MCR_{AA} and MCR_{BB} is the maximum correlation factor for the measured signal at Rogowski coil A and Rogowski coil B respectively. MCR_{AB} is the maximum correlation factor between the measured signal at Rogowski coil, A and Rogowski coil, B. The ratio of correlation, CR stated above in (7.1) is valid for both cases of $MCR_{AA} > MCR_{BB}$ or $MCR_{AA} < MCR_{BB}$. If $MCR_{AA} > MCR_{BB}$, this means that Rogowski coil A is located nearer to the PD source compared to Rogowski coil B ($L_A < L_B$). Meanwhile, if the $MCR_{AA} < MCR_{BB}$, the Rogowski coil B is located closer to the PD source, $L_A > L_B$. L_A is the distance of Rogowski coil A from the PD source, and L_B is the distance of Rogowski coil B from the PD source. While L_{AB} is the distance between Rogowski coil A and Rogowski coil B.

Based on information in (7.1), (7.2) and Equation (7.3), the distance of the PD source location from Rogowski coil A is determined as [101]:

for, $MCR_{AA} < MCR_{BB}$,

$L_A = \frac{((L_{AB}*LR) + L_{AB})}{2}$,   (7.4)

and for, $MCR_{AA} > MCR_{BB}$,

$L_A = \frac{(-(L_{AB}*L_R) + L_{AB})}{2}$.   (7.5)

7.2   Simulated study

Considering the network shown in Fig. 7.1, the EMTP-ATP is used to implement and analyze a PD monitoring system. The network is simulated for a case of PD occurrence in section AB on the CC line. The CC line and Rogowski coil model used are similar as presented

in the previous chapter. The distance between each Rogowski coil is fixed at 4 km. The simulation started with the PD source is injected on the middle of the conductor line, AB. Then, the location of PD source is removed at certain distance towards Rogowski coil, B. All measured data is stored. From the simulated study, the ratio of correlation, ROC, between two measured signals is plotted against its ratio of difference distance, LR. The ratio of correlation, ROC and the ratio of difference distance, LR, is calculated based on Equations (7.1) and (7.2) and shown in Table 7.1.

Table 7.1 The Calculation of Ratio of Correlation, ROC and Ratio of Distance, LR

L_A (m)	L_B (m)	Ratio of Distance, LR	MCR_{AA}	MCR_{BB}	MCR_{AB}	Ratio of Correlation, ROC
2000	2000	0	1.68×10^{-4}	1.68×10^{-4}	1.68×10^{-4}	0
1800	2200	0.1	1.68×10^{-4}	1.65×10^{-4}	1.65×10^{-4}	0.01464
1700	2300	0.15	1.69×10^{-4}	1.64×10^{-4}	1.66×10^{-4}	0.02866
1600	2400	0.2	1.73×10^{-4}	1.63×10^{-4}	1.68×10^{-4}	0.06187
1500	2500	0.25	1.76×10^{-4}	1.62×10^{-4}	1.67×10^{-4}	0.08781
1400	2600	0.3	1.80×10^{-4}	1.62×10^{-4}	1.69×10^{-4}	0.10933
1300	2700	0.35	1.80×10^{-4}	1.62×10^{-4}	1.71×10^{-4}	0.10785
1200	2800	0.4	1.83×10^{-4}	1.61×10^{-4}	1.71×10^{-4}	0.13118
1100	2900	0.45	1.89×10^{-4}	1.60×10^{-4}	1.73×10^{-4}	0.1679
1000	3000	0.5	1.94×10^{-4}	1.61×10^{-4}	1.76×10^{-4}	0.18281
500	3500	0.75	2.17×10^{-4}	1.58×10^{-4}	1.83×10^{-4}	0.32437
400	3600	0.8	2.37×10^{-4}	1.58×10^{-4}	1.92×10^{-4}	0.41108
300	3700	0.85	2.62×10^{-4}	1.57×10^{-4}	2.02×10^{-4}	0.52086
200	3800	0.9	2.96×10^{-4}	1.55×10^{-4}	2.13×10^{-4}	0.65943
100	3900	0.95	3.46×10^{-4}	1.54×10^{-4}	2.28×10^{-4}	0.84358
50	3950	0.975	3.78×10^{-4}	1.54×10^{-4}	2.40×10^{-4}	0.93411

The graph of the ratio of correlation against the ratio of difference distance is plotted using LAB Fit software as shown in Fig. 7.2 and the Hyperbolical sine equation $= A * \sinh(B * X) + CX$, is found as the best function correlate to this plotted. Parameters, A, B and C are 0.7923×10^{-3}, 7.588 and 0.3105. Referring to the plotted graph in Fig. 7.2, the PD source on the CC overhead lines can be localized using either Equation (7.4) or (7.5), depending on the values of the maximum correlation factor, MCR_{AA} and MCR_{BB}.

For example, if the correlation ratio, ROC = 0.0872, the ratio of difference distance, LR = 0.25. Solving Equation (7.5), the PD source location is found located at 1.5 km from Rogowski coil A. From this result, the simulated evaluation proves that an accurate PD source location can be achieved using the proposed algorithm technique. This helps to solve the problem the difficulty to get the synchronized measured signals between two measuring points.
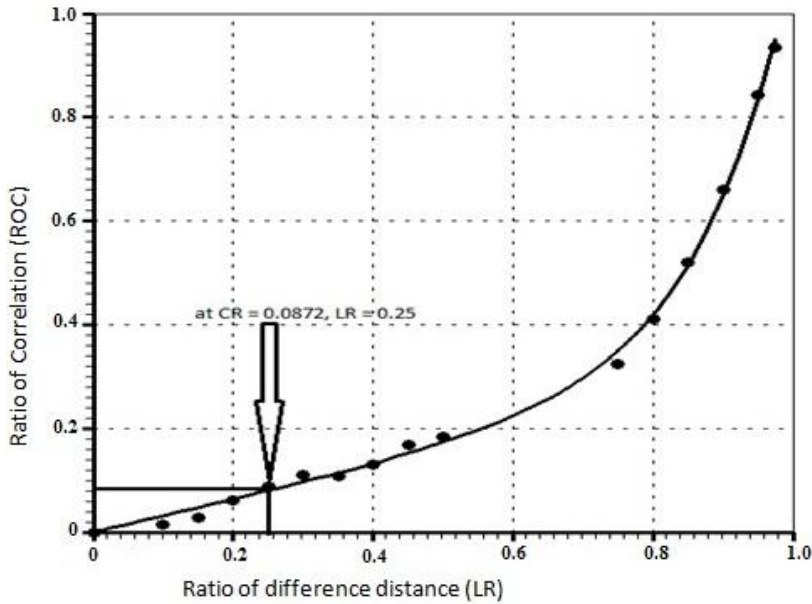
Fig. 7.2 The ratio of correlation against the ratio of difference distance.

For future work, the performance of the locator function algorithm developed in this chapter will be tested using the unsynchronized measured signals obtained from both the laboratory and from the real field. This new idea which needs more research should be done in this direction to verify the algorithm. Furthermore, the experience in the line modeling is also required.

8- Rogowski coil evaluation with different fault conditions in MV Networks

8.1   Significance of Rogowski coil for fault detection

There are possibilities that the faults on covered-conductor (CC) overhead lines occur due to other reason than partial discharge (PD), for instance, when the fault is caused by an arcing fault with characteristics of intermittent faults. As a precautionary step, the capability of the Rogowski coil to work on capturing a different fault transient traveled from the source location is evaluated. This evaluation is useful in order to make it possible to implement a fault locator technique using the same technique presented in the previous chapters. In this chapter, the Electromagnetic transient program-Alternative transient program (EMTP-ATP) test bench of a 20 kV network is developed considering the high frequency models of the Rogowski coil and the distribution network. The test bench is used to evaluate the Rogowski coil performance with different fault scenarios such as different fault types, different fault resistances and different inception angles. Furthermore, the performance of the Rogowski coil for the leaning tree and arcing fault cases is also tested. Positive results clearly show the possibility of using the Rogowski coil for locating faults in the distribution networks.

For fault detection and location, current transformers (CTs) have typically been used in measurement applications. A number of problems in application in crowded panels can be generated by the mechanical design of this particular sensor. It also only allows measurement of a single conductor. The alignment of the jaw will affect the accurate current measurement when using a typical split core or clamp on a CT. The split in the iron core requires the mating surfaces to be properly aligned for accurate measurement. Removal and installation of iron core CTs on a live conductor can result in an inductive kick. Many of these problems can be overcome by Rogowski coils. The new flexible Rogowski coil-based current probes allow the user to easily install the measurement head in tight spaces that may be inaccessible with typical iron core CT products. The user has to carry only one lightweight probe for a wide range of applications due to the variety of diameters and current ranges available. Rogowski coils also produce a safe low voltage output eliminating the hazards associated with misalignment and open secondary windings. The circuit loading and saturation concerns are virtually eliminated with the absence of an iron core.

Rogowski coils have been successfully used to measure and extract high frequency PD signals in CC overhead lines [3], [5], [56], [59]-[60], [63], [70], [87], [100] . However it has not yet been tested for fault location applications. In this work, the performance of the Rogowski

coil will be tested to measure and extract the high frequency surge transient traveled along the CC overhead and bare conductor lines due to different fault conditions. In recent times, normal CT has been used to measure this signal. However, the responses of conventional CTs at high frequencies are not flat. A Rogowski coil can be used as an alternative as evaluated in this chapter. High frequency models of the Rogowski coil and of the medium voltage (MV) network elements are implemented and solved using an ATPDraw-based pre-processing of the EMTP-ATP.

8.2   Simulated study

8.2.1   Rogowski coil and MV network modeling

The simulated model of the Rogowski coil presented in Chapter 6 is used. Its configuration and equivalent simulated circuit is shown previously in Figs. 2.2 and 2.3 in Chapter 2.

The MV network distribution lines with four feeders are shown in Fig. 8.1 where in this network the earth fault current is compensated. The overhead lines are energized by alternating current (AC) sinusoidal waveforms via a 110/20 kV delta/star transformer. The covered and uncovered overhead lines are represented using a JMarti frequency model where their configurations are shown in Fig. 8.2. A high frequency transformer model is added to the power model for accurately representing the electromagnetic transients of 21/0.42 kV load transformers [93], [94]. The parameters of this high frequency model are summarized in Fig. 8.3. The effect of the high frequency added model is where that reflection signal from the MV/LV transformers path to the network is reduced. Rogowski coils are allocated on the lines at a distance of 4 km between each other.

The compensated MV network and the corresponding measuring devices are simulated in one arrangement using the EMTP-ATP simulation environment. The performance of the Rogowski coil is evaluated concerning different fault scenarios such as resistance, leaning trees and arcing faults. The dynamic modeling of these faults is discussed in the following subsections. The evaluation is carried out using different generated fault types, different fault resistances and different fault inception angles considering the locations of the Rogowski coils shown in Fig. 8.1. Different types of faults are created in section FG in the Feeder EFGH. Rogowski coils E, F, and G are selected to evaluate their performance in order to detect different types of fault conditions considering a fault distance of 1.5 km from the Rogowski coil F on the tested MV network.
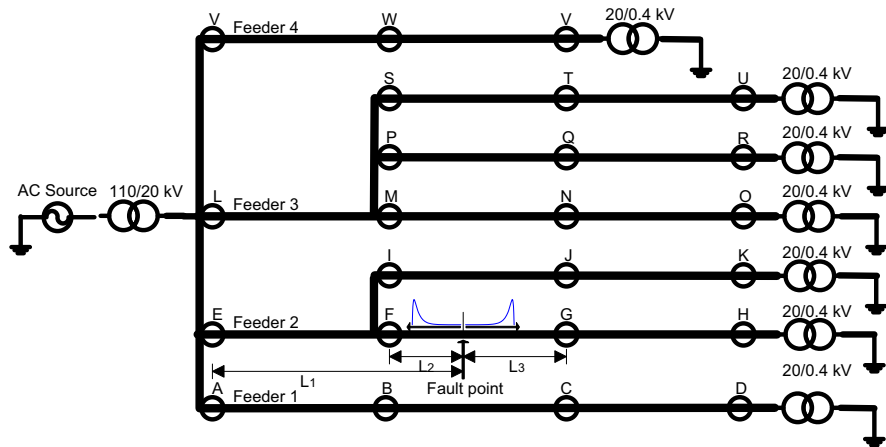
Fig. 8.1 Simulated system for 78 km distribution network. O is the Rogowski coil location [98].

(a)   (b)
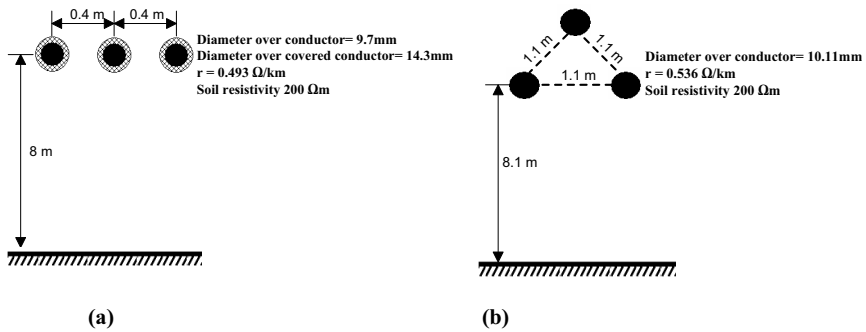
Fig. 8.2 The feeder configuration. (a) Covered conductor overhead line, (b) bare conductor line [98].
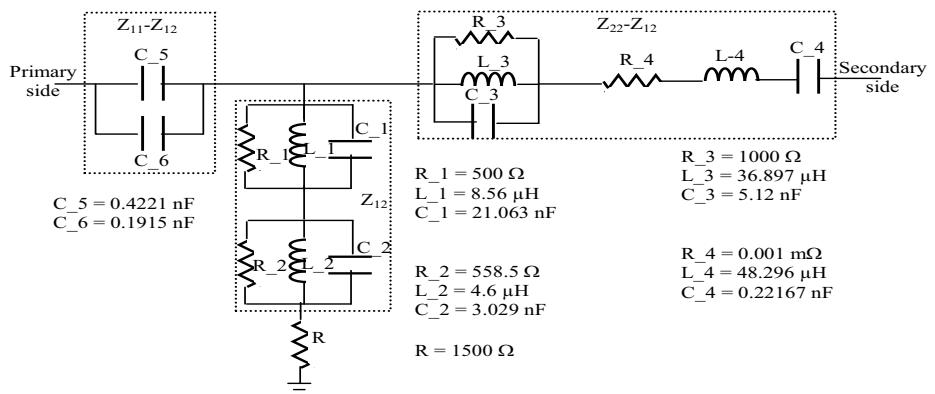
Fig. 8.3 High frequency model of MV/LV transformer and its parameters [93].

8.2.2 Model of fault due to a leaning tree

An experiment was performed to measure the characteristics of faults due to a leaning tree occurring in a 20 kV distribution network. This fault type is modeled using two series parts: a dynamic arc model and a high resistance. For the considered case study, the resistance is equal to 140 kΩ and the arc is modeled using thermal equilibrium that is adapted as in [95]:

$$\frac{dg}{dt} = \frac{1}{\tau}(G - g) \tag{8.1}$$

$$G = \frac{|i|}{U_{arc}} \tag{8.2}$$

$$\tau = A \; x \; 10^{Bg} \tag{8.3}$$

where g is the time-varying arc conductance, G is the stationary arc conductance, $|i|$ is the absolute value of the arc current, U_{arc} is a constant arc voltage parameter, τ is the arc time constant and, A and B are constants. In [95], the parameters U_{arc}, A and B were found to be 2520 V, $5.6 \; x \; 10^{-7}$ and $3.95917 \; x \; 10^{5}$, respectively. Considering the conductance at each zero crossing, the dielectric is represented by a variable resistance until the instant of reignition. It is represented using a ramp function of 0.5 MΩ/ms for a period of 1 ms after the zero-crossing and then 4 MΩ/ms until the reignition instant.

8.2.3 Model of arcing fault

A dynamic model of the arcing fault in distribution networks was presented in [96], where the dynamic arc equations (8.1) and (8.2) are the same with concerning a suitable form of the arc time constant as in [96]:

$$\tau = \tau_o (\frac{l}{l_o})^{\alpha} \tag{8.4}$$

The arc time constant τ is a function of the arc length l where τ_o is the initial arc time constant, l_o is the initial arc length and α is a coefficient of the negative value. Towards implementing this arcing fault model, the dynamic equations (8.1), (8.2) and (8.4) are solved and interacted with the network. U_{arc} is is in the form:

$$U_{arc} = (u_o + r|i|)l \tag{8.5}$$

$$u_o = 900 + \frac{400}{l} \tag{8.6}$$

$$r = 0.04 + \frac{0.008}{l} \tag{8.7}$$

where r is the resistive component per arc length, u_o is constant voltage per arc length. The values of the model parameters are: τ_o = 0.25 ms, α = -0.4 and l_o = 0.20 m. This arcing fault model is implemented considering the effect of arc elongation with a rate of change equal to 10.5 m/s. Considering the bilateral interaction between the EMTP power network and the transient analysis control system (TACS) field, the arcing equations and their corresponding parameters are implemented using the universal arc representation as addressed in [96]. The aforementioned MV network and the fault modeling are combined in a single arrangement to describe the network behaviour, accordingly.

Fig. 8.4 shows the ATPDraw circuit declaring the power feeders, the high frequency and saturable models of the load transformers, the Rogowski coil model and the univeral arc representation of the arc. The sampling frequencies are considered 100 MHz for resistance fault cases and 1 MHz for leaning-tree and arcing fault cases. This sampling frequency is chosen considering the execution time taken during simulation for each fault cases.

8.3   Performance evaluation of Rogowski coil

8.3.1   The performance considering resistance fault cases

The earth fault in phase C at the fault point in the network is shown in Fig. 8.1 where this network is with CC feeders. Fig. 8.5 shows the phase C measurements of Rogowski coils installed at E, F and G nodes. From the waveforms shown in Fig. 8.5, the fault surges can be measured using the Rogowski coils with a sufficiently large voltage range of 5 to 15 V. Furthermore, the time difference of arrival (TDOA) fault surges at the measuring nodes are clear and they can be extracted to enhance the fault location technique using traveling wave functions.

For high resistance faults, the evaluation is carried out at different values of fault resistance changed in the range 1 mΩ to 3 MΩ. Table 8.1 shows the corresponding performance of high frequency Rogowski coil measurements for single phase to ground fault. It is found that the maximum value for Rogowski coil response on phase C is higher than the other phases. This is because the fault occurs on phase C. The corresponding response of high frequency Rogowski coils on phases A and B is due to the effect of the electromagnetic and static couplings of the overhead feeder phases. From Table 8.1, increasing the fault resistance reduces the maximum voltage measured by the Rogowski coil. This is proportional to the level of transient traveling surges produced by the fault. A high resistance fault will produce less amplitude of traveling waves compared to a low resistance fault. The measured voltage is extremely reduced for fault resistances in MΩ ranges where at such fault resistances the measured voltages are low

compared to the voltages measured due to PD sources. The results confirm the suitability of the Rogowski coil to extract the earth fault surges that are extremely difficult to be found using phase current measurement when the network is a compensated network. The transients are small decaying amplitudes superimposed on fundamental waveforms. The Rogowski coil enhanced to extract those transients with discarding the fundamental component. This result is simply achieved without applying a signal processing filter.
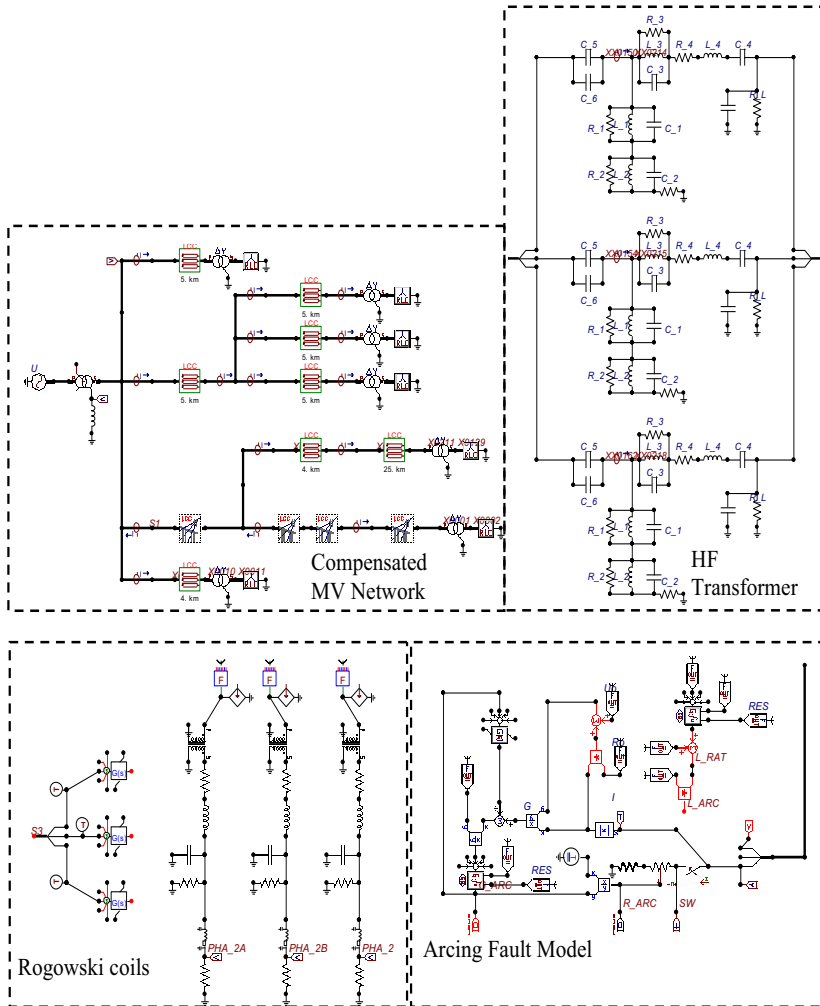
Fig. 8.4 ATPDraw circuit for the network of Fig. 8.1 [98].
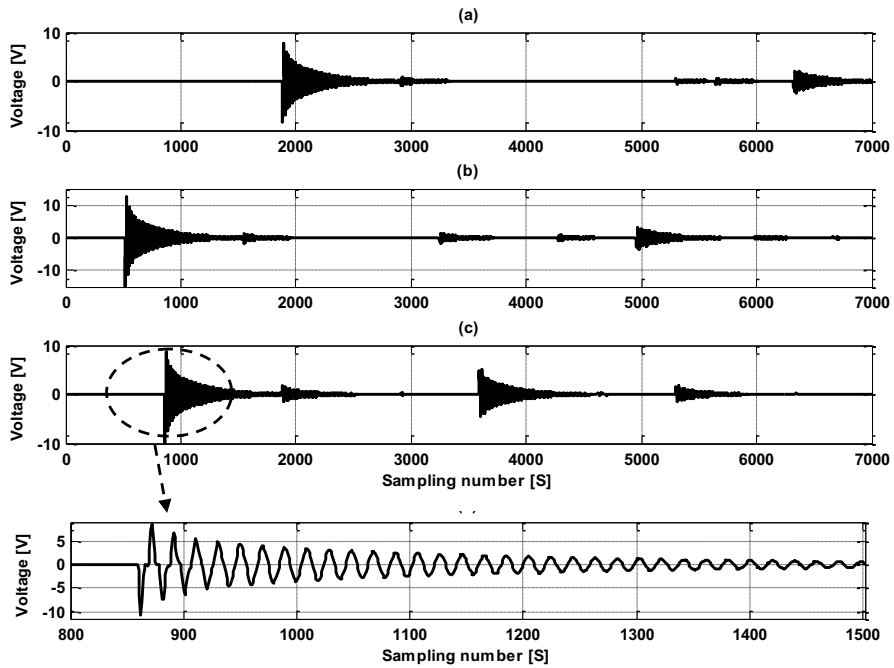
Fig. 8.5 Rogowski coil response for earth fault of phase C, (a) at Rogowski coil E, RC_E, (b) at Rogowski coil F, RC_F, (c) at Rogowski coil G, RC_G.

Table 8.1 Performance evaluation of Rogowski coil considering different resistances, R_f of single phase to ground fault

R_f(kΩ)	$V_{RCE,peak}$ (mV)			$V_{RCF,peak}$ (mV)			$V_{RCG,peak}$ (mV)		
	Phase A	Phase B	Phase C	Phase A	Phase B	Phase C	Phase A	Phase B	Phase C
0.000001	4360.1	4744.3	8443.1	7075.8	6857.1	15119.1	4971.2	5638.9	10798.7
0.001	4341.3	4724.2	8407.4	7045.2	6827.1	15053.5	4949.9	5615.0	10752.7
1	817.7	901.7	1607.4	1322.6	1311.3	2818.2	933.6	1073.6	2042.9
10	98.4	108.8	194.0	159.0	158.6	338.5	112.3	129.5	246.2
100	10.0	11.1	19.8	16.2	16.2	34.5	11.5	13.2	25.1
500	2.0	2.2	4.0	3.2	3.2	6.9	2.3	2.7	5.0
1000	1.0	1.1	2.0	1.6	1.6	3.5	1.1	1.3	2.5
2000	0.5031	0.5510	0.9870	0.8123	0.8107	1.7	0.5740	0.663	1.3
3000	0.3355	0.3656	0.6563	0.5414	0.5402	1.2	0.3825	0.443	0.839

As presented in Table 8.2, the response of high frequency Rogowski coils at points E, F, and G is increased when a two phases fault occured between phases B and C at the same fault location in Fig. 8.1. The maximum value of Rogowski coil response on phase B and C is clearly higher than phase A for each high resistance phase fault. Comparing the measured voltages due to earth faults in Table 8.1 and due to phase faults in Table 8.2, the voltages due to phase faults are higher than the earth faults where the sequence networks can help to interpret such a

100

comparative performance. Table 8.3 sumarizes the Rogowski coils response at points E,F, and G for a three-phase fault type.

Table 8.2 Performance evaluation of Rogowski coil considering different resistance, R_f for phase B to phase C fault resistivity

R_f (kΩ)	$V_{RCE,peak}$ (mV)			$V_{RCF,peak}$ (mV)			$V_{RCG,peak}$ (mV)		
	Phase A	Phase B	Phase C	Phase A	Phase B	Phase C	Phase A	Phase B	Phase C
0.000001	1967.0	24322.0	22528.0	1729.0	37470.0	37812.0	1762.0	29210.0	28109.0
0.001	1960.0	24233.0	22446.0	172.0	37329.0	37670.0	1756.0	29104.0	28007.0
1	425.0	5226.0	4847.0	377.0	7955.0	7917.0	380.0	6290.0	6022.0
10	53.0	648.0	601.0	47.0	990.0	975.0	47.0	780.0	746.0
100	5.0	66.0	62.0	5.0	102.0	100.0	5.0	80.0	76.0
500	1.0	13.0	12.0	1.0	20.0	20.0	1.0	16.0	15.0
1000	0.54	6.6	6.2	0.48	10.2	10.0	0.48	8.0	7.7
2000	0.27	3.3	3.1	0.24	5.1	5.0	0.24	4.0	3.8
3000	0.18	2.2	2.1	0.16	3.4	3.3	0.16	2.7	2.6

Table 8.3 Performance evaluation of Rogowski coil considering different resistance, R_f for three phase fault resistivity

R_f (kΩ)	$V_{RCE,peak}$ (mV)			$V_{RCF,peak}$ (mV)			$V_{RCG,peak}$ (mV)		
	Phase A	Phase B	Phase C	Phase A	Phase B	Phase C	Phase A	Phase B	Phase C
0.000001	5764.3	26912.8	21148.5	9893.4	42598.6	34492.9	5708.8	32581.1	26872.3
0.001	5696.5	26697.0	21000.5	9771.3	42244.3	34264.2	5635.5	32318.4	26683.0
1	312.7	2952.6	2692.3	361.0	4530.0	4408.2	216.3	3557.8	3361.8
10	28.6	327.5	305.1	27.0	500.9	495.3	24.5	394.5	379.0
100	2.8	33.1	30.9	2.6	50.6	50.1	2.6	39.9	38.4
500	0.56	6.6	6.2	0.51	10.1	10.0	0.52	8.0	7.7
1000	0.28	3.3	3.1	0.25	5.1	5.0	0.26	4.0	3.8
2000	0.14	1.7	1.5	0.13	2.5	2.5	0.13	2.0	1.9
3000	0.09	0.08	0.08	0.08	1.7	1.7	0.08	1.3	1.3

In the analysis of the inception angle influence, cases corresponding to single phase to ground fault with fault resistance of 1 mΩ, the inception angle varied from 0° to 90°. The results are shown in Table 8.4. The Rogowski coils response is affected by the limitation of the zero voltage point on waves faults which is regarded as a major problem for pure traveling wave techniques, but it is still adequate to give the correct response.

8.3.2   The performance considering leaning-tree and arcing fault cases

The faulty feeder is replaced by a simulated bare conductor in order to take the leaning-tree and arcing fault modeling into considerations. Figs. 8.6 and 8.7, show the Rogowski coil

performance to detect the high frequency transient signal due to the leaning of a tree and the intermittent fault respectively. The capability of the Rogowski coil to measure these high impedance faults is shown. The measurements due to a leaning tree and arcing fault are made close to zero crossing which is very difficult to measure using any other measuring transducer. Although the measured signals by Rogowski coils in these fault cases is smaller than most of the PD cases, there is still a possibility to locate the fault source location.

Table 8.4 Performance evaluation of Rogowski coil considering different inception angle for single phase fault ($R_f = 0.001\ \Omega$)

Inception angle (degree)	$V_{RCE,peak}$ (mV)			$V_{RCF,peak}$ (mV)			$V_{RCG,peak}$ (mV)		
	Phase A	Phase B	Phase C	Phase A	Phase B	Phase C	Phase A	Phase B	Phase C
0	0.8639	0.9181	1.7	1.4	1.3	3.0	0.9720	1.1	2.1
10	3802.7	4137.7	7363.6	6171.1	5980.4	13186.0	4335.6	4917.9	9418.0
30	2454.3	2670.5	4752.6	3982.9	3859.8	8510.4	2798.3	3174.1	6078.5
45	1238.2	1347.4	2397.8	2009.5	1947.4	4293.7	1411.8	1601.4	3066.8
60	62.2	67.6	120.3	100.8	97.7	215.5	70.8	80.4	153.9
90	2561.9	2787.6	4961.0	4157.5	4029.0	8883.6	2921.0	3313.3	6345.0
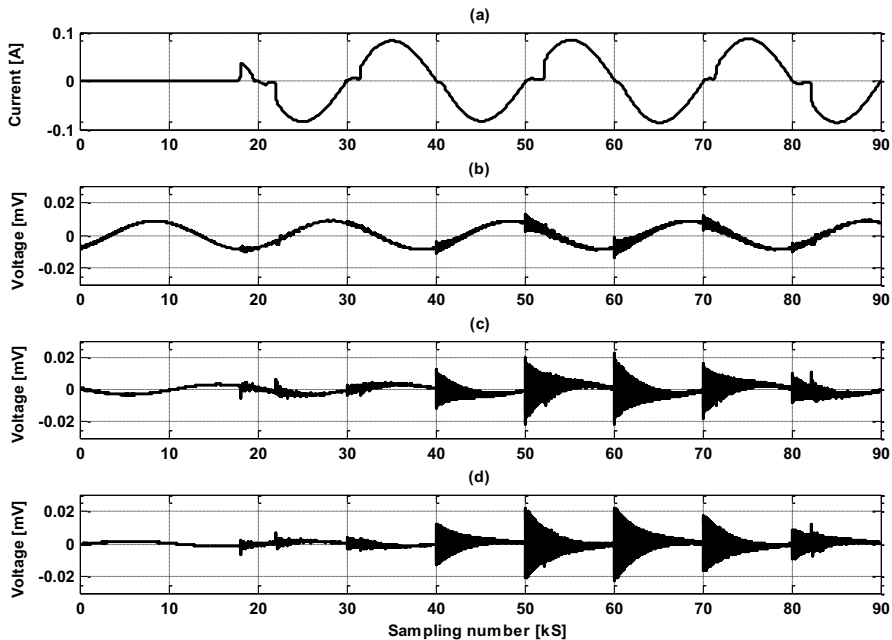
Fig. 8.6 Rogowski coils response for high impedance fault caused by a leaning tree, (a) leaning tree current fault, (b) at Rogowski coil E, RC_E, (c) at Rogowski coil F, RC_F, and (d) at Rogowski coil G, RC_G.
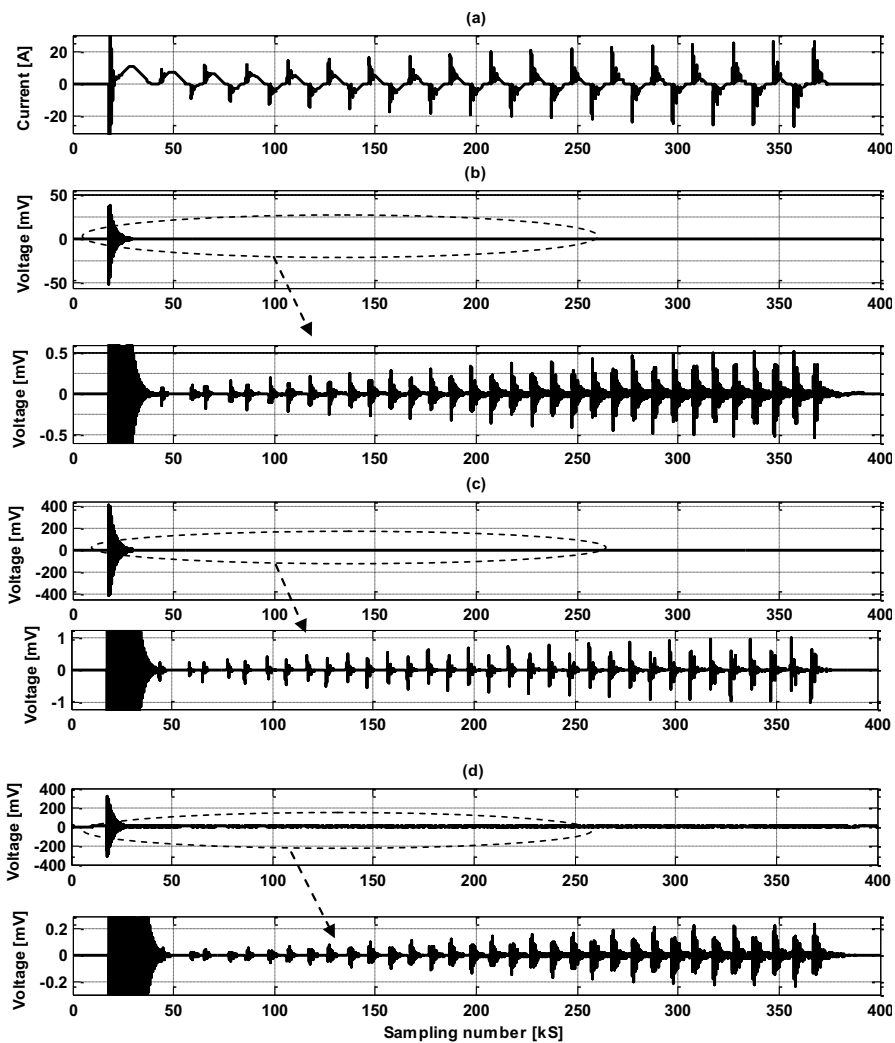
Fig. 8.7 Rogowski coils response for arcing fault, (a) arcing fault phase current (b) at Rogowski coil E, RC_E, (c) at Rogowski coil F, RC_F, and (d) at Rogowski coil G, RC_G.

In Fig. 8.6, the tree resistance is very high (140 kΩ), the fault surge and the arc reignition surges are small and therefore the Rogowski coil output is small. In Fig. 8.7, there is a high fault surge at the instant of fault starting where the arcing resistance is small. However, the intermittent characteristics at the peaks as shown in Fig. 8.7 (a) are more observed. Due to these intermittent surges, the Rogowski coil can support to confirm the fault location.

8.4 Discussion

Simulations were carried out to test the novelty of the high frequency Rogowski coil to measure and extract high frequency transient faults due to varied fault conditions. Different values of fault resistances and inception angles due to earth and phase faults were tested on the MV distribution networks in order to investigate the performance of the Rogowski coil. A high impedance fault due to a leaning tree and an intermittent fault have been modeled where their corresponding fault traveling surges have been measured and extracted by the Rogowski coil. The sensitivity of each Rogowski coil and the surge arrival time have been found proportional to the distance where the fault surge traveled up to the measuring point. In future work, a signal measured by a Rogowski coil could be used to locate the fault source location by implementing multi-end correlation techniques.

9- Conclusions and future work

9.1   Conclusions

In the last forty years, the use of covered-conductor (CC) overhead lines in distribution networks in Finland have been based on the idea of making the line more tolerable against conductor clashing and trees leaning on the conductors. This contributes a lot of space saving between the trees and conductor, and the spacing between the conductors. There is, however, a major problem associated with the CC line that is a cause for concern: the initiation of partial discharges (PDs) resulting from trees leaning on CC lines. A tree in contact with a CC line will distort the electric field around the conductor and cause PDs. PDs can be observed and they are usually an early indicator of imminent failure of the insulator. If the PD on the CC goes undetected for a certain period of time, it will lead to an outage of the distribution network connected to the CC. All leading to additional inconvenience to customers and costs for those who maintain the grid.

In this thesis, a three-phase PD monitoring system for CC overhead lines in distribution networks has been presented. These are based on single, double and multi-end measurements. A frequency-dependent CC line model (JMarti) and Rogowski coil were used as a CC overhead line model and PD measuring sensor, respectively. The performance of the aforementioned system has been experimentally evaluated based on offline and online PD measurements. For offline measurements, the pulse calibrator was used to inject a PD source into the CC overhead lines. Meanwhile, for online measurement, the CC line was energized by 110/20 kV power transformer. The concept of the twisted-coil around the CC has been introduced in order to produce a pulse similar to the PD source. In addition, PD pulses generated caused by a leaning tree have also been experimentally done. The propagation of PD pulses from the source towards its terminal-ends was measured. The localization process was done using a locator function developed during this work.

For single-end and double-end measurements, the location of the PD source on the CC overhead line was found based on the stamping time of arrival and the propagation velocity for the measured signals. Due to the inconsistency of the propagation velocity over the CC overhead lines, the new PD location technique for multi-end measurements with three synchronized measured signals has been developed without the need to be concerned about the parameter of the propagation velocity. The technique has been presented and discussed in Chapters 5 and 6 of the thesis. This technique was developed based on a combination of three

different stages of signal analysis, which are: denoising, extracting the PD features and locating the PD point.

Discrete wavelet transform (DWT) has been used to develop the denoising technique for the measured signals. The denoising performance was presented and discussed in Chapter 6. Its performance has been evaluated based on the signal to noise ratio (SNR) of the signals before and after denoising (SNR_{den}). Discrete spectral interference (DSI) and Gaussian white noise (GWN) were simulated and used as noise models. For high voltage (HV) laboratory measurement, the broadband interference white noise was generated from an energized three-phase power transformer 20 kV / 410 V AC. A high frequency transient PD pulse has been extracted from the measured signals using windowed standard deviation (STD). The advantage of windowed STD is its ability to extract non-stationary signals such as PD pulses. A multi-end correlation-based PD location technique has been employed to locate the PD source point on CC overhead lines. The theory of maximum correlation factor was used in order to find the time difference of arrival (TDOA) between PD signal arrivals at three synchronized measuring points. The advantage of this technique is the ability to locate the PD source without the need to know the first arrival time and the propagation velocity of the signals. In addition, the faulty section between the three measuring points can also be identified. The algorithm performances were evaluated using EMTP-ATP simulated PD cases and verified using an experimental measurement result. The localization accuracy was presented and discussed in Chapter 6.

For unsynchronized measured signals, the locator function algorithm was developed based on two-end correlation signals. The ratio of correlation, *ROC* has been plotted against its ratio of distance, *LR*. The hyperbolic sine equation was found to be the best function correlated with the plotted curve. This technique helps to solve the problem of the unsynchronized measured signals between two measuring points. In future, the performance of the locator function algorithm developed in this thesis could be tested using the unsynchronized measured signals obtained from both the laboratory test and the real field. More research needs to be done in this direction and field data is required to verify the algorithm. Furthermore, experience in line modeling is also required.

The capability of Rogowski coils to work on capturing different fault transients traveled from the source location has been evaluated. This evaluation is useful in order to make it possible to implement various fault locator techniques using the same technique used to locate the PDs. Different fault scenarios were simulated including earth and phase faults, arcing faults and faults due to a leaning tree. The sensitivity of each Rogowski coil and the surge arrival time have been found proportional to the distance where the fault surge traveled up to the measuring point. In future work, a signal measured by a Rogowski coil can be used to locate the fault source location by implementing multi-end correlation techniques.

It is believed that the approach in this work can contribute to improved methods of the detection and localization of insulation degradation in MV and HV power networks.

9.2 Future work

- The performance of the Rogowski coil used in this work can be improved by optimizing the design parameters. New model and design of the Rogowski coil as a cost effective and efficient PD sensor could be implemented for the other power components such as transformers, cables, switch gears and insulators, etc in a real distribution network.

- Measurements in real substations can help to evaluate the algorithm considering the collected noised data. Possible noise sources are such as from power line carrier signals, radio signals coupled in power systems and noise from power electronics equipment.

- Measurement of the PD signal in the real field area of leaning trees on CC overhead lines.

- The effect of accuracy of the PD source location on overhead CC line due to frozen ice on the CC line should be considered.

- PD location technique based-multi-end correlation developed in this work could be considered to be applied for PD and fault location in undergound cable systems too.

References

[1]   T. Leskinen, "Design of Medium Voltage and High Voltage Covered Conductor Overhead Lines", *International Conference on Electricity Distribution (CIRED)*, Barcelona, Spain, 12-15 May 2003.

[2]   *Accessories for Medium Voltage Distribution Networks - Ensto Overhead*, Report by Utility Networks, Ensto Sekko Oy, Finland, 2008.

[3]   G. M. Hashmi, *Partial Discharge Detection for Condition Monitoring of Covered-Conductor Overhead Distribution Networks Using Rogowski Coil*, Doctoral Dissertation, Helsinki University of Technology, Finland, August 2008.

[4]   P. Pakonen, "Characteristics of Partial Discharges Caused by Trees in Contact With Covered Conductor Lines", *IEEE Trans. on Dielectrics and Electrical Insulation*, Vol. 15, No. 6, pp. 1626–1633, December 2008.

[5]   G. M. Hashmi, M. Lehtonen and M. Nordman, "Modeling and Experimental Verification of On-line PD Detection in Medium Voltage Covered-Conductor Overhead Networks", *IEEE Trans. on Dielectrics and Electrical Insulation*, Vol. 17, No. 1, pp. 167–180, February 2010.

[6]   G. Xiaohua, L. Jingsheng, Z. Mingjun and Y. Miaoyuan, "Improved Performance Rogowski Coils for Power System", *IEEE Conference on Transmission, Distribution and Exposition*, Wuhan, China, Vol. 1, pp. 371-374, 7-12 September 2003.

[7]   E. F. Steennis, R. Ross, N. van Schaik, W. Boone and D. M. van Aartrijk, "Partial Discharge Diagnostics of Long and Branched Medium-Voltage Cables", *IEEE International Conference on Solid Dielectrics*, Eindhoven, Netherlands, pp. 27-30, 25-29 June 2001.

[8]   M. S. Mashikian, "Partial Discharge Location as a Diagnostic Tool for Power Cables", *IEEE Power Engineering Society Winter Meeting*, Singapore, Vol. 3, pp. 1604-1608, 23-27 January 2000.

[9]   S. Boonpoke and B. Marungsri, "Pattern Recognition of Partial Discharge by Using Simplified Fuzzy ARTMAP", *World Academy of Science, Engineering and Technology (WASET) Journal*, Vol. 65, pp. 212-219, 2010.

[10]   V. Dubickas and H. Edin, "Couplers for On-line Time Domain Reflectometry Diagnostic of Power Cables", *IEEE Conference on Electrical Insulation and Dielectric Phenomena*, Boulder, Colorado, USA, pp. 210–214, 17-20 October 2004.

[11]   J. Zhu, L. Yang, J. Jia and Q. Zhang, "The Design of Rogowski Coil with Wide Band Using for Partial Discharge Measurements", *IEEE International Symposium on Electrical Insulating Materials*, Kitakyushu, Japan, pp. 518–521, 5-9 June 2005.

[12]   P. C. J. M. Van der Wielen, J. Veen, P. A. A. F. Wouters and E. F. Steennis, "Sensors for On-line PD Detection in Medium Voltage Power Cables and Their Location in Substations", *IEEE International Conference on Properties and Applications of Dielectric Materials*, Nagoya, Japan, pp. 215–219, 1-5 June 2003.

[13]   D. A. Ward and J. L. T. Exon, "Experience with using Rogowski Coils for Transient Measurements", *IEE Colloquium on Pulsed Power Technology*, London, UK, pp. 6/1-6/4, 20 February 1992.

[14]   M. Zhu, D. J. Perreault, V. Caliskan, T. C. Neugebauer, S. Guttowski and J. G. Kassakian, "Design and Evaluation of an Active Ripple Filter with Rogowski-Coil Current Sensing", *IEEE Annual Conference on Power Electronics Specialists*, Charleston, South California, USA, Vol. 2, pp. 874-880, 27 June-1 July 1999.

[15]   C. Xiao, L. Zhao, T. Asada, W. G. Odendaal and J. D. Van Wyk, "An Overview of Integratable Current Sensor Technologies", *IEEE Conference on Industry Applications, 38th IAS Annual Meeting*, Salt Lake City, Utah, USA, Vol. 2, pp. 1251 – 1258, 12-16 October 2003.

[16]   N. H. Ahmed and N. N. Srivinas, "On-line Partial Discharge Detection in Cables", *IEEE Trans. on Dielectrics and Electrical Insulation*, Vol. 5, No. 2, pp. 181–188, April 1998.

[17] A. Kyprianou and G. E. Georghiou, "Wavelet Packet Denoising for On-Line Partial Discharge Detection in High Voltage Systems", *IEEE International Symposium on Intelligent Control & 13th Mediterranean Conference on Control and Automation*, Limassol, Cyprus, pp. 1184–1189, 27-29 June 2005.

[18] J. Veen and P. C. J. M. van der Wielen, "The Application of Matched Filters to PD Detection and Localization", *IEEE Electrical Insulation Magazine*, Vol. 19, No. 5, pp. 20-26, September 2003.

[19] I. Shim, J. J. Soraghan and W. H. Siew, "Detection of PD Utilizing Digital Signal Processing Methods - Part 3: Open-Loop Noise Reduction", *IEEE Electrical Insulation Magazine*, Vol. 17, No. 1, pp. 6-13, January 2001.

[20] J. Veen, *On-line Signal Analysis of Partial Discharges in Medium-Voltage Power Cables*, Doctoral Dissertation, Technische Universiteit, Eindhoven, Netherlands, April 2005.

[21] A. M. Elhaffar, N. I. Elkalashy and M. Lehtonen, "Experimental Investigations on Multi-end Fault Location System Based on Current Traveling Waves", *IEEE PowerTech Conference*, Lausanne, Switzerland, pp. 1141–1146, 1-5 July 2007.

[22] E. S. Tag El Din, M. Gilany, M. M. Abdel Aziz and D. K. Ibrahim, "A Wavelet-Based Fault Location Technique for Aged Power Cables", *IEEE Power Engineering Society General Meeting*, San Francisco, California, USA, Vol. 3, pp. 2485-2491, 12-16 June 2005.

[23] G. M. Hashmi, M. Lehtonen and A. Ametani, "Modeling and Experimental Verification of Covered-Conductor for PD Detection in Overhead Distribution Networks", *Institute of Electrical Engineers of Japan (IEEJ) Trans. on Power and Energy*, Vol. 130, pp. 670-678, July 2010.

[24] X. Song, C. Zhou and D. M. Hepburn, "An Algorithm for Identifying the Arrival Time of PD Pulses for PD Source Location", *IEEE Conference on Electrical Insulation and Dielectric Phenomena*, Quebec, Canada, pp. 379–382, 26-29 October 2008.

[25] P. C. J. M. van der Wielen, P. A. A. F. Wouters, J. Veen and D. M. van Aartrijk, "Synchronization of On-line PD Detection and Localization Setups Using Pulse Injection", *IEEE International Conference on Properties and Applications of Dielectric Materials*, Nagoya, Japan, pp. 327–330, 1-5 June, 2003.

[26] P. Wagenaars, P. A. A. F. Wouters, P. C. J. M. Van der Wielen and E. F. Steennis, "Accurate Estimation of the Time-of-Arrival of Partial Discharge Pulses in Cable Systems in Service", *IEEE Trans. on Dielectrics and Electrical Insulation*, Vol. 15, No. 4, pp. 1190–1199, August 2008.

[27] V. Jeyabalan and S. Usa, "Energy Based Correlation Method for Location of Partial Discharge in Transformer Winding", *Journal of Advances in Electrical and Computer Engineering*, Vol. 9, No. 1, pp. 46–51, 2009.

[28] Y. Sun, B. G. Stewart and I. J. Kemp, "Alternative Cross-Correlation Techniques for Location Estimation of PD from RF Signals", *IEEE International Conference on Universities Power Engineering (UPEC)*, Bristol, UK, pp. 143–148, 6-8 September 2004.

[29] E. Kuffel, W. S. Zaengl and J. Kuffel, *High Voltage Engineering: Fundamentals*, Elsevier, ISBN 978-0-7506-3634-6, 2nd Edition, July 2000.

[30] R. J. van Brunt, "Physics and Chemistry of Partial Discharge and Corona - Recent Advances and Future Challenges", *IEEE Trans. on Dielectrics and Electrical Insulation*, Vol. 1, No. 5, pp. 761–784, October 1994.

[31] R. Bartnikas, "Partial Discharge - Their Mechanism, Detection and Measurement", *IEEE Trans. on Dielectrics and Electrical Insulation*, Vol. 9, No. 5, pp. 763–808, October 2002.

[32] S. Karmakar, N. K. Roy and P. Kumbhakar, "Partial Discharge Measurement of Transformer with ICT Facilities", *IEEE International Conference on Power Systems (ICPS)*, Kharagpur, India, pp. 1-5, 27-29 December 2009.

[33]   A. A. Paithankar and A. D. Mokashi, "Can PD Phenomenon be Analysed by Deterministic Chaos?", *IEEE Conference on Electrical Insulation and Electrical Manufacturing & Coil Winding*, Rosemont, Illinois, USA, pp. 283-289, 22-25 September 1997.

[34]   N. Kolev, P. Darjanov, E. Gadjeva and D. Darjanova, "Partial Discharge Phenomena Simulation Using General-Purpose Analysis Programs", *IEEE International Conference on Conduction and Breakdown in Solid Dielectrics (ICSD)*, Vasteras, Sweden, pp. 149-152, 22-25 June, 1998.

[35]   C. Y. Ren, Y. H. Cheng, P. Yan, Y. H. Sun and T. Shao, "Simulation of Partial Discharges in Single and Double Voids using SIMULINK", *IEEE Conference on Power Modulator*, Arlington, Virgina, USA, pp. 120-123, 14-18 May 2004.

[36]   L. Satish and W. S. Zaengl, "Artificial Neural Networks for Recognition of 3D Partial Discharge Patterns", *IEEE Trans. on Dielectrics and Electrical Insulation*, Vol. 1, No. 2, pp. 265–275, April 1994.

[37]   L. Kojovic, "Rogowski Coils Suit Relay Protection and Measurement", *IEEE Computer Applications in Power*, Vol. 10, No. 3, pp. 47-52, July 1997.

[38]   CIGRE Working Group D1.37, *Guidelines for Basic and Practical Aspects of Partial Discharge Detection Using Conventional and Unconventional Methods*, CIGRE Technical Brochure, August 2011.

[39]   L. E. Lundgaard, "Partial Discharge - Part XIV: Acoustic Partial Discharge Detection-Practical Application", *IEEE Electrical Insulation Magazine*, Vol. 8, No. 5, pp. 34-43, September 1992.

[40]   L. E. Lundgaard, "Partial Discharge - Part XIII: Acoustic Partial Discharge Detection-Fundamental Considerations", *IEEE Electrical Insulation Magazine*, Vol. 8, No. 4, pp. 25-31, July 1992.

[41]   R. Schwarz and M. Muhr, "Modern Technologies in Optical Partial Discharge Detection", *IEEE Conference on Electrical Insulation and Dielectric Phenomena (CEIDP)*, Vancouver, Canada, pp. 163-166, 14-17 October 2007.

[42]   R. Schwarz, M. Muhr and S. Pack, "Evaluation of Partial Discharge Impulses with Optical and Conventional Detection Systems", *International Symposium on High Voltage Engineering*, Tsinghua University, Beijing, China, pp. 1-4, 25-29 August 2005.

[43]   S. Tominaga, H. Kuwahara, K. Hirooka and T. Yoshioka, "SF6 Gas Analysis Technique and its Application for Evaluation of Internal Conditions in SF6 Gas Equipment", *IEEE Trans. on Power Apparatus and Systems*, Vol. 100, No. 9, pp. 4196-4206, September 1981.

[44]   M. Kaufhold, S. S. Bamji and A. T. Bulinski, "Optical Detection of Partial Discharges in Gas-Insulated Systems", *IEEE Conference on Electrical Insulation and Dielectric Phenomena*, Millbrae, California, USA, Vol. 2, pp. 618-623, 20-23 October 1996.

[45]   A. Ametani, "Power System Transient Analysis by EMTP", *Middle-East Power Systems Conference (MEPCON)*, Hellwan University, Egypt, pp. 1-12, 29-31 December 2001.

[46]   J. R. Marti and L. R. Linares, "Real-Time EMTP-Based Transients Simulation", *IEEE Trans. on Power Systems*, Vol. 9, No. 3, pp. 1309-1317, August 1994.

[47]   R. H. Lasseter, *Electromagnetic Transient Program (EMTP)*: *Vol. 4, Workbook IV (TACS)*, Technical Report, EPRI Research Project, USA, June 1989.

[48]   L. Prikler and H. K. Hoidalen, *ATPDraw Version 3.5 for Windows 9x/NT/2000/XP – Users' Manual,* Report by SINTEF Energy Research, Norway, October 2002.

[49]   G. M. Hashmi, M. Nordman and M. Lehtonen, "A Partial Discharge Detection Concept for Wireless Sensors in Covered-Conductors Distribution System", *Europe's Premier Conference on Electrical Insulation (INSUCON2006)*, Birmingham, UK, 24-26 May 2006.

[50]   H. W. Dommel, *Electromagnetic Transients Program (EMTP) – Rule Book*, Oregon, USA, 1984.

[51]   W. S. Meyer and T. H. Liu, *Alternative Transients Program (*ATP*) Rule Book,* Report by Canadian/American EMTP User Group, 1987-2000.

113

[52]   L. Prikler and H. K. Hoidalen, *ATPDraw Version 5.6 for Windows 9x/NT/2000/XP/Vista - User's Manual,* Report by NTNU, Norway and SINTEF Energy Research, Budapest, Hungary, November 2009.

[53]   G. M. Hashmi and M. Lehtonen, "Covered-Conductor Overhead Distribution Line Modeling and Experimental Verification for Determining its Line Characteristics", *IEEE Power Engineering Society (PES) Conference and Exposition in Africa*, Johannesburg, South Africa, pp. 1-7, 16-20 July 2007.

[54]   A. Ametani, N. Nagaoka and R. Koide, "Wave Propagation Characteristics on an Overhead Conductor Above Snow", *Electrical Engineering in Japan*, Vol. 134, No. 3, pp. 26–33, February 2001.

[55]   G. M. Hashmi and M. Lehtonen, "Effects of Rogowski Coil and Covered-Conductor Parameters on the Performance of PD Measurements in Overhead Distribution Networks," *International Journal of Innovations in Energy Systems and Power*, Vol. 4, No. 2, pp. 14–21, October 2009.

[56]   G. M. Hashmi, M. Isa and M. Lehtonen, "Modeling Online Three-Phase PD Monitoring System for MV Overhead Covered-Conductors", *International Conference on Power Systems Transients (IPST2009)*, Kyoto, Japan, 3-6 June 2009.

[57]   J. R. Marti, "Accurate Modeling of Frequency-Dependent Transmission Lines in Electromagnetic Transients Simulations", *IEEE Trans. on Power Apparatus and Systems*, Vol. 101, No.1, pp. 147-157, January 1982.

[58]   G. M. Hashmi and M. Lehtonen, "On-line PD Measuring System Modeling and Experimental Verification for Covered-Conductor Overhead Distribution Networks", *IEEE Mediterranean Conference on Control and Automation (MED07)*, Athens, Greece, pp. 1-6, 27-29 June 2007.

[59]   G. M. Hashmi, M. Lehtonen, M. Nordman and M. Isa, "Sensors for On-line Partial Discharge Detection in Covered-Conductor Overhead Distribution Networks", *International Conference on Electrical and Control Technologies (ECT2009)*, Kaunas, Lithuania, pp. 272-277, 7-8 May 2009.

[60]   M. Isa, G. M. Hashmi and M. Lehtonen, "Comparative Study of On-line Three Phase PD Monitoring Systems for Overhead Covered Conductor Distribution Lines", *IEEE International Conference on Universities Power Engineering (UPEC2009),* Glasgow, Scotland, pp. 1-5, 1-4 September 2009.

[61]   B. Badrzadeh and S. M. Shahrtash, "Partial Discharge Site Location in Power Cables: Application to On-line and Off-line Approach", *IEEE Conference on Australasian Universities Power Engineering (AUPEC2002)*, Melbourne, Australia, 29 September-2 October 2002.

[62]   H. Zhang, *Advanced Techniques Application of On-line Partial Discharge Detection in Power Cables*, Doctoral Thesis, University of New South Wales, Australia, August 2006.

[63]   M. Isa, G. M. Hashmi and M. Lehtonen, "EMTP-ATP Representation of Three-Phase Partial Discharge Monitoring System for Covered Conductors in Overhead Distribution Lines", *European EMTP-ATP Conference*, Delft, Netherlands, 26-28 October 2009.

[64]   L. Kojovic, "Rogowski Coil Transient Performance and ATP Simulations for Applications in Protective Relaying", *International Conference on Power Systems Transients (IPST'05)*, Montreal, Canada, 19-23 June 2005.

[65]   D. A. Ward and J. L. T. Exon, "Using Rogowski Coils for Transient Current Measurements", *Engineering Science and Education Journal*, Vol. 2, No. 3, pp. 105-113, June 1993.

[66]   S. Abe and A. Matsushita, "Induced Pulse Voltage in Twisted Vicalloy Wire with Compound Magnetic Effect", *IEEE Trans. on Magnetics*, Vol. 31, No. 6, pp. 3152-3154, November 1995.

[67]   N. I. Elkalashy, N. G. Tarhuni, A. M. Elhaffar and M. Lehtonen, "Evaluation of Chirp Detector-Based Travelling Wave Localization of Earth Faults in MV Networks", *IET International Conference on Developments in Power System Protection (DPSP2010)*, Manchester, UK, pp. 1-5, 29 March-1 April 2010.

[68]   A. M. Elhaffar, *Power Transmission Line Fault Location Based on Current Traveling Waves*, Doctoral Dissertation, Helsinki University of Technology, Finland, March 2008.

[69]   Z. Feng, L. Jun, Z. Li and Y. Zhihao, "A New Fault Location Method Avoiding Wave Speed and Based on Traveling Waves for EHV Transmission line", *IEEE International Conference on Electric Utility Deregulation and Restructuring and Power Technologies (DRPT2008)*, Nanjuing, China, pp. 1753-1757, 6-9 April 2008.

[70]   M. Isa, N. I. Elkalashy, N. Tarhuni, G. M. Hashmi and M. Lehtonen, "Experimental Evaluation of Rogowski Coil Performance for Locating PD in Energized Overhead Covered-Conductor Feeder", *Middle-East Power Systems Conference (MEPCON2010)*, Cairo, Egypt, pp. 572-577, 19-21 December 2010.

[71]   G. A. Mizusawa, *Performance of Hyperbolic Position Location Techniques for Code Division Multiple Access*, Master Thesis, Virginia Polytechnic Institute and State University, Blacksburg, Virginia, USA, 1996.

[72]   V. Jeyabalan and S. Usa, "Partial Discharge Location in Transformers Using Frequency Domain Correlation", *IEEE International Conference on Power Engineering (IPEC)*, Singapore, pp. 197-200, 3-6 December 2007.

[73]   W. A. Gardner and C. K. Chen, "Signal-Selective Time-Difference-of-Arrival Estimation for Passive Location of Man-Made Signal Sources in Highly Corruptive Environments, Part 1: Theory and Method", *IEEE Trans. on Signal Processing*, Vol. 40, No. 5, pp. 1168-1184, May 1992.

[74]   C. K. Chen and W. A. Gardner, "Signal-Selective Time-Difference-of-Arrival Estimation for Passive Location of Man-Made Signal Sources in Highly Corruptive Environments, Part II: Algorithms and Performance", *IEEE Trans. on Signal Processing*, Vol. 40, No. 5, pp. 1185-1197, May 1992.

[75]   C. H. Knapp and G. C. Carter, "The Generalized Correlation Method for Estimation of Time Delay", *IEEE Trans. on Acoustics, Speech and Signal Processing*, Vol. 24, No. 4, pp. 320-327, 1976.

[76]   G. C. Carter, "Coherence and Time Delay Estimation", *Proceedings of the IEEE*, Vol. 75, No. 2, pp. 236-255, February 1987.

[77]   P. R. Roth, "Effective Measurements Using Digital Signal Analysis", *IEEE Spectrum*, Vol. 8, No. 4, pp. 62-70, April 1971.

[78] W. R. Hahn and S. A. Tretter, "Optimum Processing for Delay-Vector Estimation in Passive Signal Arrays", *IEEE Trans. on Information Theory*, Vol. 19, No. 5, pp. 608-614, September 1973.

[79] X. Ma, C. Zhou and I. J. Kemp, "Interpretation of Wavelet Analysis and Its Application in Partial Discharge Detection", *IEEE Trans. on Dielectrics and Electrical Insulation*, Vol. 9, No. 3, pp. 446–457, June 2002.

[80] M. Gilany, D. K. Ibrahim and E. S. Tag El Din, "Traveling-Wave-Based Fault-Location Scheme for Multiend-Aged Underground Cable System", *IEEE Trans. on Power Delivery*, Vol. 22, No. 1, pp. 82–89, January 2007.

[81] H. Zhang, T. R. Blackburn, B. T. Phung and D. Sen, "A Novel Wavelet Transform Technique for On-line Partial Discharge Measurements - Part 1: WT De-noising Algorithm", *IEEE Trans. on Dielectrics and Electrical Insulation*, Vol. 14, No. 1, pp. 3–14, February 2007.

[82] H. Zhang, T. R. Blackburn, B. T. Phung and D. Sen, "A Novel Wavelet Transform Technique for On-line Partial Discharge Measurements - Part 2: On-site Noise Rejection Application", *IEEE Trans. on Dielectrics and Electrical Insulation*, Vol. 14, No. 1, pp. 15–22, February 2007.

[83] A. M. Elhaffar, N. I. Elkalashy, N. G. Tarhuni, M. F. Abdel-Fattah and M. Lehtonen, "Evaluation of Probabilistic-Based Selectivity Technique for Earth Fault Protection in Medium Voltage Networks", *IEEE Conference on PowerTech*, Bucharest, Romania, pp. 1–5, 28 June-2 July 2009.

[84] A. M. Gouda, A. El-Hag, T. K. Abdel-Galil, M. M. A. Salama and R. Bartnikas, "On-line Detection and Measurement of Partial Discharge Signals in a Noisy Environment", *IEEE Trans. on Dielectrics and Electrical Insulation*, Vol. 15, No. 4, pp. 1162–1173, August 2008.

[85] W. Li, "Research on Extraction of Partial Discharge Signals Based on Wavelet Analysis," *IEEE International Conference on Electronic Computer Technology*, Macau, China, pp. 545–548, 20-22 February 2009.

[86]   N. I. Elkalashy, A. M. Elhaffar, M. F. Abdel-Fattah, M. Lehtonen and N. G. Tarhuni, "Windowed Standard Deviation-Based Transient Feature Extraction for Earth Fault Protection in Medium Voltage Networks", *IEEE International Conference on Universities Power Engineering (UPEC)*, Glasgow, UK, pp. 1-4, 1-4 September 2009.

[87]   M. Isa, N. I. Elkalashy, M. Lehtonen, G. M. Hashmi and M. S. Elmusrati, "Multi-end Correlation-Based PD Location Technique for Medium Voltage Covered-Conductor Lines", *IEEE Trans. on Dielectrics and Electrical Insulation*, Vol. 19, No. 3, pp. 936-946, June 2012.

[88]   G. Asada, M. Dong, T. Lin, F. Newberg, G. Pottie, W. Kaiser and H. O. Marcy, "Wireless Integrated Network Sensors: Low Power Systems on a Chip", *IEEE European Solid-State Circuits Conference*, Den Hague, Netherlands, pp. 9-12, 22-24 September 1998.

[89]   D. Estrin, R. Govindan, J. Heidemann and S. Kumar, "Next Century Challenges: Scalable Coordination in Sensor Networks", *International Conference on Mobile Computing and Networking*, Seattle, Washington, USA, pp. 263-270, 25-30 October 1999.

[90]   L. Girod and D. Estrin, *Development and Characterization of an acoustic rangefinder*, Technical Report 00-728, Department of Computer Science, University of Southern California, California, USA, 2000.

[91]   K. Yao, R. E. Hudson, C. W. Reed, D. Chen and F. Lorenzelli, "Blind Beamforming on a Randomly Distributed Sensor Array System", *IEEE Journal on Selected Areas in Communications*, Vol. 16, No. 8, pp. 1555–1567, October 1998.

[92]   C. Intanagonwiwat, R. Govindan and D. Estrin, "Directed Diffusion: A Scable and Robust Communication Paradigm for Sensor Networks", *Annual International Conference on Mobile Computing and Networks*, Boston, Massachusetts, USA, pp. 56-67, 6-11 August 2000.

[93]   N. A. Sabiha and M. Lehtonen, "Lightning-Induced Overvoltages Transmitted over Distribution Transformer with Medium Voltage Spark-Gap Operation - Part I: High-Frequency Transformer Model with Medium Voltage Spark-Gap", *IEEE Trans. on Power Delivery*, Vol. 25, No. 4, pp. 2472-2480, October 2010.

[94]   N. A. Sabiha and M. Lehtonen, "Combining High Frequency and Saturable models of Distribution Transformer for Lightning-Induced Overvoltage Superimposed on AC Voltage" *European EMTP-ATP Conference*, Espoo, Finland, pp. 176-184, 16-18 August 2010.

[95]   N. I. Elkalashy, M. Lehtonen, H. A. Darwish, M. A. Izzularab and A. I. Taalab, "Modeling and Experimental Verification of High Impedance Arcing Fault in Medium Voltage Networks", *IEEE Trans. on Dielectrics and Electrical Insulation*, Vol. 14, No. 2, pp. 375- 383, April 2007.

[96]   M. Kizilcay and P. L. Seta, "Digital Simulation of Fault Arcs in Medium-Voltage Distribution Networks", *Power Systems Computation Conference (PSCC)*, Liege, Belgium, pp. 1-7, 22-26 August 2005.

[97]   H. Darwish and N. Elkalashy, "Universal Arc Representation Using EMTP", *IEEE Trans. on Power Delivery*, Vol. 20, No. 2, pp. 772-779, April 2005.

[98]   M. Isa, M. Lehtonen, G. M. Hashmi and N. I. Elkalashy, "Rogowski Coil Evaluation with Different Fault Conditions in Medium Voltage Distribution Networks", *International Journal of Electrical Engineering and Technology (IJEET)*, Vol. 3, No. 1, pp. 85-96, January 2012.

[99]   G. M. Hashmi, M. Lehtonen and M. Nordman, "Calibration of On-line Partial Discharge Measuring System Using Rogowski coil in Covered-Conductor Overhead Distribution Networks", *IET Science, Measurement and Technology,* Vol. 5, No. 1, pp. 5–13, January 2011.

[100]   M. Isa, N. I. Elkalashy, G. M. Hashmi, M. Shafiq and M. Lehtonen, "Three Measuring Points for Partial Discharge Location in Energized Covered-Conductor Overhead Distribution Lines: Algorithm and Experimental Evaluation", *International Review of Electrical Engineering (IREE)*, Vol. 7, No. 4, pp. 5221-5229, August 2012.

[101]   M. Isa, N. I. Elkalashy, G. M. Hashmi, M. Shafiq and M. Lehtonen, "Correlation Evaluation of Unsynchronized Multi-End Windows for Locating Partial Discharge Sources in Covered-Conductor Overhead Lines", *International Review of Modeling and Simulations (IREMOS)*, Vol. 5, No. 4, pp. 1854-1857, August 2012.

[102] A. Ametani, R. Koide and N. Nagaoka, "Effect of Snow on Wave Propagation Characteristics on an Overhead Single Conductor", *International Conference on Electrical Engineering (ICEE)*, Hong Kong, pp. 55-58, 16-18 August 1999.

Fault on distribution line networks may cause excessive power interruption to customers and large costs for the distributor. The thesis provides a technique which can locate partial discharges (PDs), which is one of the major causes of fault in covered-conductor (CC) line, by using multi-end correlation technique. In Finland covered-conductor overhead lines are commonly used in medium voltage networks because the loads are widely distributed in forested terrain. Such networks are exposed to leaning trees which will produce PDs prior to complete breakdown. The PDs, if undetected for a certain period of time, will lead to an outage of the distribution networks. In the technique developed, the PDs can be detected with multiple Rogowski coil sensors and located using the algorithm developed. The technique will help in improving the detection and localization reliability of PDs due to leaning trees on CC overhead distribution lines, and will provide protection improvements against the breakdown in distribution network.

BUSINESS +
ECONOMY

ART +
DESIGN +
ARCHITECTURE

SCIENCE +
TECHNOLOGY

CROSSOVER

**DOCTORAL
DISSERTATIONS**